2019-01-01

Using Coherence to Improve the Calculation of Active Acoustic Intensity with the Phase and Amplitude Gradient Estimator Method

Mylan Ray Cook
Brigham Young University

Using Coherence to Improve the Calculation of Active Acoustic Intensity with the Phase and Amplitude Gradient Estimator Method

Mylan Ray Cook

A thesis submitted to the faculty of
Brigham Young University
in partial fulfillment of the requirements for the degree of

Master of Science

Kent L. Gee, Chair
Scott D. Sommerfeldt
Tracianne B. Neilsen

Department of Physics and Astronomy

Brigham Young University

ABSTRACT

Using Coherence to Improve the Calculation of Active Acoustic Intensity with the Phase and Amplitude Gradient Estimator Method

Mylan Ray Cook
Department of Physics and Astronomy, BYU
Master of Science

Coherence, which gives the similarity of signals received at two microphone locations, can be a powerful tool for calculating acoustic quantities, particularly active acoustic intensity. To calculate active acoustic intensity, a multi-microphone probe is often used, and therefore coherence between all microphone pairs on the probe can be obtained. The phase and amplitude gradient estimator (PAGE) method can be used to calculate intensity, and is well suited for many situations. There are limitations to this method—such as multiple sources or contaminating noise in the sound field—which can cause significant error. When there are multiple sources or contaminating noise present, the coherence between microphone pairs will be reduced. A coherence-based approach to the PAGE method, called the CPAGE method, is advantageous.

Coherence is useful in phase unwrapping. For the PAGE method to be used at frequencies where the probe microphone spacing is larger than half a wavelength (above the spatial Nyquist frequency), the phase of transfer functions between microphone pairs must be unwrapped. Phase differences are limited to a 2π radian interval, so unwrapping—adding integer multiples of 2π radians to create a continuous phase relation across frequency—is necessary to allow computation of phase gradients. Using coherence in phase unwrapping can improve phase gradient calculation, which in turn leads to improved intensity calculation.

Because phase unwrapping is necessary above the spatial Nyquist frequency, the PAGE method is best suited to dealing with broadband signals. For narrowband signals, which lack coherent phase information at many frequencies, the PAGE method can give erroneous intensity results. One way to improve calculation is with low-level additive broadband noise, which provides coherent phase information that can improve phase unwrapping, and thereby improve intensity calculation. There are limitations to this approach, as additive noise can have a negative impact on intensity calculation with the PAGE method.

The CPAGE method, fortunately, can account for contaminating noise in some situations. A magnitude adjustment—which arises naturally from investigation of the bias errors of the PAGE method—can account for the additional pressure amplitude caused by the contaminating noise, improving pressure magnitude calculations. A phase gradient adjustment—using a coherence-weighted least squares algorithm—can likewise improve phase gradient calculations. Both adjustments depend upon probe microphone coherence values. Though not immune to contaminating noise, this method can better account for contaminating noise. Further experimental work can verify the effectiveness of the CPAGE method.

Keywords: coherence, active acoustic intensity, phase gradient, bias errors, broadband

Table of Contents

List of Figures

List of Tables:

Chapter 1

Introduction

1.1 Motivation

In many signal processing applications, at least a certain amount of coherence is necessary, and ideally perfect coherence.[1,2] For many experimental situations, where some contaminating noise is present, however, coherence cannot be assumed. This noise affects accurate measurements, which leads to inaccurate results for signal properties.[3] The reduced coherence does contain information about the contaminating noise, however, and so it is possible to use coherence values to account for some of the inaccuracy caused by the noise. This idea is utilized to improve the calculation of active acoustic intensity using the Phase and Amplitude Gradient Estimator (PAGE) method.

Active acoustic intensity is a measure of the propagating energy in a sound field. This measure is often used for source characterization—to explain how it radiates sound—and localization—to find sources from which sound emanates. It is a frequency-domain vector quantity, and as such consists of a magnitude and direction, which points in the direction of sound propagation.[4] It is obtained from either measuring or calculating the pressure and particle velocity at a specific spatial location. Particle velocity measurements are difficult, especially when any net flow exists in the sound field. Some methods measure the pressure using a compact probe with multiple microphones, then use Euler's equation to obtain the particle velocity from the calculated pressure gradient.[5]

Both the traditional (or finite difference or p-p) method and the PAGE method use this approach. The traditional method uses real and imaginary parts of the complex pressure to obtain the pressure gradient, and is largely unaffected by contaminating noise, but is limited in its frequency range.[6] The PAGE method was developed in part to increase the frequency range over which this calculation is considered valid, and uses the pressure magnitude and phase.[7-9] This method is extremely useful for many situations; however, it is particularly susceptible to errors caused by contaminating noise. The PAGE method is also better suited to dealing with broadband signals, and at higher frequencies narrowband results can be unreliable.

Applications of using the PAGE method to calculate intensity for narrowband signals are investigated. It is found that additive low-level broadband noise—where the additive noise source and signal source have a small angular separation as seen at the probe location—can improve intensity calculations above the spatial Nyquist frequency (the limit of the traditional method, the frequency at which microphone probe spacing is equal to half of a wavelength), as the broadband noise provides needed phase information across frequency. This can increase the number of situations in which the PAGE method can be employed.

To further improve applications for the PAGE method, a coherence-based method known as the CPAGE method is developed herein. The CPAGE method makes a few adjustments in how the intensity is calculated with the PAGE method, based on probe coherence values. One adjustment is improving transfer function phase unwrapping by using coherence. This is useful at frequencies above which the traditional method is used. Another adjustment is using the coherence to remove pressure amplitude caused by uncorrelated noise. A phase gradient adjustment is also implemented, by using the coherence in a weighted least-squares algorithm instead of the least-

squares algorithm employed by the PAGE method. These adjustments make the CPAGE method more robust for dealing with contaminating noise than the PAGE method.

1.2 Thesis outline

This thesis is composed of four separate papers—each comprising a single chapter of this thesis—which have been published, or are being adapted and submitted for publication. As such, each has its own introduction and conclusion, and relevant definitions and equations are given in each chapter. Each addresses a specific property of or difficulty encountered with the PAGE method, and explains how coherence can be used to improve calculations.

Chapter 2, accepted for publication in the *Journal of the Acoustical Society of America* (JASA),[10] discusses the bias errors of the traditional and PAGE methods, and shows how large an impact contaminating noise can have on calculations. These errors become extremely large for the PAGE method when the contaminating noise is significant, but a correction to account for the pressure amplitude caused by the contaminating noise is found. The implementation of this correction is discussed in Chapter 5, where the CPAGE method itself is described.

Chapter 3, which is currently being submitted for publication in JASA,[11] deals with a different challenge, namely that of using the PAGE method with narrowband signals. The PAGE method relies on broadband noise to increase the effective frequency range, and can often be erroneous for higher frequencies. Though contaminating noise negatively impacts calculation of intensity for broadband sources, for a narrowband source additive low-level broadband noise can be advantageous. It can provide phase information necessary to correctly unwrap phase values, and hence improve calculation of intensity. The benefits and limitations of this approach are discussed in further detail in this chapter.

Chapter 4, which has been published in *Proceedings of Meetings on Acoustics*,[12] discusses a coherence-based phase unwrapping algorithm. Phase unwrapping is crucial to the effectiveness of the PAGE method at higher frequencies, and the coherence can be used to drastically improve unwrapping. Improved unwrapping can then yield more accurate pressure phase gradient calculations, which improves the calculation of intensity.

Chapter 5, which is being adapted for submission as an Express Letter in the *Journal of the Acoustical Society of America*, is where the adjustments implemented in the CPAGE method are explained in detail. These adjustments include a magnitude correction (as found in Chapter 2) and a phase gradient correction. The improvements make for a more robust method for calculating active acoustic intensity, which then increases applications for the phase and amplitude gradient version of calculating intensity. The effectiveness of the CPAGE method is examined, along with some limitations and failings.

Chapter 6 contains the final conclusions for this thesis. The CPAGE method serves to increase the number of situations in which the PAGE method can be used. Similarly, though usually reliant upon broadband signals to obtain accurate results at high frequencies, additive low-level broadband noise can increase the effectiveness of the PAGE method for dealing with narrowband signals. The adjustments to the PAGE method, while not making for a perfect solution to every situation, can make the CPAGE method better able to deal with real-world applications where contaminating noise is present. Future applications for this method are also explained in this concluding chapter.

Chapter 2

The effects of contaminating noise on the calculation of active acoustic intensity for pressure gradient methods

Bias errors for two-dimensional active acoustic intensity using multi-microphone probes have been previously calculated for both the traditional cross-spectral and the Phase and Amplitude Gradient Estimator (PAGE) methods.[8] Here, these calculations are expanded to include errors due to contaminating noise, as well as probe orientation. The noise can either be uncorrelated at each microphone location or self-correlated; the self-correlated noise is modeled as a plane wave with a varying angle of incidence. The intensity errors in both magnitude and direction are dependent on the signal-to-noise ratio (SNR), frequency, source properties, incidence angles, probe configuration, and processing method. The PAGE method is generally found to give more accurate results, especially in direction; however, uncorrelated noise with a low SNR (below 10-15 dB) and low frequency (wavelengths more than ¼ the microphone spacing) can yield larger errors in magnitude than the traditional method—though a correction for this is possible. Additionally, contaminating noise does not necessarily impact the possibility of using the PAGE method for broadband signals beyond a probe's spatial Nyquist frequency.

2.1 Introduction

Intensity is an important acoustic measure, and is useful for applications such as source characterization and localization. Acoustic source characterization in real-world environments can

be subject to inaccuracies caused by contaminating noise, whether acoustic, fluid mechanical (e.g. wind) or electrical. These inaccuracies extend to vector acoustic intensity calculations made from pressure measurements obtained with multiple-microphone probes. Intensity, or more specifically active acoustic intensity, is the time-averaged energy flux density. For a given frequency and location, it is a vector-valued quantity that describes the magnitude and direction of the propagating acoustic energy. Accurate estimates of both complex pressure and particle velocity are necessary because intensity is calculated with their product.[13]

Traditionally, acoustic intensity has been calculated using a multi-microphone processing method developed in the 1970s known as the p-p method or finite difference method.[13-15] This method—which here is referred to as the traditional method—estimates the pressure gradient by taking finite sums and differences of the real and imaginary components of the frequency domain complex pressures. The intensity is therefore calculated by using cross-spectral values from the microphones on the intensity probe. Another processing method available is the phase and amplitude gradient estimator (PAGE) method.[9] Instead of using the real and imaginary components of the complex pressures, it uses the magnitude and phase components. The intensity in this case is calculated using auto-spectral values and the arguments of cross-spectral values.[7,13,16,17] Because of differences between the traditional and PAGE methods, the calculated intensity can vary depending on which method is used.

In order to compare the effectiveness of these two methods, calculated intensity can be compared to the known analytical intensity to find the bias errors. A bias error gives a measure of the difference between analytical solutions and the values obtained by using a specific processing method. These errors can depend on many different factors. Previous work has shown how

different bias errors are obtained for various probe geometries for both methods using either a plane-wave source or a monopole source.[17-19]

These previous studies are now expanded to investigate the effects contaminating noise and probe rotation have on the bias errors. The effects of both correlated and uncorrelated contaminating noise are investigated for a single probe geometry, followed by a summary of the effects of using different probe geometries. In general, the PAGE method has lower bias errors in the calculated intensity direction than the traditional method, and in most cases the intensity magnitude bias errors are lower as well. However, for low-level signals at low frequencies, the traditional method may yield a better intensity calculation. In general, the traditional method has larger bias errors than the PAGE method at higher frequencies (wavelengths less than ¼ the microphone spacing), and also when self-correlated noise is present.

2.2 Methodology

The active acoustic intensity $\boldsymbol{I}$ at a point is calculated in the frequency domain as

$$\boldsymbol{I} = \frac{1}{2}\mathrm{Re}\{p\boldsymbol{u}^*\}, \qquad (1)$$

where p is the complex pressure, $\boldsymbol{u}$ is the vector complex particle velocity, and Re indicates the real part. (Bold letters indicate vector quantities, and * indicates complex conjugation.) By using Euler's equation, the complex particle velocity can be obtained from the gradient of the complex pressure as

$$\boldsymbol{u} = \frac{j}{\omega\rho_0}\nabla p, \qquad (2)$$

where j is the imaginary unit, ω is the angular frequency, and ρ_0 is the fluid density. Accurate calculation of the intensity therefore depends upon an accurate calculation of the pressure gradient,

as well as the pressure. The two processing methods calculate the pressure gradient differently, which leads to different bias errors.

For probe configurations where the intensity is calculated in two dimensions, the bias errors—the difference between the analytical intensity $\boldsymbol{I}$ and the calculated intensity $\boldsymbol{I}_{\mathrm{calc}}$—consist of a magnitude error and an angular error, defined respectively as

$$L_{\epsilon,\boldsymbol{I}} = 10\log_{10}\left(\frac{|\boldsymbol{I}_{\mathrm{calc}}|}{|\boldsymbol{I}|}\right) \text{ dB}, \tag{3}$$

$$\theta_{\epsilon,\boldsymbol{I}} = \theta_{\mathrm{calc}} - \theta, \tag{4}$$

where θ and θ_{calc} are the directions of $\boldsymbol{I}$ and $\boldsymbol{I}_{\mathrm{calc}}$ as polar angle in the plane of the probe, respectively. Perfect calculation would yield $L_{\epsilon,\boldsymbol{I}} = 0$ dB and $\theta_{\epsilon,\boldsymbol{I}} = 0°$. Previous studies have shown how these bias errors differ in an ideal, noiseless field where the source is located at a specific angular location relative to the probes investigated.[8] Expanding upon this work, the effects of both probe orientation and contaminating noise present in the sound field are taken into consideration.

When trying to localize or characterize acoustic sources of interest, the presence of contaminating noise introduces several additional variables to bias error calculations. Though independent of the source of interest, the contaminating noise can either be uncorrelated or self-correlated at the microphone probe location, e.g., an extraneous acoustic signal that arrives at a specified angle relative to the probe, yielding a specific phase relationship for the noise itself. In practice, it is possible for the contaminating noise to fall between these two extremes, being partially self-correlated. Both the degree of correlation and the relative amplitude of the signal to the contaminating noise amplitude, or the signal-to-noise ratio (SNR), will further affect the bias errors.

The bias errors vary with frequency. The traditional method has an upper frequency limit—known as the spatial Nyquist frequency f_N, which is the frequency at which the microphone spacing is equal to ½ of a wavelength—above which intensity results are not considered valid.[18] The PAGE method can be used above f_N for broadband signals with the use of phase unwrapping.[12] Though frequencies above f_N are not discussed in this paper, the equations for the bias errors for the PAGE method—with a broadband source and broadband noise—remain valid up to frequencies at which probe scattering effects must be taken into account, so long as phase unwrapping can be performed correctly. When phase values do not exhibit jumps of more than π radians between frequency bins, phase unwrapping is trivial. For narrowband sources, low-level additive broadband noise can actually improve estimation of intensity above f_N with the PAGE method, so long as certain conditions are met; these results will be presented in a forthcoming paper, as only frequencies below f_N are investigated herein.

The remainder of this paper addresses the effects of extraneous noise on the bias errors from the calculation of active intensity using the traditional and PAGE methods. Section 2.3 of this paper deals with uncorrelated noise using a five-microphone orthogonal probe, pictured in Fig. 2.1. This probe was chosen as it has a center microphone to directly measure the pressure, as well as two pairs of orthogonally positioned microphones, which can be used to test for symmetry. For this probe, f_N is reached when $ka = \pi$, where k is the wavenumber and a is the microphone probe radius. Section 2.4 deals with self-correlated or plane-wave-like (directional constant-amplitude) noise with the same probe geometry. Different probe geometries are discussed in Section 2.5 in regards to both correlated and uncorrelated noise. The reason for using a as the probe radius rather than simply the microphone spacing is for comparison of different probe geometries with the same

overall probe dimensions. Equations for all of the cases described can be found in the tables in Section 2.7.

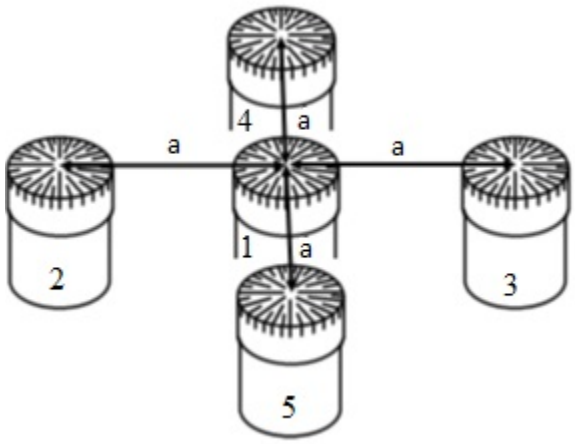

Figure 2.1: A five-microphone orthogonal probe. The microphones are numbered 1 to 5, and in the x-y plane of the probe—where $\hat{x}$ goes from 1 to 3 and $\hat{y}$ goes from 1 to 4—have positions (0,0), (-a,0), (a,0), (0,a), and (0,-a), respectively.

2.3 Bias errors caused by uncorrelated contaminating noise

In the frequency domain, the total complex pressure at microphone μ is obtained by summing the pressure due to the source and the pressure due to the contaminating noise,

$$p_\mu = p_{s_\mu} + p_{n_\mu} = A_{s_\mu} e^{-jk\phi_{s_\mu}} + A_{n_\mu} e^{-jk\phi_{n_\mu}}, \qquad (5)$$

where A is the pressure amplitude, ϕ is the phase, and the subscripts s and n indicate source and contaminating noise, respectively. If the complex pressure due to the contaminating noise exhibits a position-dependent relationship in phase and magnitude—e.g. equal amplitude at each position and phase differences proportional to the distance between microphones—the noise is said to be correlated. When no such relationship exists, the noise is uncorrelated.[20] Some examples of uncorrelated noise are electrical noise in the microphone and data acquisition system or pressures at the level of the noise floor.

Using the pressure measurements from the microphones, the auto-spectral and cross-spectral values—needed to calculate the intensity—can be obtained using the procedure laid out in Section 6.1.3 of Bendat and Piersol[20] as, respectively,

$$G_{\mu\mu} = G_{s_\mu s_\mu} + G_{s_\mu n_\mu} + G_{n_\mu s_\mu} + G_{n_\mu n_\mu}, \tag{6}$$

$$G_{\mu\nu} = G_{s_\mu s_\nu} + G_{s_\mu n_\nu} + G_{n_\mu s_\nu} + G_{n_\mu n_\nu}. \tag{7}$$

Using the ensemble average, the individual terms are given by

$$G_{\mu\nu} = \begin{Bmatrix} p_\mu p_\nu^* & \text{if the signals of } \mu \text{ and } \nu \text{ are correlated} \\ 0 & \text{if the signals of } \mu \text{ and } \nu \text{ are uncorrelated} \end{Bmatrix}. \tag{8}$$

Because the contaminating noise is uncorrelated with the source, all cross terms between the source and contaminating noise are zero. For the cross-spectrum, because the noise is itself uncorrelated at different locations, $G_{n_\mu n_\nu}$ is also zero using ensemble averaging. Though uncorrelated noise does not necessarily exhibit any specific amplitude relationship, it is reasonable to assume—especially for relatively compact probes and well-matched microphones—that the SNR is equal at each microphone position, so $A_{n_\mu} = A_{n_\nu} \equiv A_n$. The auto-spectral and cross-spectral values can then be simplified to give

$$G_{\mu\mu} = A_{s_\mu}^2 + A_n^2, \tag{9}$$

$$G_{\mu\nu} = A_{s_\mu} A_{s_\nu} e^{-jk\left(\phi_{s_\mu} - \phi_{s_\nu}\right)}. \tag{10}$$

2.3.1 Plane-wave source

The first source considered is a plane wave, for which the amplitude at each microphone location is the same, so $A_{s_\mu} = A_{s_\nu} \equiv A_s$. The plane wave propagates with an angle θ_s with respect to the positive x axis or $\hat{x}$, as the probe coordinates in Fig. 2.1 have been defined. This results in auto and cross-spectral values such as

$$G_{11} = \cdots = G_{55} = A_s^2 + A_n^2, \tag{11}$$

$$G_{12} = A_s^2 e^{jka\cos\theta_s}. \tag{12}$$

The analytical result for the intensity caused by a plane wave of amplitude A_s in the absence of contaminating noise is

$$\boldsymbol{I} = \frac{A_s^2}{2\rho_0 c}\cos\theta_s\,\hat{x} + \frac{A_s^2}{2\rho_0 c}\sin\theta_s\,\hat{y} = \frac{A_s^2}{2\rho_0 c}\widehat{\theta_s}, \tag{13}$$

where $c = \omega/k$ is the sound speed.

Using Eq. (*13*), the formulae for calculating the orthogonal components of the intensity bias, $I_{\hat{x}}$ and $I_{\hat{y}}$, can be found in Table 2.5 in Section 2.7 (which also includes other probe configurations, discussed further on). The total bias errors are then given by

$$L_{\epsilon,\boldsymbol{I}} = 10\log_{10}\left(\sqrt{I_{\hat{x}}^2 + I_{\hat{y}}^2}\right) = 5\log_{10}\left(I_{\hat{x}}^2 + I_{\hat{y}}^2\right), \tag{14}$$

$$\theta_{\epsilon,\boldsymbol{I}} = \tan^{-1}\left(\frac{I_{\hat{y}}}{I_{\hat{x}}}\right) - \theta_s. \tag{15}$$

All equations given are complete, but are dependent upon several independent variables. Therefore, in order to present and interpret the results in a concise manner, the absolute value of the bias errors is averaged across all angles of incidence θ_s, and this average bias error is used for the following figures. This averaging allows results to be presented as only a function of ka and SNR, where $\text{SNR} = 10\log_{10}\left(\frac{A_s^2}{A_n^2}\right)$. In many cases this averaging does not have a large effect, though for complete results the equations in the tables in the appendix should be used, rather than just looking at the figures—most notably this averaging can obscure the effect of probe rotation very near a monopole source. It should be noted that for the traditional method, as ka approaches f_N the intensity magnitude is usually underestimated rather than overestimated,[16] so—since the absolute value is used—the bias errors give how much the traditional method under-calculates the intensity. Conversely, contaminating noise usually causes the PAGE method to

calculate a larger value for the intensity than the analytic solution, so the bias errors give this over-calculated value.

Table 2.1: Orthogonal intensity bias components and bias errors for a plane-wave source and uncorrelated noise. Similar equations for other probe geometries are given in Table 2.6.

Plane-wave source uncorrelated noise	Traditional	PAGE
$I_{\hat{x}}$	$\frac{\sin(ka\cos\theta_s)}{ka}$	$\left(1+10^{\frac{-\mathrm{SNR}}{10}}\right)\cos\theta_s$
$I_{\hat{y}}$	$\frac{\sin(ka\sin\theta_s)}{ka}$	$\left(1+10^{\frac{-\mathrm{SNR}}{10}}\right)\sin\theta_s$
$L_{\epsilon,\boldsymbol{I}}$	$5\log_{10}\left(\left(\frac{\sin(ka\cos\theta_s)}{ka}\right)^2+\left(\frac{\sin(ka\sin\theta_s)}{ka}\right)^2\right)$	$10\log_{10}\left(1+10^{\frac{-\mathrm{SNR}}{10}}\right)$
$\theta_{\epsilon,\boldsymbol{I}}$	$\tan^{-1}\left(\frac{\sin(ka\sin\theta_s)}{\sin(ka\cos\theta_s)}\right)-\theta_s$	0

Since the traditional method calculates the intensity using weighted cross-spectra, and since uncorrelated noise terms cancel out in cross-spectral values, the bias errors for the traditional method here are independent of SNR (see Table 2.1). As such—and due to the averaging across all angles of incidence—the magnitude and bias errors are plotted as only a function of ka in Fig. 2.2. Though uncorrelated noise does not affect the bias errors for the traditional method, larger errors are seen for large values of ka (above 0.5), which illustrate the bandwidth limitation of the traditional method.

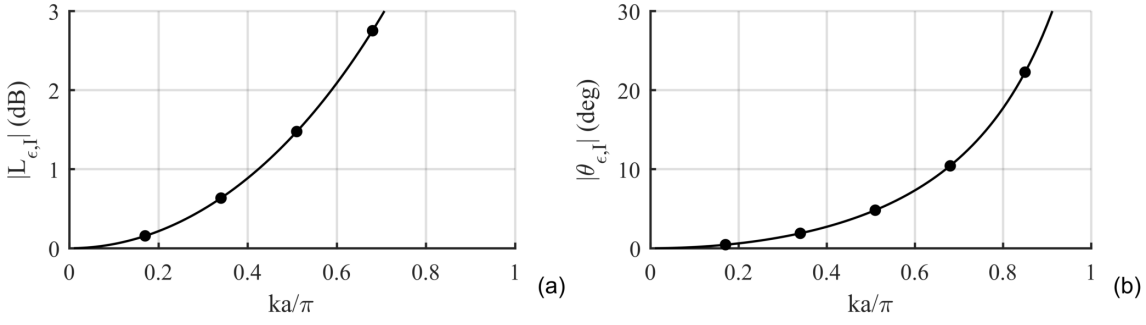

Figure 2.2: Traditional method bias errors in (a) the magnitude and (b) the direction of the active intensity calculated for a plane-wave source with uncorrelated contaminating noise using a five-microphone orthogonal probe. The bias errors are plotted as a function of only ka because the results are independent of SNR and are averaged across all possible angles of incidence.

Unlike the traditional method, the PAGE method calculates intensity using weighted auto-spectra and the arguments of cross-spectra. Because of this, the bias errors depend heavily on the SNR, but are independent of ka when the phase can be unwrapped correctly (see Table 2.1). Note also that the magnitude and angular portions of the bias errors are entirely separable—the magnitude bias depends on the auto-spectral values, while the angular bias depends on cross-spectral values, and the total bias is the product of the two. Additionally, for this case the bias errors are independent of the angle of incidence, so the averaging is redundant. The results are seen in Fig. 2.3, and are plotted as a function of SNR.

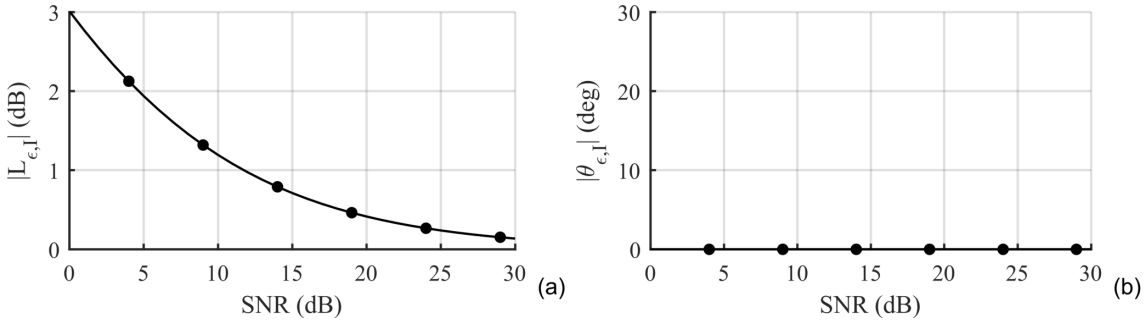

Figure 2.3: PAGE method bias errors in (a) the magnitude and (b) the direction of the active intensity calculated for a plane-wave source with uncorrelated contaminating noise. This method is dependent on SNR but independent of ka. Note the horizontal axis is different than that in Fig. 2.2.

Interestingly, for an incident plane wave and uncorrelated contaminating noise there is no angular bias incurred by using the PAGE method, as seen in Fig. 2.3(b). This accuracy is because the intensity is computed by using the arguments of cross-spectra, for which uncorrelated noise cancels out, and due to the separable nature of the magnitude and angle errors. For a plane-wave source with uncorrelated contaminating noise, the PAGE method computes the direction perfectly regardless of frequency, microphone spacing, SNR, or angle of incidence.

The magnitude bias errors for the PAGE method are very predictable, and depend solely upon SNR, as seen in Fig. 2.3(a). The increase in sound pressure level, and therefore the bias, is singularly dependent on the additional squared pressure due to the contaminating noise. Because of this, there is a doubling of pressure from the noiseless case, or a rise of 3 dB, when the SNR approaches zero.[21] For large SNR values, the magnitude error asymptotically approaches zero as expected.

Because the magnitude bias is so predictable and independent of (the zero-valued) angular bias, a simple correction can be used to scale the PAGE intensity magnitude appropriately using the SNR or the coherence. The coherence between microphone pairs can be calculated using the auto-spectral and cross-spectral values; for the plane-wave source, it is identical for each microphone pair and is

$$\gamma_{\mu\nu}^2 = \frac{\left|G_{\mu\nu}\right|^2}{G_{\mu\mu}G_{\nu\nu}} = \frac{1}{\left(1+\frac{A_n^2}{A_s^2}\right)^2} = \frac{1}{\left(1+10^{-\frac{\mathrm{SNR}}{10}}\right)^2}. \qquad (16)$$

The square root of the coherence is the correction factor needed to account for the presence of the uncorrelated noise:

$$\sqrt{\gamma_{\mu\nu}^2} = \frac{1}{1+10^{-\frac{\mathrm{SNR}}{10}}}. \qquad (17)$$

If this scaling factor is multiplied by the computed intensity before it is converted to a decibel value—or equivalently a corresponding dB value can be subtracted from the computed intensity level—then $L_{\epsilon,\boldsymbol{I}}$ for the PAGE method would be zero for any SNR. Since the magnitude and angular parts are separable, this scaling factor would have no adverse effects on the calculation of the angle. This correction works perfectly for a plane-wave source with contaminating uncorrelated noise, and may be useful for other source and contaminating noise situations;[22-26] this correction is further explored in Section 5.4.1.

With or without correction, the PAGE method computes the correct intensity angle for a plane-wave source with uncorrelated noise, regardless of the values for ka, SNR, or angle of incidence. For low SNR values and very low ka values, the traditional method can better estimate the intensity level; however, the magnitude obtained by the PAGE method can be corrected to obtain zero magnitude error. It is also useful to note that for broadband sources, the results for the PAGE method are the same for frequencies above f_N, with phase unwrapping of the transfer function applied.[12]

2.3.2 Monopole source

For a monopole sound source, the pressure amplitude is inversely proportional to the distance r between the source and the position of interest. By representing the monopole amplitude with the complex magnitude $\tilde{A}$, and letting $A_s^2 = \frac{|\tilde{A}|^2}{r^2}$, the analytical solution is

$$\boldsymbol{I} = \frac{\left|\tilde{A}\right|^2}{2\rho_0 c r^2}\hat{\theta}_s = \frac{A_s^2}{2\rho_0 c}\hat{\theta}_s. \tag{18}$$

The auto-spectral value for microphone 1 and the cross-spectral value between microphone 1 and microphone 2 due to the monopole source with uncorrelated contaminating noise are then

$$G_{11} = \frac{\left|\tilde{A}\right|^2}{r^2} + A_n^2 = A_s^2 + A_n^2, \tag{19}$$

$$G_{12} = \frac{\left|\tilde{A}\right|^2 e^{jka\cos\theta_s}}{r^2 - ra\cos\theta_s} = \frac{A_s^2 e^{jka\cos\theta_s}}{1 - \frac{a}{r}\cos\theta_s} \equiv \frac{A_s^2 e^{jka\cos\theta_s}}{1 - \beta\cos\theta_s}. \tag{20}$$

Similar auto-spectral and cross-spectral expressions can be given for the other microphone pairs. To simplify the results, the variable β is defined such that $\beta \equiv \frac{a}{r} = \frac{ka}{kr}$, which can take on any value between zero and one. In the near field of the monopole, as $\beta \to 1$, the bias errors are

very different from the far field, where $\beta \to 0$ and the solutions converge to those of a plane-wave source. The resulting intensity components are found in Table 2.2.

Table 2.2: Intensity bias error components for a monopole source with uncorrelated noise. The bias errors $L_{\epsilon,\boldsymbol{I}} = 5\,log_{10}\left(I_{\hat{x}}^2 + I_{\hat{y}}^2\right)$ and $\theta_{\epsilon,\boldsymbol{I}} = tan^{-1}\left(\frac{I_{\hat{y}}}{I_{\hat{x}}}\right) - \theta_s$ are not given explicitly here since they do not easily simplify. Equations for other probe geometries are given in Table 2.7.

Monopole source uncorrelated noise	Traditional	PAGE
$I_{\hat{x}}$	$\frac{\sin\left(kr-kr\sqrt{1-2\beta\cos\theta_s+\beta^2}\right)}{2ka\sqrt{1-2\beta\cos\theta_s+\beta^2}} - \frac{\sin\left(kr-kr\sqrt{1+2\beta\cos\theta_s+\beta^2}\right)}{2ka\sqrt{1+2\beta\cos\theta_s+\beta^2}}$	$\left(1+10^{\frac{-\text{SNR}}{10}}\right)\left(\frac{1}{2\beta}\sqrt{1+2\beta\cos\theta_s+\beta^2} - \frac{1}{2\beta}\sqrt{1-2\beta\cos\theta_s+\beta^2}\right)$
$I_{\hat{y}}$	$\frac{\sin\left(kr-kr\sqrt{1-2\beta\sin\theta_s+\beta^2}\right)}{2ka\sqrt{1-2\beta\sin\theta_s+\beta^2}} - \frac{\sin\left(kr-kr\sqrt{1+2\beta\sin\theta_s+\beta^2}\right)}{2ka\sqrt{1+2\beta\sin\theta_s+\beta^2}}$	$\left(1+10^{\frac{-\text{SNR}}{10}}\right)\left(\frac{1}{2\beta}\sqrt{1+2\beta\sin\theta_s+\beta^2} - \frac{1}{2\beta}\sqrt{1-2\beta\sin\theta_s+\beta^2}\right)$

The meaning of the SNR for a monopole source is slightly different than that for a plane-wave source, since the SNR depends on the distance between a monopole source and the probe. This means that the SNR for the monopole source is the SNR at the probe location. For the monopole source, $\text{SNR} = 10\log_{10}\left(\frac{A_s^2}{A_n^2}\right) = 10\log_{10}\left(\frac{|\tilde{A}|^2}{r^2 A_n^2}\right)$, which is dependent on r. This means that if the probe were to physically be moved away from the source, the source amplitude would have to be increased—or the noise amplitude would need to be decreased—to maintain the same signal-to-noise ratio. In practice since the source amplitude is rarely known, the SNR is usually defined at a given location.

For the monopole source with uncorrelated noise, the traditional method is still independent of SNR, and therefore identical to the noiseless case presented previously by Whiting et al. (2017).[8] As the value of β decreases, the bias errors no longer increase monotonically, which can be seen in Fig. 2.4. The magnitude bias is greater for small values of ka (below about 0.5), beyond even

3 dB when $\beta \to 1$. Interestingly, the increase caused by larger ka values appear later than for the plane-wave source; for some intermediate values of ka the total bias actually decreases. The trends for the angular bias are the same, with an angular bias of nearly 10° for small ka values (below 0.5) as $\beta \to 1$; see Fig. 2.4(b).

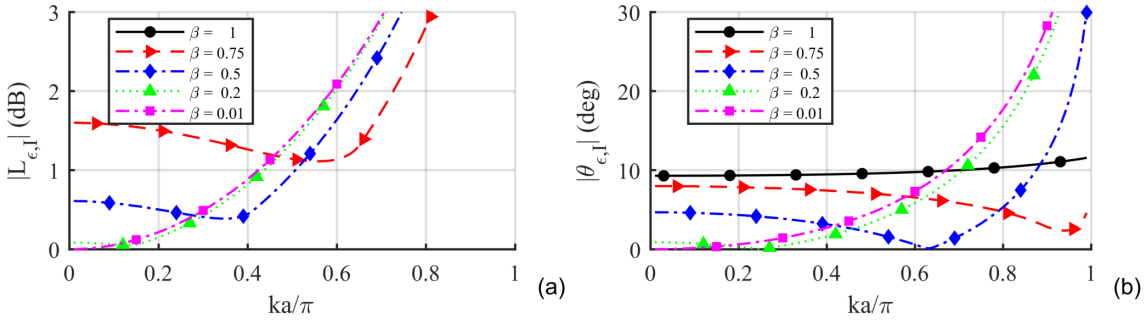

Figure 2.4: Traditional method bias errors in (a) the magnitude and (b) the direction of the active intensity calculated for a monopole source with uncorrelated contaminating noise using a five-microphone orthogonal probe. Results are averaged across angle of incidence. In (a) the bias errors for $\beta = 1$ are greater than 3 dB for all values of ka.

For the PAGE method, the bias errors for the monopole source are still independent of ka but must be averaged across the angle of incidence as is done with the traditional method. The angular error is constant over SNR as in the plane-wave case, though non-zero; as $\beta \to 1$ the angular error approaches approximately 2°, as seen in Fig. 2.5(b). For small SNR values (less than about 10 dB), the PAGE method intensity magnitude errors are actually decreased slightly as β increases, seen in Fig. 2.5(a). For higher SNR values (above 10 dB), however, these errors are increased slightly—this is a product of averaging across all angle of incidence. As $\beta \to 1$, the actual bias errors can show a large variance across angle of incidence. For a more complete representation, the equations in Table 2.7 should be used. Generally, biases are larger for $\theta_s \approx 0°$ than for $\theta_s \approx 45°$.

Moving close to a monopole source has a greater effect on the traditional method than it does on the PAGE method. The PAGE method is again better for computing the intensity angle, though is not perfect and can be offset by about 2°. The magnitude offset from the plane-wave case is within about 0.7 dB for all SNR values. For the traditional method at low ka values, the magnitude can be offset by more than 3 dB, and the angular offset can be near 10°.

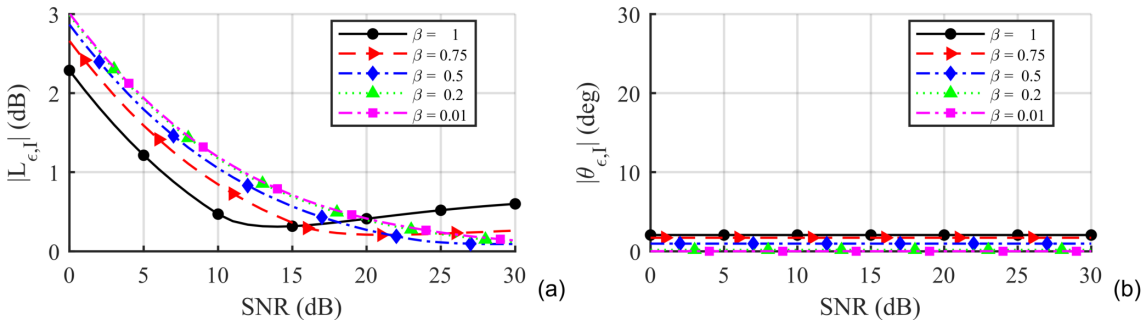

Figure 2.5: PAGE method bias errors in (a) the magnitude and (b) the direction of the active intensity calculated for a monopole source with uncorrelated contaminating noise using a five-microphone orthogonal probe, averaged across angle of incidence.

2.4 Bias errors caused by self-correlated noise

Turning now to self-correlated noise, which is still assumed to be uncorrelated with the source, the problem becomes more complicated. Assuming the contaminating noise source is not close to the probe (within a few wavelengths), the noise can be assumed to be plane-wave-like (directional, amplitude-constant) in nature. However, this plane-wave noise comes from a specific direction θ_n and can have a very large impact on bias errors. This additional variable is not a problem when dealing with equations, though it does create additional difficulties when trying to illustrate results. Objectively averaging across possible noise directions is not possible. Instead, an angular separation θ_{sep} between the source and noise directions can be defined such that $\theta_{\text{sep}} =$

$|\theta_s - \theta_n| \leq 180°$. Results can then be averaged across the angle of incidence to obtain the bias errors as a function of ka, SNR, and angular separation.

As now shown for both plane-wave and monopole sources, the traditional method is most sensitive to the value of ka and the PAGE method is most dependent on the SNR. However, neither is completely independent of the other variable, and both depend heavily on the separation angle.

2.4.1 Plane-wave source

For an incident plane-wave source of interest and contaminating plane-wave noise—uncorrelated with the source—the more complicated impact of correlated noise is immediately apparent from the equations in Table 2.3. There are more independent variables, and the angular and magnitude portions are now entangled for both methods. Figures for the bias errors are presented, but can only capture a portion of the big picture.

Table 2.3: Intensity components for a plane-wave source with correlated noise. The total bias errors for magnitude and direction are $L_{\epsilon,\boldsymbol{I}} = 5\,log_{10}\left(I_{\hat{x}}^2 + I_{\hat{y}}^2\right)$ *and* $\theta_{\epsilon,\boldsymbol{I}} = tan^{-1}\left(\frac{I_{\hat{y}}}{I_{\hat{x}}}\right) - \theta_s$. *Equations for other probe geometries are given in Table 2.9.*

Plane-wave source correlated noise	Traditional	PAGE
$I_{\hat{x}}$	$\frac{\frac{\sin(ka\cos\theta_s)}{ka}}{10^{\frac{-\text{SNR}}{10}}\frac{\sin(ka\cos\theta_n)}{ka}}$	$\left(1+10^{\frac{-\text{SNR}}{10}}\right)\frac{1}{2ka}\arg\left\{e^{2jka\cos\theta_s}+10^{\frac{-\text{SNR}}{10}}e^{2jka\cos\theta_n}\right\}$
$I_{\hat{y}}$	$\frac{\frac{\sin(ka\sin\theta_s)}{ka}}{10^{\frac{-\text{SNR}}{10}}\frac{\sin(ka\sin\theta_n)}{ka}}$	$\left(1+10^{\frac{-\text{SNR}}{10}}\right)\frac{1}{2ka}\arg\left\{e^{2jka\sin\theta_s}+10^{\frac{-\text{SNR}}{10}}e^{2jka\sin\theta_n}\right\}$

The traditional method is not very adept at dealing with correlated noise. Fig. 2.6(a) shows the bias errors as a function of separation angle θ_{sep} and ka value for a few representative SNR values. With a large SNR, the expected errors for large ka values are easily seen. With lower SNR values, there is a tradeoff between magnitude and angular accuracy as the separation angle

changes. For $\theta_{\text{sep}} \approx 0°$ there is no angular error—again for small ka values (less than 0.5) only—but a large magnitude error. For larger separation angles, the magnitude is more accurately calculated, while the angular error is larger. For large values of ka both the magnitude and angular errors are extreme.

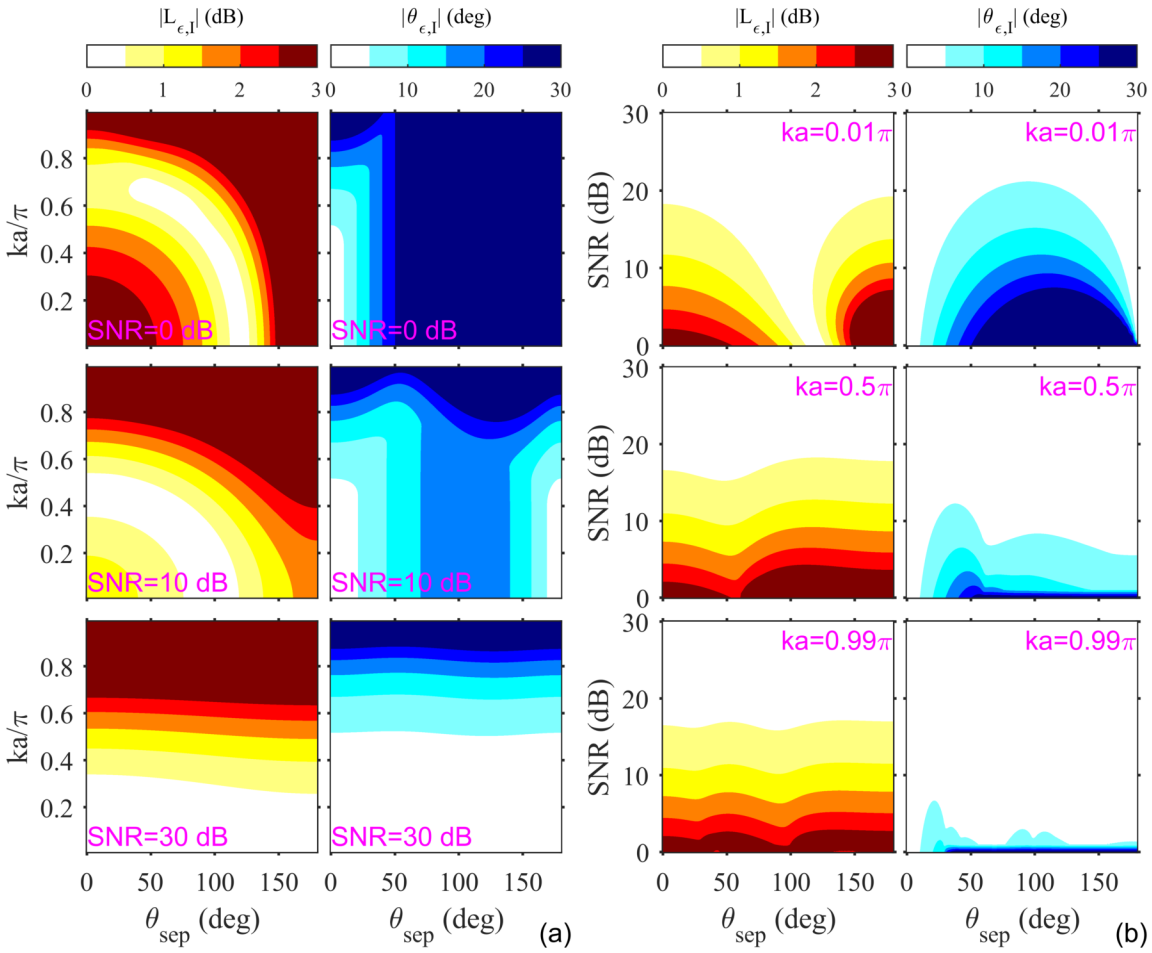

Figure 2.6: Bias errors for a plane-wave source with contaminating correlated noise using (a) the traditional method and (b) the PAGE method.

The PAGE method does not cause any bias error whenever the SNR exceeds about 20 dB, as shown in Fig. 2.6(b). For lower SNR values the direction can still be computed fairly accurately, most especially when there is enough phase information to obtain the correct phase gradient, i.e. for larger values of ka. The magnitude errors are a bit more complicated. For low values of ka

there is more dependence on the separation angle than there is for larger values of ka. For any given separation angle, the magnitude and angular calculation is better for a larger SNR value, as seen in Fig. 2.6(b).

The PAGE method is less dependent on separation angle than the traditional method. For low ka values and low SNR values (SNR near zero), both methods show similar errors. However, for the plane-wave source with plane-wave noise, the PAGE method outperforms the traditional method as either ka increases or, most especially, as the SNR increases.

2.4.2 Monopole source

Results are again separated for the monopole source based upon the value of β, as done in Section 2.3. For the sake of brevity, results for only two values of β are portrayed—one near the source and the other as close to the monopole source as possible—in Fig. 2.7 and Fig. 2.8, while the intensity values are given in Table 2.4. As $\beta \to 0$, the monopole source errors approach those of the plane-wave source.

Table 2.4: Intensity components for a monopole source with uncorrelated noise. The total bias errors are $L_{\epsilon,\boldsymbol{I}} = 10\,log_{10}\left(\sqrt{I_{\hat{x}}^2 + I_{\hat{y}}^2}\right)$ *and* $\theta_{\epsilon,\boldsymbol{I}} = tan^{-1}\left(\frac{I_{\hat{y}}}{I_{\hat{x}}}\right) - \theta_s$. *Equations for other probe geometries are given in Table 2.9.*

Monopole source correlated noise	Traditional	PAGE
$I_{\hat{x}}$	$\frac{\sin\left(kr-kr\sqrt{1-2\beta\cos\theta_s+\beta^2}\right)}{2ka\sqrt{1-2\beta\cos\theta_s+\beta^2}} - \frac{\sin\left(kr-kr\sqrt{1+2\beta\cos\theta_s+\beta^2}\right)}{2ka\sqrt{1+2\beta\cos\theta_s+\beta^2}} + 10^{\frac{-\text{SNR}}{10}}\frac{\sin(ka\cos\theta_n)}{ka}$	$\left(1+10^{\frac{-\text{SNR}}{10}}\right)\frac{1}{2ka} * \arg\left\{e^{jkr\left(\sqrt{1+2\beta\cos\theta_s+\beta^2}-\sqrt{1-2\beta\cos\theta_s+\beta^2}\right)} + 10^{\frac{-\text{SNR}}{10}}\sqrt{1-2\beta^2\cos 2\theta_s+\beta^4}e^{2jka\cos\theta_n}\right\}$
$I_{\hat{y}}$	$\frac{\sin\left(kr-kr\sqrt{1-2\beta\sin\theta_s+\beta^2}\right)}{2ka\sqrt{1-2\beta\sin\theta_s+\beta^2}} - \frac{\sin\left(kr-kr\sqrt{1+2\beta\sin\theta_s+\beta^2}\right)}{2ka\sqrt{1+2\beta\sin\theta_s+\beta^2}} + 10^{\frac{-\text{SNR}}{10}}\frac{\sin(ka\sin\theta_n)}{ka}$	$\left(1+10^{\frac{-\text{SNR}}{10}}\right)\frac{1}{2ka} * \arg\left\{e^{jkr\left(\sqrt{1+2\beta\sin\theta_s+\beta^2}-\sqrt{1-2\beta\sin\theta_s+\beta^2}\right)} + 10^{\frac{-\text{SNR}}{10}}\sqrt{1+2\beta^2\cos 2\theta_s+\beta^4}e^{2jka\sin\theta_n}\right\}$

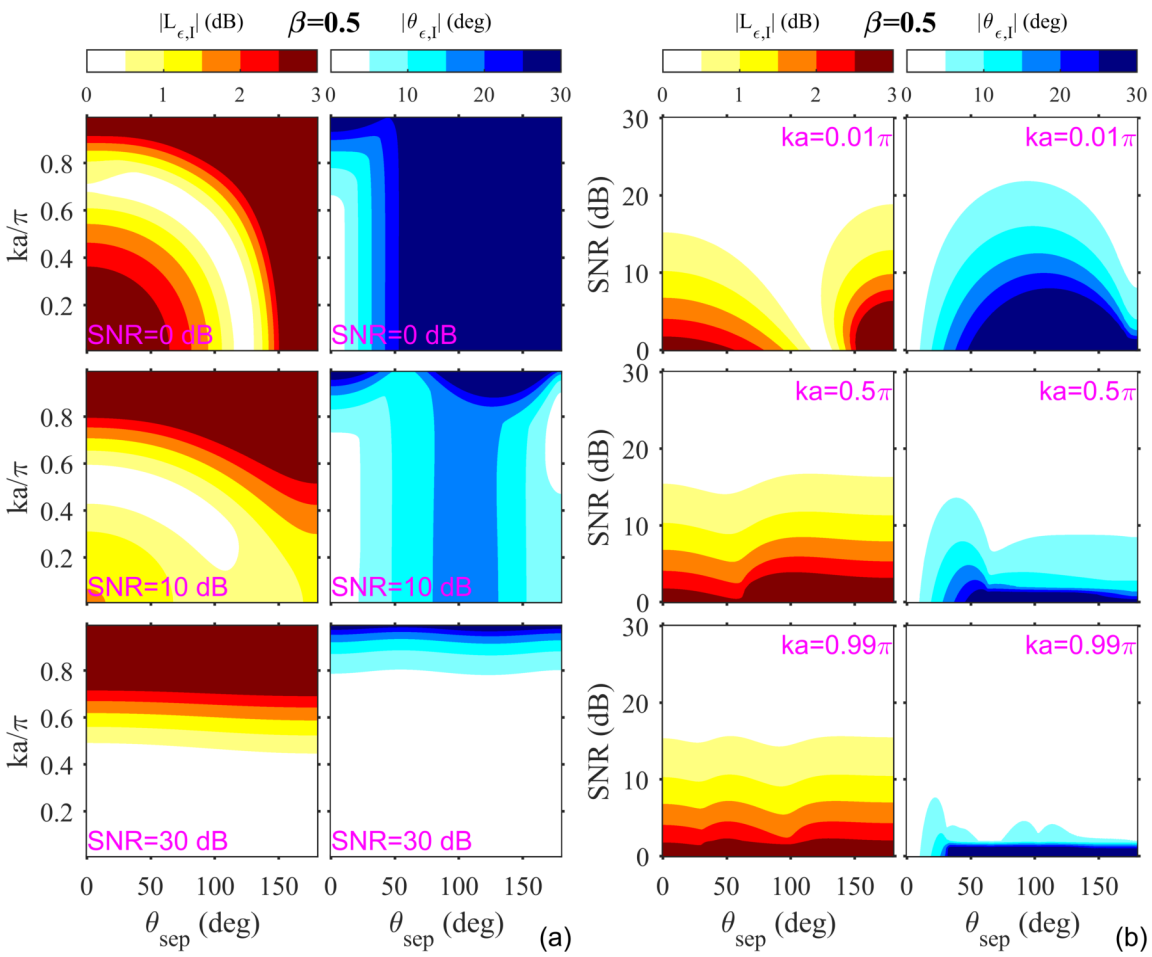

Figure 2.7: Bias errors for a monopole source located a distance $r = 2a$ $\left(\beta = \frac{ka}{kr} = 0.5\right)$ *from the probe center with contaminating correlated noise using (a) the traditional method and (b) the PAGE method.*

Both methods are seen to exhibit significant errors in the near field (as $\beta \to 1$) of a monopole with plane-wave noise. The PAGE method is better at computing the magnitude for all but the lowest SNR values, below a value of around 10 dB, depending on the separation angle. As $\beta \to 1$, the PAGE method clearly outperforms the traditional method for positive SNR values.

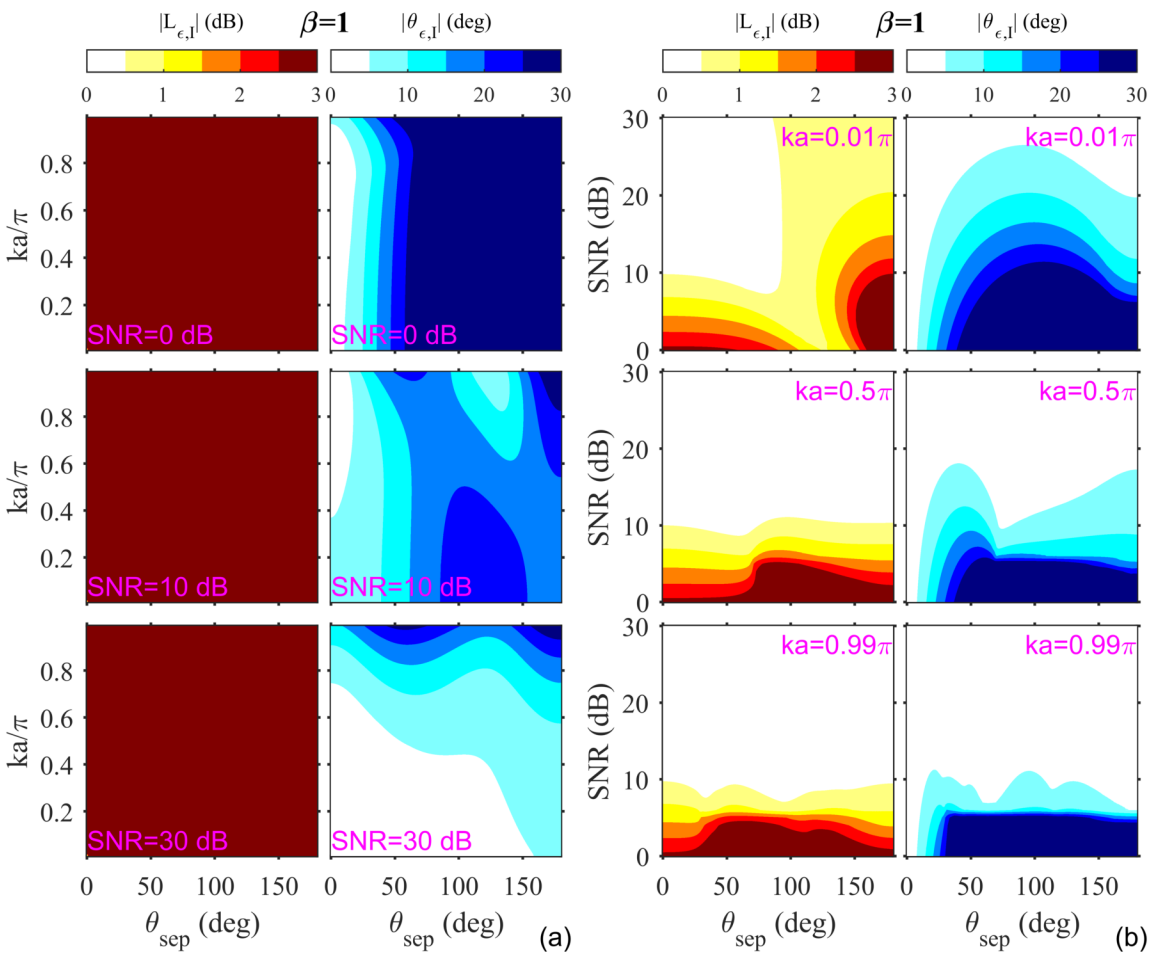

Figure 2.8: Bias errors for a monopole source located a distance $r = a$ $\left(\beta = \frac{ka}{kr} = 1\right)$ *from the probe center with contaminating correlated noise using (a) the traditional method and (b) the PAGE method.*

In terms of angular error, both methods behave similarly for small values of ka (below 0.5) and small SNR values. For an SNR above about 10 dB the bias errors for the PAGE method are much smaller than those for the traditional method, regardless of the value of ka. The PAGE method can perform better at higher ka values because the phase gradient can be calculated more accurately—even with noise present. For small values of ka, even small amounts of noise can lead to an inaccurate phase gradient calculation.

2.5 The effects of probe geometry

Previous results were given for a specific five-microphone orthogonal probe geometry, since the probe symmetry with orthogonal pairs made the equations for the bias errors relatively simple. However, different probes can be used to calculate intensity, and each probe can estimate the pressure gradient—or the central pressure when there is no microphone in the center—differently, leading to different bias errors. Two other two-dimensional probe geometries, for which noiseless bias errors were previously investigated,[8] are considered herein.

By removing the center microphone from the probe seen in Fig. 2.1, the four-microphone orthogonal probe seen in Fig. 2.9(a) can be obtained. The bias errors obtained can differ largely from the results seen in the previous sections, while in other cases are exactly the same. The main reason for the differences is that instead of obtaining the pressure at the center microphone directly, an average must be computed to obtain the approximate pressure at the probe center. When the pressure does not vary rapidly, this averaging does not cause significant adverse effects, but near a monopole source the differences can be drastic. Additionally, when using the traditional method, the effective microphone spacing is now twice what it was for the five microphone probe, so f_N is now reached at $ka = \frac{\pi}{2}$ instead of $ka = \pi$. Note that the effective doubling in microphone spacing for this probe is simply a result of not having a center microphone—the probe radius is still the same.

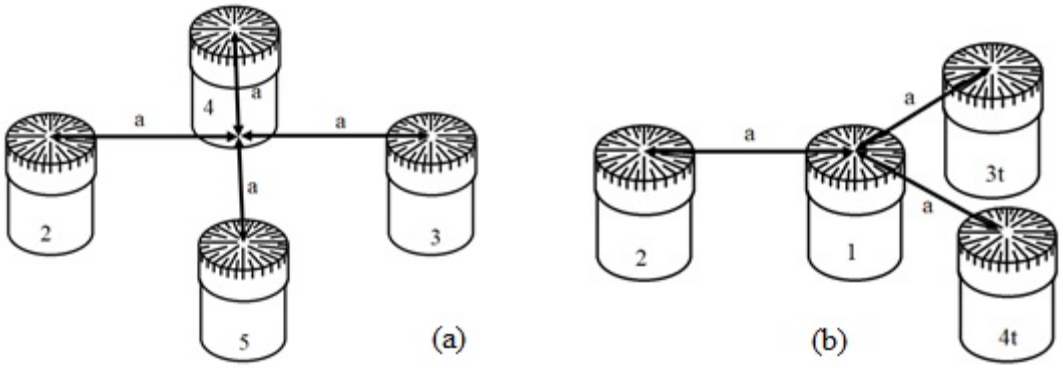

Figure 2.9: Two alternate probe geometries that can be used to calculate intensity. The four-microphone orthogonal probe (a) is referred to as 4_O and the four-microphone triangular probe (b) is referred to as 4_T. The five-microphone orthogonal probe in Fig. 2.1 is referred to as 5_O. Note there is no microphone 1 for 4_O, and are numbered 2 through 5 to match the numbering for 5_O.

The third probe of interest consists of a center microphone surrounded by three microphones in an equilateral triangle configuration, each separated from the center microphone by a distance a. Since there is a center microphone, this probe generally works better than the four microphone orthogonal probe. For the sake of brevity, only the most significant differences caused by probe geometry are presented. The five microphone probe will hereafter be referred to as 5_O, the four microphone orthogonal probe as 4_O, and the four microphone triangular probe as 4_T.

2.5.1 Uncorrelated noise

For the traditional method, 4_O and 5_O perform similarly with two noted differences (which can be seen in Fig. 2.10). First, since 4_O has effectively double the microphone spacing of 5_O, the bias errors are reached at ½ the value of ka. Second, very near a monopole source, 4_O must estimate the center pressure, yielding larger errors.

Using the traditional method with a plane-wave source, 4_T is identical to 5_O in calculating the magnitude, but can better calculate the intensity direction, seen in Fig. 2.10(a). Near a

monopole source, 4_T is worse at calculating both the direction and magnitude of the intensity, seen in Fig. 2.10(b) and Fig. 2.10(c). This is due to the effective microphone spacing in orthogonal directions being $3a/2$ and $\sqrt{3}a/2$, so the random incidence average shows great variability. As $\beta \to 1$, when the probe is as close to the source as possible, the bias errors all exceed 3 dB with large angular errors.

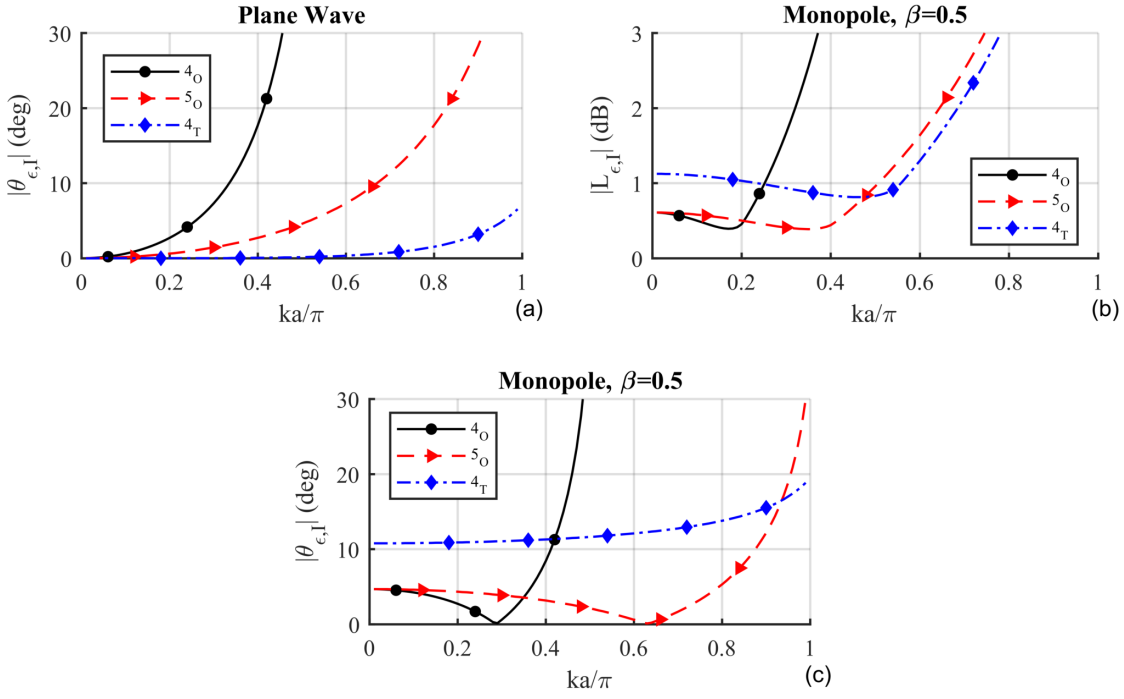

Figure 2.10: Bias errors for different probe geometries with contaminating uncorrelated noise using the traditional method. Only cases where the different probe geometries exhibit marked differences are pictured. The angular error for a plane wave source with uncorrelated noise is given in (a), while (b) shows the magnitude error and (c) shows the angular error for a monopole source.

For the PAGE method, the results for each probe configuration are exactly the same for a plane-wave source with uncorrelated noise, and so are not shown. In the near field of a monopole ($\beta \approx 1$), however, the probes give noticeably different results. Probe 5_O is much better at estimating the angle. This improvement results from having four microphones to calculate the angle with another mic at the center, while 4_T has only three for the angle. Probe 4_O has to estimate

the center pressure, making it the least effective of the three probe geometries at calculating the intensity direction. In regards to magnitude, 4_O is very inaccurate, again due to the lack of a direct center pressure measurement. Whether the bias errors for 4_T are less than or greater than those for 5_O depends on the value of β and the SNR. These results can be seen in Fig. 2.11. Again note that for $\beta \approx 1$, averaging across angle of incidence provides an incomplete representation. Biases are larger for $\theta_s \approx 0°$ than for $\theta_s \approx 45°$.

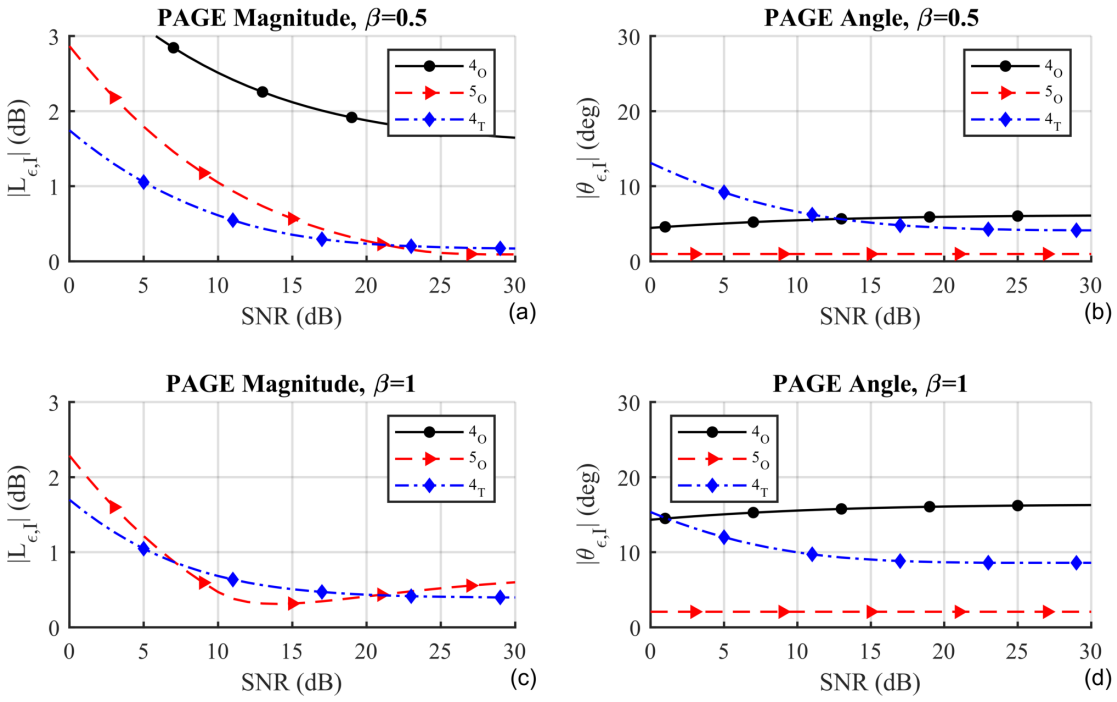

Figure 2.11: Probe comparison of bias errors for a monopole source at two distances ($\beta = 0.5$ and $\beta = 1$) with contaminating uncorrelated noise using the PAGE method. Both magnitude and direction errors are shown for both cases. In (c) the bias errors for 4_O are greater than 3 dB for all SNR values below 30 dB.

2.5.2 Correlated noise

To avoid using a large number of two-dimensional plots to compare probe geometries, figures are not presented in this section; rather, simple conclusions are stated. See the tables in the appendix for further comparison of bias errors for the different probe geometries.

With the traditional method, 4_O and 5_O have essentially identical bias errors except for very near the monopole source, when the difference in microphone spacing is accounted for. 4_T is worse at calculating the angle for large values of θ_{sep}, though the errors caused by high values of ka appear later than for the other probes, and the magnitude estimation can be slightly better. Near a monopole source, all probes exhibit large magnitude errors, while the angular error varies rapidly with SNR and ka for each probe configuration.

For the PAGE method, the same general trends hold for correlated noise as for uncorrelated noise. For a plane-wave source, each probe performs the same. Near a monopole source, 4_O exhibits greater errors than those for 5_O, which again is a result of estimating the center pressure. In regards to the effects of separation angle, larger values of ka are again less affected while lower values can show marked differences. For SNR values greater than 20 dB the bias errors are extremely low, though some errors are obtained in the extreme monopole near field, most notably for 4_O, in which case either 4_T or 5_O performs better, depending on β and the SNR.

2.6 Conclusions

Contaminating noise can have a great impact on the calculation of active acoustic intensity. The differences in how the traditional method and the PAGE method calculate the intensity lead to different intensity results. The PAGE method is nearly always better at computing the intensity direction, regardless of the source properties or noise type. This is because it uses the phase values of cross-spectra, and the magnitude and phase portions are separable for plane wave signals, while for monopole sources the magnitude and phase portions are somewhat loosely intertwined. Any time the SNR exceeds about 20 dB, the bias errors using the PAGE method are small in comparison to the traditional method. In regards to magnitude, it is possible to correct for the extra measured

pressure caused by uncorrelated contaminating noise; this is further investigated in Chapter 5. Near a monopole source, 5_O is the probe with the least bias in most cases, though for some situations 4_T can work better, depending on the exact values of β and the SNR. For plane-wave sources, each probe configuration is essentially the same.

The main problem with the traditional method is its bandwidth limitation. For any large values of ka (above 0.5) the bias errors are never insignificant. The magnitude and angular biases are invariably intertwined. In some cases, the magnitude and angular inaccuracies can cancel to cause smaller biases, though this is a complicated interaction. For small values of ka (less than 0.5) with small SNR values (below 10-15 dB), the traditional method can sometimes better calculate the intensity magnitude. The probe that performs most consistently is 5_O, though depending on the situation either of the other probes can be more efficient.

Small SNR values (below 10 dB) can have adverse effects on the calculation of the PAGE method, though it is possible to correct for this, especially when the contaminating noise is uncorrelated (see Chapter 5). Angularly separated signals do not impact the PAGE method as much as the traditional method, especially for higher ka values. Whenever large values of ka are of interest (above 0.5), or when the SNR exceeds about 20 dB, the PAGE method gives more reliable results than the traditional method.

2.7 Chapter 2 Appendix

Equation tables are included herein. Table 2.5 gives the equations for how the orthogonal components of the intensity bias errors, $I_{\hat{x}}$ and $I_{\hat{y}}$, are calculated for the different probe configurations, using the auto-spectral and cross-spectral values. The following tables give the simplified intensity bias components for plane-wave and monopole sources with uncorrelated and

self-correlated contaminating noise. In each case, perfect calculation would yield $I_{\hat{x}} = \cos\theta_s$ and $I_{\hat{y}} = \sin\theta_s$. The magnitude and angular biases are given by $L_{\epsilon,\boldsymbol{I}} = 10\log_{10}\left(\sqrt{I_{\hat{x}}^2 + I_{\hat{y}}^2}\right) = 5\log_{10}\left(I_{\hat{x}}^2 + I_{\hat{y}}^2\right)$ and $\theta_{\epsilon,\boldsymbol{I}} = \tan^{-1}\left(\frac{I_{\hat{y}}}{I_{\hat{x}}}\right) - \theta_s$.

Table 2.5: The analytical expressions for intensity bias given in orthogonal directions. Note the arguments of cross-spectra are used, though the arguments of the transfer functions are equivalent (since they differ by a factor of auto-spectra, which are always real and so do not alter the argument).

Calculated intensity bias error components			
4 mic orthogonal	$I_{\hat{x}}$	Trad	$-\frac{Im\{G_{23}\}}{2kaA_S^2}$
		PAGE	$-\frac{\left(\sqrt{G_{22}}+\sqrt{G_{33}}\right)^2 \arg\{G_{23}\}}{8kaA_S^2}$
	$I_{\hat{y}}$	Trad	$\frac{Im\{G_{45}\}}{2kaA_S^2}$
		PAGE	$\frac{\left(\sqrt{G_{44}}+\sqrt{G_{55}}\right)^2 \arg\{G_{45}\}}{8kaA_S^2}$
5 mic orthogonal	$I_{\hat{x}}$	Trad	$\frac{Im\{G_{12}\}-Im\{G_{13}\}}{2kaA_S^2}$
		PAGE	$-\frac{G_{11}\arg\{G_{23}\}}{2kaA_S^2}$
	$I_{\hat{y}}$	Trad	$-\frac{Im\{G_{14}\}-Im\{G_{15}\}}{2kaA_S^2}$
		PAGE	$\frac{G_{11}\arg\{G_{45}\}}{2kaA_S^2}$
4 mic triangular	$I_{\hat{x}}$	Trad	$-\frac{Im\{G_{13t}+G_{14t}-2G_{12}\}}{3kaA_S^2}$
		PAGE	$-\frac{G_{11}(\arg\{G_{24t}\}+\arg\{G_{23t}\})}{3kaA_S^2}$
	$I_{\hat{y}}$	Trad	$\frac{Im\{G_{14t}-G_{13t}\}}{\sqrt{3}kaA_S^2}$
		PAGE	$\frac{G_{11}\arg\{G_{3t4t}\}}{\sqrt{3}kaA_S^2}$

Table 2.6: Intensity bias error components for a plane-wave source with contaminating uncorrelated noise.

Plane-wave source, uncorrelated noise			
4 mic orthogonal	$I_{\hat{x}}$	Trad	$\frac{\sin(2ka\cos\theta_s)}{2ka}$
		PAGE	$\left(1+10^{\frac{-\mathrm{SNR}}{10}}\right)\cos\theta_s$
	$I_{\hat{y}}$	Trad	$\frac{\sin(2ka\sin\theta_s)}{2ka}$
		PAGE	$\left(1+10^{\frac{-\mathrm{SNR}}{10}}\right)\sin\theta_s$
5 mic orthogonal	$I_{\hat{x}}$	Trad	$\frac{\sin(ka\cos\theta_s)}{ka}$
		PAGE	$\left(1+10^{\frac{-\mathrm{SNR}}{10}}\right)\cos\theta_s$
	$I_{\hat{y}}$	Trad	$\frac{\sin(ka\sin\theta_s)}{ka}$

Plane-wave source, uncorrelated noise			
		PAGE	$\left(1+10^{\frac{-\mathrm{SNR}}{10}}\right)\sin\theta_s$
4 mic triangular	$I_{\hat{x}}$	Trad	$\frac{\sin\left(\frac{1}{2}ka\cos\theta_s\right)\cos\left(\frac{\sqrt{3}}{2}ka\sin\theta_s\right)+\sin(ka\cos\theta_s)}{\frac{3}{2}ka}$
		PAGE	$\left(1+10^{\frac{-\mathrm{SNR}}{10}}\right)\cos\theta_s$
	$I_{\hat{y}}$	Trad	$\frac{\cos\left(\frac{1}{2}ka\cos\theta_s\right)\sin\left(\frac{\sqrt{3}}{2}ka\sin\theta_s\right)}{\frac{\sqrt{3}}{2}ka}$
		PAGE	$\left(1+10^{\frac{-\mathrm{SNR}}{10}}\right)\sin\theta_s$

Table 2.7: Intensity bias error components for a monopole source with contaminating uncorrelated noise.

Monopole source, uncorrelated noise			
4 mic orthogonal	$I_{\hat{x}}$	Trad	$\frac{\sin\left(kr\sqrt{1+2\beta\cos\theta_s+\beta^2}-kr\sqrt{1-2\beta\cos\theta_s+\beta^2}\right)}{2ka\sqrt{1-2\beta^2\cos 2\theta_s+\beta^4}}$
		PAGE	$\left(\frac{1}{2}\sqrt{\frac{1}{1-2\beta\cos\theta_s+\beta^2}+10^{\frac{-\mathrm{SNR}}{10}}}+\frac{1}{2}\sqrt{\frac{1}{1+2\beta\cos\theta_s+\beta^2}+10^{\frac{-\mathrm{SNR}}{10}}}\right)^2\left(\frac{1}{2\beta}\sqrt{1+2\beta\cos\theta_s+\beta^2}-\frac{1}{2\beta}\sqrt{1-2\beta\cos\theta_s+\beta^2}\right)$
	$I_{\hat{y}}$	Trad	$\frac{\sin\left(kr\sqrt{1-2\beta\sin\theta_s+\beta^2}-kr\sqrt{1+2\beta\sin\theta_s+\beta^2}\right)}{2ka\sqrt{1+2\beta^2\cos 2\theta_s+\beta^4}}$
		PAGE	$\left(\frac{1}{2}\sqrt{\frac{1}{1-2\beta\sin\theta_s+\beta^2}+10^{\frac{-\mathrm{SNR}}{10}}}+\frac{1}{2}\sqrt{\frac{1}{1+2\beta\sin\theta_s+\beta^2}+10^{\frac{-\mathrm{SNR}}{10}}}\right)^2\left(\frac{1}{2\beta}\sqrt{1+2\beta\sin\theta_s+\beta^2}-\frac{1}{2\beta}\sqrt{1-2\beta\sin\theta_s+\beta^2}\right)$
5 mic orthogonal	$I_{\hat{x}}$	Trad	$\frac{\sin\left(kr-kr\sqrt{1-2\beta\cos\theta_s+\beta^2}\right)}{2ka\sqrt{1-2\beta\cos\theta_s+\beta^2}}-\frac{\sin\left(kr-kr\sqrt{1+2\beta\cos\theta_s+\beta^2}\right)}{2ka\sqrt{1+2\beta\cos\theta_s+\beta^2}}$
		PAGE	$\left(1+10^{\frac{-\mathrm{SNR}}{10}}\right)\left(\frac{1}{2\beta}\sqrt{1+2\beta\cos\theta_s+\beta^2}-\frac{1}{2\beta}\sqrt{1-2\beta\cos\theta_s+\beta^2}\right)$
	$I_{\hat{y}}$	Trad	$\frac{\sin\left(kr-kr\sqrt{1-2\beta\sin\theta_s+\beta^2}\right)}{2ka\sqrt{1-2\beta\sin\theta_s+\beta^2}}-\frac{\sin\left(kr-kr\sqrt{1+2\beta\sin\theta_s+\beta^2}\right)}{2ka\sqrt{1+2\beta\sin\theta_s+\beta^2}}$
		PAGE	$\left(1+10^{\frac{-\mathrm{SNR}}{10}}\right)\left(\frac{1}{2\beta}\sqrt{1+2\beta\sin\theta_s+\beta^2}-\frac{1}{2\beta}\sqrt{1-2\beta\sin\theta_s+\beta^2}\right)$
4 mic triangular	$I_{\hat{x}}$	Trad	$\frac{\sin\left(kr-kr\sqrt{1-2\beta\cos\theta_s+\beta^2}\right)}{\frac{3}{2}ka\sqrt{1-2\beta\cos\theta_s+\beta^2}}+\frac{\sin\left(\frac{1}{2}ka\cos\theta_s+\frac{\sqrt{3}}{2}ka\sin\theta_s\right)}{3ka+3\beta\left(\frac{1}{2}ka\cos\theta_s+\frac{\sqrt{3}}{2}ka\sin\theta_s\right)}-\frac{\sin\left(\frac{1}{2}ka\cos\theta_s-\frac{\sqrt{3}}{2}ka\sin\theta_s\right)}{3ka+3\beta\left(\frac{1}{2}ka\cos\theta_s-\frac{\sqrt{3}}{2}ka\sin\theta_s\right)}$
		PAGE	$\left(1+10^{\frac{-\mathrm{SNR}}{10}}\right)\left(\frac{1}{3}\cos\theta_s+\frac{2}{3\beta}\left(1-\sqrt{1-2\beta\cos\theta_s+\beta^2}\right)\right)$
	$I_{\hat{y}}$	Trad	$\frac{\sin\left(\frac{1}{2}ka\cos\theta_s+\frac{\sqrt{3}}{2}ka\sin\theta_s\right)}{\sqrt{3}ka+\sqrt{3}\beta\left(\frac{1}{2}ka\cos\theta_s+\frac{\sqrt{3}}{2}ka\sin\theta_s\right)}-\frac{\sin\left(\frac{1}{2}ka\cos\theta_s-\frac{\sqrt{3}}{2}ka\sin\theta_s\right)}{\sqrt{3}ka+\sqrt{3}\beta\left(\frac{1}{2}ka\cos\theta_s-\frac{\sqrt{3}}{2}ka\sin\theta_s\right)}$
		PAGE	$\left(1+10^{\frac{-\mathrm{SNR}}{10}}\right)\sin\theta_s$

Table 2.8: Intensity bias error components for a plane-wave source with contaminating plane-wave noise.

Plane-wave source, plane-wave noise			
4 mic orthogonal	$I_{\hat{x}}$	Trad	$\frac{\sin(2ka\cos\theta_s)}{2ka} + 10^{\frac{-\text{SNR}}{10}}\frac{\sin(2ka\cos\theta_n)}{2ka}$
		PAGE	$\left(1+10^{\frac{-\text{SNR}}{10}}\right)\frac{1}{2ka}\arg\left\{e^{2jka\cos\theta_s}+10^{\frac{-\text{SNR}}{10}}e^{2jka\cos\theta_n}\right\}$
	$I_{\hat{y}}$	Trad	$\frac{\sin(2ka\sin\theta_s)}{2ka} + 10^{\frac{-\text{SNR}}{10}}\frac{\sin(2ka\sin\theta_n)}{2ka}$
		PAGE	$\left(1+10^{\frac{-\text{SNR}}{10}}\right)\frac{1}{2ka}\arg\left\{e^{2jka\sin\theta_s}+10^{\frac{-\text{SNR}}{10}}e^{2jka\sin\theta_n}\right\}$
5 mic orthogonal	$I_{\hat{x}}$	Trad	$\frac{\sin(ka\cos\theta_s)}{ka} + 10^{\frac{-\text{SNR}}{10}}\frac{\sin(ka\cos\theta_n)}{ka}$
		PAGE	$\left(1+10^{\frac{-\text{SNR}}{10}}\right)\frac{1}{2ka}\arg\left\{e^{2jka\cos\theta_s}+10^{\frac{-\text{SNR}}{10}}e^{2jka\cos\theta_n}\right\}$
	$I_{\hat{y}}$	Trad	$\frac{\sin(ka\sin\theta_s)}{ka} + 10^{\frac{-\text{SNR}}{10}}\frac{\sin(ka\sin\theta_n)}{ka}$
		PAGE	$\left(1+10^{\frac{-\text{SNR}}{10}}\right)\frac{1}{2ka}\arg\left\{e^{2jka\sin\theta_s}+10^{\frac{-\text{SNR}}{10}}e^{2jka\sin\theta_n}\right\}$
4 mic triangular	$I_{\hat{x}}$	Trad	$\frac{\sin\left(\frac{1}{2}ka\cos\theta_s\right)\cos\left(\frac{\sqrt{3}}{2}ka\sin\theta_s\right)+\sin(ka\cos\theta_s)}{\frac{3}{2}ka} + 10^{\frac{-\text{SNR}}{10}}\frac{\sin\left(\frac{1}{2}ka\cos\theta_n\right)\cos\left(\frac{\sqrt{3}}{2}ka\sin\theta_n\right)+\sin(ka\cos\theta_n)}{\frac{3}{2}ka}$
		PAGE	$\left(1+10^{\frac{-\text{SNR}}{10}}\right)\left(\frac{1}{3ka}\arg\left\{e^{j\left(\frac{3}{2}ka\cos\theta_s-\frac{\sqrt{3}}{2}ka\sin\theta_s\right)}+10^{\frac{-\text{SNR}}{10}}e^{j\left(\frac{3}{2}ka\cos\theta_n-\frac{\sqrt{3}}{2}ka\sin\theta_n\right)}\right\}+\frac{1}{3ka}\arg\left\{e^{j\left(\frac{3}{2}ka\cos\theta_s+\frac{\sqrt{3}}{2}ka\sin\theta_s\right)}+10^{\frac{-\text{SNR}}{10}}e^{j\left(\frac{3}{2}ka\cos\theta_n+\frac{\sqrt{3}}{2}ka\sin\theta_n\right)}\right\}\right)$
	$I_{\hat{y}}$	Trad	$\frac{\cos\left(\frac{1}{2}ka\cos\theta_s\right)\sin\left(\frac{\sqrt{3}}{2}ka\sin\theta_s\right)}{\frac{\sqrt{3}}{2}ka} + 10^{\frac{-\text{SNR}}{10}}\frac{\cos\left(\frac{1}{2}ka\cos\theta_n\right)\sin\left(\frac{\sqrt{3}}{2}ka\sin\theta_n\right)}{\frac{\sqrt{3}}{2}ka}$
		PAGE	$\left(1+10^{\frac{-\text{SNR}}{10}}\right)\frac{1}{\sqrt{3}ka}\arg\left\{e^{\sqrt{3}jka\sin\theta_s}+10^{\frac{-\text{SNR}}{10}}e^{\sqrt{3}jka\sin\theta_n}\right\}$

Table 2.9: Intensity bias error components for a monopole source with contaminating plane-wave noise.

Monopole source, plane-wave noise			
4 mic orthogonal	$I_{\hat{x}}$	Trad	$\frac{\sin\left(kr\sqrt{1+2\beta\cos\theta_s+\beta^2}-kr\sqrt{1-2\beta\cos\theta_s+\beta^2}\right)}{2ka\sqrt{1-2\beta^2\cos2\theta_s+\beta^4}} + 10^{\frac{-\text{SNR}}{10}}\frac{\sin(2ka\cos\theta_n)}{2ka}$
		PAGE	$\left(\frac{1}{2}\sqrt{\frac{1}{1-2\beta\cos\theta_s+\beta^2}+10^{\frac{-\text{SNR}}{10}}}+\frac{1}{2}\sqrt{\frac{1}{1+2\beta\cos\theta_s+\beta^2}+10^{\frac{-\text{SNR}}{10}}}\right)^2\left(\frac{1}{2ka}\arg\left\{e^{jkr\left(\sqrt{1+2\beta\cos\theta_s+\beta^2}-\sqrt{1-2\beta\cos\theta_s+\beta^2}\right)}+10^{\frac{-\text{SNR}}{10}}\sqrt{1-2\beta^2\cos2\theta_s+\beta^4}e^{2jka\cos\theta_n}\right\}\right)$
	$I_{\hat{y}}$	Trad	$\frac{\sin\left(kr\sqrt{1-2\beta\sin\theta_s+\beta^2}-kr\sqrt{1+2\beta\sin\theta_s+\beta^2}\right)}{2ka\sqrt{1+2\beta^2\cos2\theta_s+\beta^4}} + 10^{\frac{-\text{SNR}}{10}}\frac{\sin(2ka\sin\theta_n)}{2ka}$

Monopole source, plane-wave noise			
		PAGE	$\left(\frac{1}{2}\sqrt{\frac{1}{1-2\beta\sin\theta_s+\beta^2}+10^{\frac{-\mathrm{SNR}}{10}}}+\frac{1}{2}\sqrt{\frac{1}{1+2\beta\sin\theta_s+\beta^2}+10^{\frac{-\mathrm{SNR}}{10}}}\right)^2\left(\frac{1}{2ka}\arg\left\{e^{jkr\left(\sqrt{1+2\beta\sin\theta_s+\beta^2}-\sqrt{1-2\beta\sin\theta_s+\beta^2}\right)}+10^{\frac{-\mathrm{SNR}}{10}}\sqrt{1+2\beta^2\cos 2\theta_s+\beta^4}e^{2jka\sin\theta_n}\right\}\right)$
5 mic orthogonal	$I_{\hat{x}}$	Trad	$\frac{\sin\left(kr-kr\sqrt{1-2\beta\cos\theta_s+\beta^2}\right)}{2ka\sqrt{1-2\beta\cos\theta_s+\beta^2}}-\frac{\sin\left(kr-kr\sqrt{1+2\beta\cos\theta_s+\beta^2}\right)}{2ka\sqrt{1+2\beta\cos\theta_s+\beta^2}}+10^{\frac{-\mathrm{SNR}}{10}}\frac{\sin(ka\cos\theta_n)}{ka}$
		PAGE	$\left(1+10^{\frac{-\mathrm{SNR}}{10}}\right)\left(\frac{1}{2ka}\arg\left\{e^{jkr\left(\sqrt{1+2\beta\cos\theta_s+\beta^2}-\sqrt{1-2\beta\cos\theta_s+\beta^2}\right)}+10^{\frac{-\mathrm{SNR}}{10}}\sqrt{1-2\beta^2\cos 2\theta_s+\beta^4}e^{2jka\cos\theta_n}\right\}\right)$
	$I_{\hat{y}}$	Trad	$\frac{\sin\left(kr-kr\sqrt{1-2\beta\sin\theta_s+\beta^2}\right)}{2ka\sqrt{1-2\beta\sin\theta_s+\beta^2}}-\frac{\sin\left(kr-kr\sqrt{1+2\beta\sin\theta_s+\beta^2}\right)}{2ka\sqrt{1+2\beta\sin\theta_s+\beta^2}}+10^{\frac{-\mathrm{SNR}}{10}}\frac{\sin(ka\sin\theta_n)}{ka}$
		PAGE	$\left(1+10^{\frac{-\mathrm{SNR}}{10}}\right)\left(\frac{1}{2ka}\arg\left\{e^{jkr\left(\sqrt{1+2\beta\sin\theta_s+\beta^2}-\sqrt{1-2\beta\sin\theta_s+\beta^2}\right)}+10^{\frac{-\mathrm{SNR}}{10}}\sqrt{1+2\beta^2\cos 2\theta_s+\beta^4}e^{2jka\sin\theta_n}\right\}\right)$
4 mic triangular	$I_{\hat{x}}$	Trad	$\frac{\sin\left(kr-kr\sqrt{1-2\beta\cos\theta_s+\beta^2}\right)}{\frac{3}{2}ka\sqrt{1-2\beta\cos\theta_s+\beta^2}}+\frac{\sin\left(\frac{1}{2}ka\cos\theta_s+\frac{\sqrt{3}}{2}ka\sin\theta_s\right)}{3ka+3\beta\left(\frac{1}{2}ka\cos\theta_s+\frac{\sqrt{3}}{2}ka\sin\theta_s\right)}-\frac{\sin\left(\frac{1}{2}ka\cos\theta_s-\frac{\sqrt{3}}{2}ka\sin\theta_s\right)}{3ka+3\beta\left(\frac{1}{2}ka\cos\theta_s-\frac{\sqrt{3}}{2}ka\sin\theta_s\right)}+10^{\frac{-\mathrm{SNR}}{10}}\frac{\sin\left(\frac{1}{2}ka\cos\theta_n\right)\cos\left(\frac{\sqrt{3}}{2}ka\sin\theta_n\right)+\sin(ka\cos\theta_n)}{\frac{3}{2}ka}$
		PAGE	$\left(1+10^{\frac{-\mathrm{SNR}}{10}}\right)\left(\frac{1}{3ka}\arg\left\{e^{j\left(kr-kr\sqrt{1-2\beta\cos\theta_s+\beta^2}+\frac{1}{2}ka\cos\theta_s-\frac{\sqrt{3}}{2}ka\sin\theta_s\right)}+10^{\frac{-\mathrm{SNR}}{10}}\sqrt{1-2\beta\cos\theta_s+\beta^2}\left(1+\frac{1}{2}\beta\cos\theta_s-\frac{\sqrt{3}}{2}\beta\sin\theta_s\right)e^{j\left(\frac{3}{2}ka\cos\theta_n-\frac{\sqrt{3}}{2}ka\sin\theta_n\right)}\right\}+\frac{1}{3ka}\arg\left\{e^{j\left(kr-kr\sqrt{1-2\beta\cos\theta_s+\beta^2}+\frac{1}{2}ka\cos\theta_s+\frac{\sqrt{3}}{2}ka\sin\theta_s\right)}+10^{\frac{-\mathrm{SNR}}{10}}\sqrt{1-2\beta\cos\theta_s+\beta^2}\left(1+\frac{1}{2}\beta\cos\theta_s+\frac{\sqrt{3}}{2}\beta\sin\theta_s\right)e^{j\left(\frac{3}{2}ka\cos\theta_n-\frac{\sqrt{3}}{2}ka\sin\theta_n\right)}\right\}\right)$
	$I_{\hat{y}}$	Trad	$\frac{\sin\left(\frac{1}{2}ka\cos\theta_s+\frac{\sqrt{3}}{2}ka\sin\theta_s\right)}{\sqrt{3}ka+\sqrt{3}\beta\left(\frac{1}{2}ka\cos\theta_s+\frac{\sqrt{3}}{2}ka\sin\theta_s\right)}-\frac{\sin\left(\frac{1}{2}ka\cos\theta_s-\frac{\sqrt{3}}{2}ka\sin\theta_s\right)}{\sqrt{3}ka+\sqrt{3}\beta\left(\frac{1}{2}ka\cos\theta_s-\frac{\sqrt{3}}{2}ka\sin\theta_s\right)}+10^{\frac{-\mathrm{SNR}}{10}}\frac{\cos\left(\frac{1}{2}ka\cos\theta_n\right)\sin\left(\frac{\sqrt{3}}{2}ka\sin\theta_n\right)}{\frac{\sqrt{3}}{2}ka}$
		PAGE	$\left(1+10^{\frac{-\mathrm{SNR}}{10}}\right)\left(\frac{1}{\sqrt{3}ka}\arg\left\{e^{\sqrt{3}jka\sin\theta_s}+10^{\frac{-\mathrm{SNR}}{10}}\left(1+\beta\cos\theta_s+\frac{1}{2}\beta^2\cos 2\theta_s-\frac{1}{4}\beta^2\right)e^{\sqrt{3}jka\sin\theta_n}\right\}\right)$

Chapter 3

Bandwidth extension of narrowband intensity calculations using additive, low-level broadband noise

Calculation of acoustic intensity using the phase and amplitude gradient estimator (PAGE) method has been shown to increase the effective upper frequency limit beyond the traditional p-p method when the source of interest is broadband in frequency.[7] For narrowband sources, it has been shown that intensity can still be calculated without bias error up to the spatial Nyquist frequency.[27] Herein it is shown that when frequencies above the spatial Nyquist frequency are of interest for narrowband sources, additive low-level broadband noise can improve intensity calculations. To be effective, the angular separation between the source and the additive noise source should be less than 30°, with improved results for smaller angular separation. The upper frequency limit for the bandwidth extension depends on the angular separation, the sound speed, and the probe microphone spacing. Assuming the signal-to-additive-noise ratio (SNR_a) is larger than 10 dB, the maximum level and angular bias errors incurred by the additive broadband noise are less than 0.5 dB and 2.5°, respectively.

3.1 Introduction

Active acoustic intensity, hereafter referred to as simply intensity, is an energy-based acoustic measure obtained by the product of acoustic pressure and particle velocity. As a vector quantity, it gives the magnitude and direction of the propagating acoustic energy. Intensity is often

used for source characterization, since the direction of propagation can identify which regions of a source are radiating more dominantly. Many additional applications of intensity have been explored.[28,29]

Acoustic intensity can be computed in several ways; one of the most prevalent methods is referred to as the p-p method, in which a probe with multiple microphones is used to estimate the gradient of pressure by using the change in the real and imaginary pressure components divided by the microphone spacing.[15,30] The p-p method is hereafter referred to as the traditional method. One significant limitation of the traditional method is that the microphone spacing must be small relative to the acoustic wavelength. The particle velocity is underestimated when the microphone spacing begins to be sufficiently large relative to a wavelength, which leads to errors at high frequencies. At much lower frequencies, inherent or residual microphone phase mismatch can cause significant errors. Between these two frequency limitations, there is only a fairly limited bandwidth over which the traditional method can be adequately used. These and other errors have been discussed at length,[31- 38] and many have tried to overcome the errors using varying experimental sensor placement or processing.[39,40]

To overcome some of the problems of the traditional method, especially for high-amplitude jet and rocket noise, the Phase and Amplitude Gradient Estimator (PAGE) method was developed.[9,41] Instead of using formulations which split the complex pressure into real and imaginary parts, as is done in the traditional method, the formulations for the PAGE method represent the complex pressure with a magnitude and phase, based on expressions from Mann et. al.[42] and Mann and Tichy.[43] The expression for intensity with the PAGE method is

$$\boldsymbol{I} = \frac{1}{\rho_0 \omega} P^2 \nabla \phi, \qquad (21)$$

where P represents the pressure magnitude and $\nabla\phi$ represents the pressure phase gradient, where ρ_0 is the air density and ω is the angular frequency. These expressions are advantageous—particularly in propagating fields—because the pressure magnitude and phase manifest less spatial variation than the real and imaginary components of pressure, which allows for a more accurate estimation of the particle velocity across a wider range of frequencies.

Using the PAGE method allows for calculation of intensity at much higher frequencies than does the traditional method. The bias errors for both methods have been investigated,[41] and in general the bias errors for the PAGE method are less than or equal to those of the traditional method. The effects of contaminating noise have likewise been investigated.[10]

The PAGE method generally relies upon phase information in broadband signals to obtain valid intensity results at frequencies above the probe spatial Nyquist frequency, denoted f_N. With narrowband signals, phase information can be sparse enough that the phase gradient may not be calculated reliably above f_N. For distinct tones, the sparsity of phase information in frequency space can make calculation of intensity at these higher frequencies especially erroneous. Fortunately, there is a simple solution. When more phase information is lacking, additive low-level broadband noise with similar directionality can often provide phase information so that the PAGE method can be used effectively with narrowband signals—whether tonal or band-limited—above f_N. [27]

In this chapter, the theoretical and experimental effects of additive broadband noise on obtaining intensity estimates for narrowband signals—specifically tonal frequencies—are discussed. In Section 3.2, the theory for the intensity from a plane-wave source and contaminating broadband noise is developed. The analytical bias errors are presented in Section 3.3. In Section

3.4, experimental results are presented and compared to the analytical results, with conclusions following in the final section.

3.2 Methodology

In this section, the mathematical theory for how additive broadband noise can improve intensity calculation for narrowband signals is developed. Necessary parameters are discussed, followed by the mathematical derivations and bias errors. Practical simplifications are then made, and a guide to when additive broadband noise is helpful is provided.

3.2.1 Preliminary parameters

3.2.1.1 Spatial Nyquist frequency

With the traditional method, the effective upper frequency limit for reliable intensity calculation is the spatial Nyquist frequency, f_N: the frequency at which the microphone spacing is equal to half of an acoustic wavelength, $f_N = \frac{c}{2a}$. This spatial sampling requirement means that microphones in an intensity probe must be placed closer together to calculate intensity for higher frequencies, which can not only increase the effects of scattering, but also increase phase mismatch errors at lower frequencies. Probe configuration and orientation can change the effective microphone spacing and yields an effective spatial Nyquist frequency, $f_{N,\text{eff}}$. As $f_{N,\text{eff}}$ is approached—even at frequencies below $\frac{1}{2} f_{N,\text{eff}}$—the particle velocity is underestimated, so inaccurate intensities are calculated well below $f_{N,\text{eff}}$. In general, angular estimates are valid up to frequencies near $f_{N,\text{eff}}$, while magnitude estimates are only valid up to around one-half of $f_{N,\text{eff}}$.[10] However, the PAGE method yields accurate magnitude and phase estimates up to $f_{N,\text{eff}}$ and also

at higher frequencies if the phase gradient can be accurately calculated. Accurate calculation requires the use of phase unwrapping.

3.2.1.2 Phase unwrapping

To calculate the phase gradient, the phases of the transfer functions between microphone pairs are used. Because the phase differences obtained from transfer functions are restricted to a 2π radian interval, a linear phase difference in frequency space wraps or jumps between π radians and $-\pi$ radians at odd integer multiples of $f_{N,\text{eff}}$, as illustrated by the solid line in Fig. 3.1. The phase is unwrapped by adding multiples of 2π radians to create a continuous phase relationship (dashed line in Fig. 3.1). In this manner the correct overall phase gradient can be obtained.[12,44]

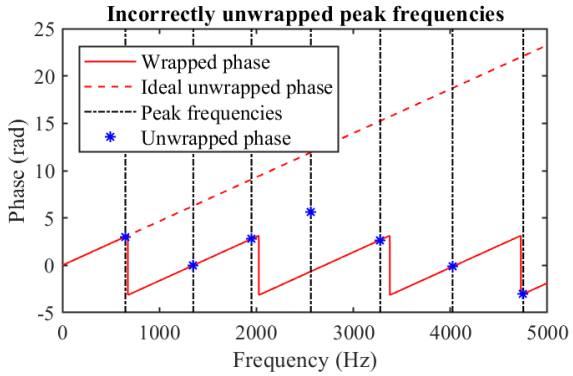

Figure 3.1: An example of ideal wrapped and unwrapped phase values (red) for a broadband signal coming from the same angular direction as a narrowband signal. The sparsity of phase information—none between peak frequencies (black)—for the narrowband signal leads to unreliable unwrapped phase values (blue), and can therefore lead to flawed phase gradient estimates for narrowband signals.

Phase unwrapping works well for broadband signals with sufficient coherence between microphones, most especially for signals with a linear phase relationship.[12] For narrowband signals, or signals composed of discrete frequencies, however, the sparsity of frequency-dependent phase information can cause problems with phase unwrapping. Incorrectly unwrapped phase

values lead to inaccurate phase gradient estimates, and therefore incorrect intensity vectors for frequencies above $f_{N,\mathrm{eff}}$. As seen in Fig. 3.1, the phase gradient obtained for peak frequencies from inaccurately unwrapped phase values can be extremely flawed, and can even trend in the opposite direction. Wrapped phase values at frequencies where there is a signal, hereafter referred to as peak frequencies, are measured for the source, but can be sparse. In contrast, for frequencies without a signal—called noise frequencies—the phase values come from the ambient noise rather than from the source. These phase values have no relation to the phase that would be caused by the source at that frequency, and so are not valid for source properties. Phase unwrapping for narrowband signals is therefore prone to error without additional phase information, which is where additive low-level broadband noise can be helpful.

3.2.1.3 Signal-to-noise ratios

The effects of—and bias errors caused by—contaminating noise in the sound field have been previously investigated.[10] When the signal-to-noise ratio (SNR) is sufficiently large, the contaminating noise does not significantly affect the calculation of intensity. For narrowband sources where frequencies of interest are above f_N, additive broadband noise can actually be helpful. Additive broadband noise provides coherent phase information across the probe at noise frequencies, which can improve unwrapping and, therefore, lead to better intensity calculations. The additive noise must necessarily be higher in level than the ambient noise, which is quantified by comparing two signal-to-noise ratios: The signal-to-additive-noise ratio is denoted by $\mathrm{SNR_a}$, while the signal-to-ambient-noise ratio is simply the usual SNR. When $\mathrm{SNR_a} < \mathrm{SNR}$, the additive noise can provide coherent phase information, which can allow for meaningful phase unwrapping, which results in more accurate phase gradient estimates at peak frequencies.

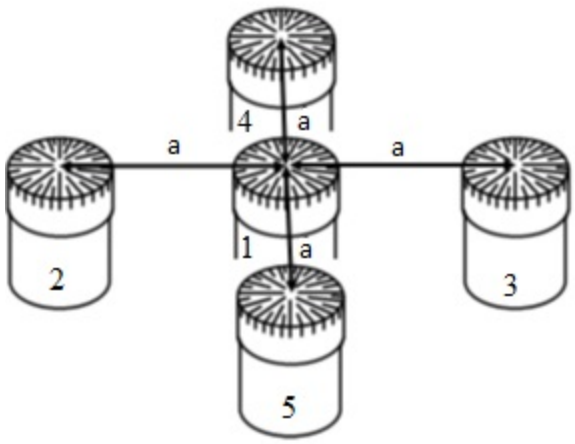

Figure 3.2: A five-microphone orthogonal probe. The microphones are numbered 1 to 5, and have positions (x,y) = (0,0), (-a,0), (a,0), (0,a), and (0,-a), respectively.

3.2.2 Mathematical foundation

3.2.2.1 Derivations

The benefit of additive noise can be illustrated using the five-microphone orthogonal probe pictured in Fig. 3.2. This probe is chosen because symmetry can be employed and calculations are simplified by using pairs of orthogonal microphones.[27] The intensity for this probe using the PAGE method calculation is

$$\boldsymbol{I}_{\text{calc}} = \frac{-G_{11}\arg\{H_{23}\}}{4ka\rho_0 c}\hat{x} + \frac{G_{11}\arg\{H_{45}\}}{4ka\rho_0 c}\hat{y}, \qquad (22)$$

where G_{11} is the auto-spectrum of the central microphone, $H_{\mu\nu}$ is the transfer function between microphones μ and ν, c is the sound speed, ρ_0 is the air density, and k is the wavenumber. For a plane wave signal of pressure amplitude A_s coming from an angle θ_s, and additive plane wave noise—which is self-correlated, though uncorrelated with the source[10]—of amplitude A_n coming from an angle θ_n,

$$G_{11} = A_s^2 + A_n^2, \qquad (23)$$

$$\arg\{H_{23}\} = \arg\left\{A_s^2 e^{-2jka\cos\theta_s} + A_n^2 e^{-2jka\cos\theta_n}\right\}, \quad (24)$$

$$\arg\{H_{45}\} = \arg\left\{A_s^2 e^{-2jka\sin\theta_s} + A_n^2 e^{-2jka\sin\theta_n}\right\}. \quad (25)$$

For the peak frequencies of a narrowband signal with low-level additive noise, $A_s^2 \gg A_n^2$, so the additive noise causes a negligibly small change in transfer function arguments. At noise frequencies, $A_s \approx 0$, and the transfer function phase values obtained from the additive noise are used for unwrapping. The signal-only values at peak frequencies are $G_{11} = A_s^2$, $\arg\{H_{23}\} = -2ka\cos\theta_s$, and $\arg\{H_{45}\} = -2ka\sin\theta_s$. As long as the angular separation $|\theta_s - \theta_n|$ is not too large, these values can be obtained, as is further outlined below. When there is any angular separation, some error is unavoidably introduced.

When angular separation becomes too large, phase unwrapping can fail, which causes inaccurate intensity calculation. The frequency resolution used in processing Δf also has an impact on the unwrapping—too few points between peak frequencies results in poor unwrapping. The phase can be unwrapped correctly if the phase difference of the transfer functions at the peak frequency, f_p, and the adjacent noise frequency, $f_n = f_p \pm \Delta f$, is less than π radians, i.e.,

$$\left|\arg\{H_{23}(f_p)\} - \arg\{H_{23}(f_p \pm \Delta f)\}\right| \leq \pi, \quad (26)$$

$$\left|\arg\{H_{45}(f_p)\} - \arg\{H_{45}(f_p \pm \Delta f)\}\right| \leq \pi. \quad (27)$$

Note that for band-limited signals rather than for discrete tones $f_p \pm \Delta f$ is not necessarily a noise frequency. Equations (*26*) and (*27*) do not need to be checked for validity in this case, only when $f_p \pm \Delta f$ is a noise frequency; the latter case is where the phase values exhibit the greatest change. The frequency when these inequalities are no longer satisfied defines an upper frequency limit, f_{lim}, above which the bias errors sharply increase since unwrapping fails. By assuming $A_s^2(f_p) \gg A_n^2(f_p)$ and $A_s^2(f_n) \approx 0$ [a relatively large signal-to-additive-noise ratio (SNR_a) and a negligible signal amplitude at noise frequencies] and solving for the maximum value of f where Eqs. (*26*) and (*27*) hold, the maximum frequency value is found to be

$$f_{\text{lim}} = \min\left\{\frac{c - 4a\Delta f|\cos\theta_n|}{4a|\cos\theta_n - \cos\theta_s|}, \quad \frac{c - 4a\Delta f|\sin\theta_n|}{4a|\sin\theta_n - \sin\theta_s|}\right\}. \tag{28}$$

This value gives the upper frequency limit for when additive low-level broadband noise will help improve intensity calculation above f_N.

3.2.2.2 Bias errors

When only frequencies below f_{lim} are considered, the bias errors for the calculated intensity due to additive noise are small. An example of the bias error is shown by considering a plane-wave signal consisting of a series of discrete peak frequencies. The analytical intensity for the plane wave signal of pressure amplitude A_s travelling in the $\hat{\theta}_s$ direction is

$$\boldsymbol{I}(\omega) = \frac{A_s^2(\omega)}{2\rho_0 c}\,\hat{\theta}_s. \tag{29}$$

The magnitude and direction bias errors are calculated, respectively, as

$$L_{\epsilon,\boldsymbol{I}} = 10\log_{10}\left(\frac{\boldsymbol{I}_{\text{calc}}}{\boldsymbol{I}}\right)\text{ dB}, \tag{30}$$

$$\theta_{\epsilon,\boldsymbol{I}} = \theta_{\text{calc}} - \theta_s. \tag{31}$$

Using the PAGE method for acoustic vector intensity, the magnitude bias error in decibels at peak frequencies for the five-microphone probe in Fig. 3.2 is given by

$$\begin{aligned} L_{\epsilon,\boldsymbol{I}} &= 10\log_{10}\left(\sqrt{\left|\frac{-G_{11}\arg\{H_{23}\}}{2kaA_s^2}\right|^2 + \left|\frac{-G_{11}\arg\{H_{45}\}}{2kaA_s^2}\right|^2}\right) \\ &= 10\log_{10}\left(1 + \frac{A_n^2}{A_s^2}\left(\frac{2ka + \sin\left(2ka(\cos\theta_n - \cos\theta_s)\right)\cos\theta_s + \sin\left(2ka(\sin\theta_n - \sin\theta_s)\right)\sin\theta_s}{2ka}\right) + O\left(\frac{A_n^4}{A_s^4}\right)\right) \\ &= 10^{1-\frac{\text{SNR}_a}{10}}\left(\frac{2ka + \sin\left(2ka(\cos\theta_n - \cos\theta_s)\right)\cos\theta_s + \sin\left(2ka(\sin\theta_n - \sin\theta_s)\right)\sin\theta_s}{2ka}\right) + O\left(10^{-2*\frac{\text{SNR}_a}{10}}\right) \end{aligned} \tag{32}$$

while the angular bias in radians is given by

$$\begin{aligned} \theta_{\epsilon,\boldsymbol{I}} &= \tan^{-1}\frac{-\arg\{H_{45}\}}{-\arg\{H_{23}\}} - \theta_s = \tan^{-1}\frac{-\arg\left\{A_s^2 e^{-2jka\sin\theta_s} + A_n^2 e^{-2jka\sin\theta_n}\right\}}{-\arg\left\{A_s^2 e^{-2jka\cos\theta_s} + A_n^2 e^{-2jka\cos\theta_n}\right\}} - \theta_s \\ &= \frac{A_n^2}{A_s^2}\frac{\sin\left(2ka(\sin\theta_n - \sin\theta_s)\right)\cos\theta_s - \sin\left(2ka(\cos\theta_n - \cos\theta_s)\right)\sin\theta_s}{2ka} + O\left(\frac{A_n^4}{A_s^4}\right) \end{aligned} \tag{33}$$

$$= 10^{-\frac{\mathrm{SNR_a}}{10}} \frac{\sin\left(2ka(\sin\theta_n - \sin\theta_s)\right)\cos\theta_s - \sin\left(2ka(\cos\theta_n - \cos\theta_s)\right)\sin\theta_s}{2ka} + O\left(10^{-2*\frac{\mathrm{SNR_a}}{10}}\right)$$

The maximum errors across θ_s and θ_n for frequencies below f_{lim} can be obtained from (the exact solutions of) Eqs. (*32*) and (*33*) to give the maximum error as a function of only $\mathrm{SNR_a}$:

$$\left|L_{\epsilon,I}\right| < 10^{1-\frac{\mathrm{SNR_a}}{10}} * 0.5 \text{ dB}, \tag{34}$$

$$\left|\theta_{\epsilon,I}\right| = 10^{1-\frac{\mathrm{SNR_a}}{10}} * 6°. \tag{35}$$

The maximum bias errors were found by assuming $A_s(f_p) \gg A_n(f_p)$. Equations (*34*) and (*35*) are only valid, therefore, if the $\mathrm{SNR_a}$ is larger than about 10 dB. For $\mathrm{SNR_a} \geq 10$ dB the magnitude error is always less than 0.5 dB and the angular error is always less than 6°. If instead the value of the $\mathrm{SNR_a}$ is 20 dB, the maximum angular error is less than 1° while the magnitude error is imperceptible. Note also that these maximum errors decrease with a smaller separation angle between signal and broadband noise sources, which also serves to increase f_{lim}.

3.2.2.3 Practical simplifications

For cases with a significantly large angular separation between the signal and additive noise sources, f_{lim} can actually be reached before the effective spatial Nyquist frequency for the probe,

$$f_{N,\mathrm{eff}} = \min\left\{\left|\frac{c}{2a\cos\theta_s}\right|, \quad \left|\frac{c}{2a\sin\theta_s}\right|\right\}. \tag{36}$$

When $f_{\mathrm{lim}} < f_{N,\mathrm{eff}}$, the additive noise negatively affects the PAGE method calculation of intensity below $f_{N,\mathrm{eff}}$. In practice, to avoid negatively impacting the intensity calculation the angular separation should be limited to

$$|\theta_s - \theta_n| \leq 0.5 \text{ rad} \approx 28.6°. \tag{37}$$

If Eq. (*37*) holds and $4a\Delta f|\sin\theta_n| \ll c$, then f_{lim} can be simplified as

$$f_{\mathrm{lim}} \approx \frac{c}{4a|\theta_s - \theta_n|_{\mathrm{rad}}}. \tag{38}$$

The maximum errors as a function of $\mathrm{SNR_a}$ then become

$$\left|L_{\epsilon,\boldsymbol{I}}\right| < 10^{1-\frac{\mathrm{SNR_a}}{10}} * 0.5 \text{ dB}, \tag{39}$$

$$\left|\theta_{\epsilon,\boldsymbol{I}}\right| = 10^{1-\frac{\mathrm{SNR_a}}{10}} * 2.5°. \tag{40}$$

In summary, certain conditions must be met for the additive noise to be useful. First, the additive noise needs to be low-level relative to the signal, while still greater than the ambient noise level. Second, the angular separation between the signal and additive noise sources must not be too large. The frequency limit above which the additive noise is no longer particularly useful depends on this angular separation. Decreasing the angular separation increases the frequency limit. The bias errors caused by the additive noise depend on the angular separation and the $\mathrm{SNR_a}$, though a maximum error bound for frequencies below the frequency limit can be obtained by using the $\mathrm{SNR_a}$ value alone.

3.2.2.4 Guide to effective additive noise

Consolidating all of these approximations, guidelines emerge for when additive noise is useful and the accuracy of the resulting intensity calculation. For a plane-wave like signal, additive plane-wave noise is useful when

- Signal and noise sources are separated by less than $\sim 28°$, and
- $\mathrm{SNR_a} \geq 10$ dB.

When these conditions are met,

- The upper frequency limit is f_{lim} as given in Eq. (*38*), and depends on the microphone spacing, sound speed, and angular separation of sources, and
- The calculated intensity magnitude and direction for frequencies below f_{lim} is always accurate to within 0.5 dB and $2.5°$, respectively, of the analytical intensity. The accuracy increases with a decreasing angular separation and/or a larger $\mathrm{SNR_a}$.

3.3 Analytical results

Bias errors depend on how the data are processed. If Δf is negligibly small, and the $\mathrm{SNR_a}$ is large (greater than 20 dB), then the magnitude and direction intensity bias errors—shown in Fig. 3.3 and Fig. 3.4 as a function of ka and θ_n, assuming $\theta_s = 0°$—for a plane wave source can be obtained. The black line representing f_{lim} is shown: it outlines regions of high error, and delineates the frequency division above which additive noise is no longer helpful. There are two distinct overlapping error lobes seen—symmetric about $\pm 90°$ and $\pm 180°$—whose lower bounds for ka coincide with the two different values for f_{lim} given in Eq. (*28*) (and multiples of these values), and give the limits for when the phase cannot be unwrapped in either one of or both of the two orthogonal directions.

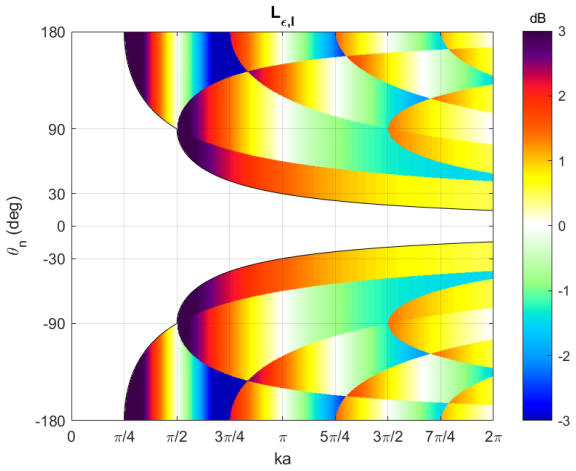

Figure 3.3: Analytical bias errors for PAGE-calculated intensity level for a plane wave source using the probe in Fig. 3.2, given as a function of ka and noise angle θ_n, assuming $SNR_a \geq 20\ dB$ and $\theta_s = 0$.

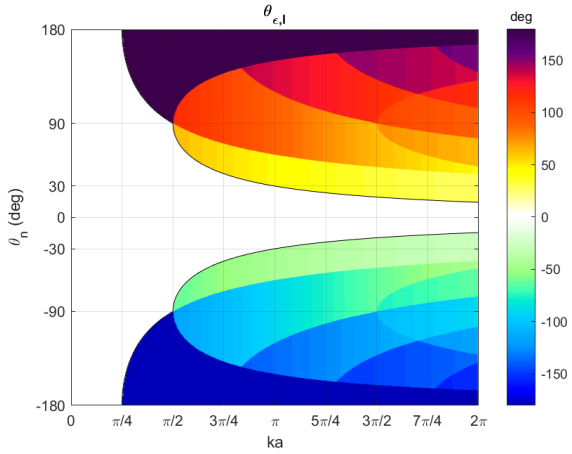

Figure 3.4: Analytical bias errors for PAGE-calculated intensity direction for a plane wave source using the probe in Fig. 3.2, given as a function of ka and noise angle θ_n, assuming $SNR_a \geq 20\ dB$ and $\theta_s = 0$.

These analytical results are extremely promising: the errors below f_{lim} are small and are easily quantified. To allow for experimental verification, analytical results are shown for a specific example. The signal is a sawtooth source with additive broadband brown noise. The sawtooth has a peak frequency of 250 Hz, with overtones which decrease in amplitude. The brown noise likewise rolls off, such that the SNR_a at each peak frequency is the same. Values of $\theta_s = 0°, \Delta f = 1\ \text{Hz}, c = 343\,\frac{\text{m}}{\text{s}}, a = 5.08\ \text{cm}$, and $\text{SNR} = 34\ \text{dB}$ are used.

The analytical magnitude bias errors for this particular setup are show in Fig. 3.5, while the analytical angular bias errors are shown in Fig. 3.6. The figures show the bias errors at the peak frequencies, plotted with an angular resolution of 2.5° and angular limits of $\theta_n = \pm 90°$. The analytical bias errors below f_{lim} are the same as when no discrete processing resolution is assumed, but the error lobes seen above f_{lim} are fundamentally different because of the discrete frequency bin width used in this example.

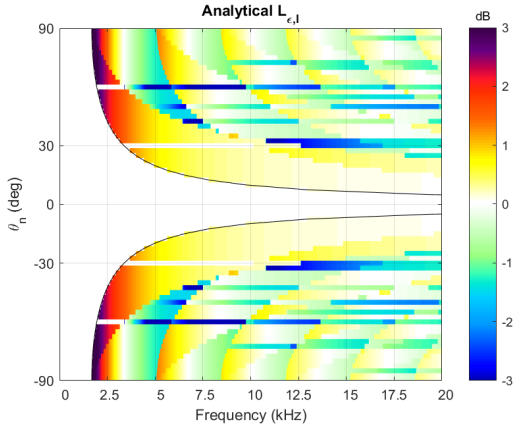

Figure 3.5: Analytical bias errors for PAGE-calculated intensity magnitude using the probe in Fig. 3.2 for a 250 Hz sawtooth source and additive noise with $\theta_s = 0°, \Delta f = 1\ Hz, c = 343\frac{m}{s}, a = 5.08\ cm$, *and* $SNR_a = 34\ dB$. *The black lines give the value of* f_{lim}.

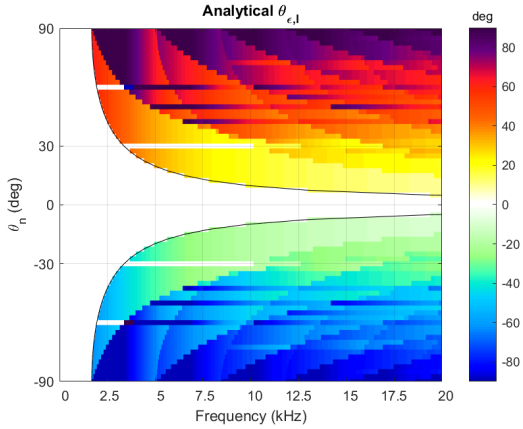

Figure 3.6: Analytical bias errors for PAGE-calculated intensity direction using the probe in Fig. 3.2 for a 250 Hz sawtooth source and additive noise with $\theta_s = 0°, \Delta f = 1\ Hz, c = 343\frac{m}{s}, a = 5.08\ cm$, *and* $SNR_a = 34\ dB$. *The black lines give the value of* f_{lim}.

Many horizontal lines appear in the bias error plots when using discrete values. They are caused by unwrapping errors, which as previously noted depend on the frequency bin width used in processing. At f_{lim}, or at the frequencies where one error lobe crosses another, the unwrapping errors propagate up to higher frequency bins. Despite the analytical differences when using a specific value of Δf, there is no discernable difference below f_{lim}, meaning bias errors in both magnitude and direction are still minimal.

3.4 Experimental verification

3.4.1 Experimental setup

The analytical bias errors in Fig. 3.5 and Fig. 3.6 are now compared to those obtained experimentally. Measurements were taken in the BYU fully anechoic chamber, which has a lower cutoff frequency of approximately 80 Hz. The microphone probe pictured in Fig. 3.2 was used, where the probe radius was $a = 5.08$ cm. A loudspeaker generated a 250 Hz sawtooth wave signal, and was placed on a stand such that $\theta_s = 0°$. The loudspeaker used for the additive noise was placed on the arm of a turntable which was rotated in angular increments of $2.5°$. This second loudspeaker was raised slightly higher than the first, so that the loudspeakers could be located the same distance—approximately 2 meters—from the probe, but so that the rotating arm didn't hit the first loudspeaker. The second loudspeaker on the arm broadcasted brown noise such that the $\mathrm{SNR_a}$ at peak frequencies was approximately 34 dB. Using this experimental setup, which is pictured in Fig. 3.7, and processing with a frequency bin width of $\Delta f = 1$ Hz where the sound speed was $c = 343 \frac{m}{s}$, the results shown in Fig. 3.8 and Fig. 3.9 should ideally match the analytical results seen in Fig. 3.5 and Fig. 3.6, respectively.

Figure 3.7: Experimental setup. The source loudspeaker location is fixed, while the additive noise loudspeaker is on a rotating arm to have variable angular separation.

3.4.2 Experimental results

Bias errors are found by comparing experimentally-obtained vector intensity to the analytical intensity for a 250 Hz sawtooth wave using Eqs. (*30*) and (*31*). The analytical angle for the intensity is 0°, so the direction bias errors, shown in Fig. 3.9, are simply

$$\theta_{\epsilon,\boldsymbol{I}} = \theta_{\text{calc}}. \tag{41}$$

The analytical intensity magnitude is obtained by using the sound pressure level measured by the center microphone, and hence is $G_{11}/\rho_0 c$. The level bias errors, shown in Fig. 3.8, are then

$$L_{\epsilon,\boldsymbol{I}} = 10\log_{10}\left(\frac{L_{\text{calc}}}{G_{11}/\rho_0 c}\right). \tag{42}$$

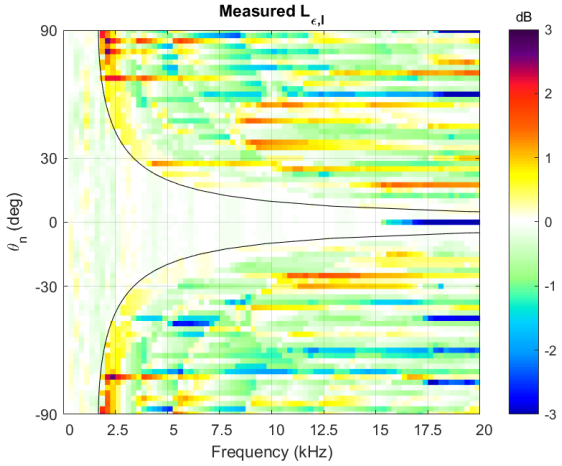

Figure 3.8: Experimental bias errors for PAGE-calculated intensity magnitude using the probe in Fig. 3.2 for a 250 Hz sawtooth signal and additive noise with $\theta_s = 0°, \Delta f = 1\ Hz, c = 343\frac{m}{s}, a = 5.08\ cm$, *and* $SNR_a = 34\ dB$. *The corresponding analytical level bias errors are seen in Fig. 3.5.*

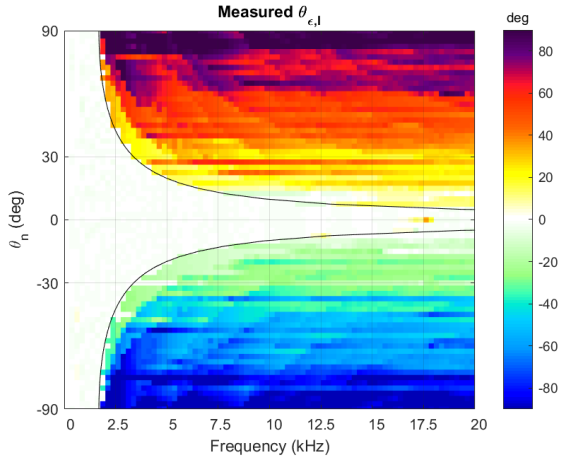

Figure 3.9: Experimental bias errors for PAGE-calculated intensity direction using the probe in Fig. 3.2 for a 250 Hz sawtooth signal and additive noise with $\theta_s = 0°, \Delta f = 1\ Hz, c = 343\frac{m}{s}, a = 5.08\ cm$, *and* $SNR_a = 34\ dB$. *The corresponding analytical direction bias errors are seen in Fig. 3.6.*

The experimental results exhibit remarkable agreement with the analytical results. The frequency limit f_{lim} matches the analytical result. Above f_{lim}, the error lobe edges can be clearly seen, as can the horizontal lines caused by unwrapping with discrete frequency bins. Interestingly, the error lobes—though clearly present—are somewhat different than the analytical results. This is possibly caused by the inherent three-dimensional nature of the experimental setup.

Below f_{lim}, the errors are extremely small, with one noted exception; for $\theta_n = 0°$ the non-trivial error above around 15 kHz is caused by probe scattering.[45] The level bias is especially noticeable, because scattering off the front microphone shields the center microphone, the auto-spectrum of which is used to give the analytical intensity level. For this reason, other small, non-zero angular separation angles do not exhibit these increased bias errors. Below f_{lim}, the benefits of additive broadband noise are clearly manifest.

3.5 Conclusions

When certain conditions are met, adding broadband noise to narrowband signals can greatly improve the calculation of active acoustic intensity using the PAGE method. Below the spatial Nyquist frequency the PAGE method can obtain accurate intensity vectors with or without additive noise. Above the spatial Nyquist frequency, the additive broadband noise provides phase information to improve unwrapping, which yields more accurate intensity vectors. The conditions for when additive noise is beneficial are (1) The $\mathrm{SNR_a}$ should exceed 10 dB at peak signal frequencies, and (2) the signal and additive noise sources should be separated by less than $\sim 28°$. An upper frequency limit f_{lim} can be computed from the angular separation, sound speed, and microphone spacing, given in Eq. (*38*), above which additive noise is no longer beneficial.

For certain probe configurations, scattering can occur before f_{lim} is reached. To reduce scattering, a greater microphone separation distance is beneficial.[45] Probe rotation such that microphones no longer shield one another is also a viable option. Increasing the microphone separation also decreases the spatial Nyquist frequency, which reduces the useable bandwidth when using the traditional method for calculating intensity; for the PAGE method, a greater microphone separation distance decreases f_{lim}, though as the angular separation between the signal and additive noise sources goes to zero, f_{lim} becomes infinite. The experimental upper frequency limit necessarily depends on probe scattering, microphone spacing, and angular separation of the sources.

As a general guideline, a smaller angular separation between the signal and the additive broadband noise source can yield a higher upper frequency limit for PAGE-based intensity calculation of narrowband noise. As long as the $\mathrm{SNR_a}$ exceeds 10 dB at peak frequencies, the intensity bias errors are minimal—within 0.5 dB and 2.5° of the magnitude and direction of the

analytical intensity. These errors decrease with increasing $\mathrm{SNR_a}$ and decreasing angular separation.

Chapter 4

Coherence-based phase unwrapping for broadband acoustic signals

4.1 Introduction

Complex-valued functions are often separated into real and imaginary values. For functions that demonstrate periodicity, a separation into magnitude and phase values is often more useful. As a simple example, consider a unit phasor rotating in the complex plane as a function of frequency, $e^{j\omega t}$. The real part is represented by a cosine wave, and the imaginary part by a sine wave. The magnitude is constant, and the phase is piecewise linear, an example of which can be seen in the upper left plot of Fig. 4.1. These phase values are known as the *wrapped phase*, because they are limited to an interval of 2π radians. The values are aliased or wrapped, giving only the relative phase angle. The *absolute phase* gives the total angle—including complete cycles of the phasor as a function of frequency—instead of the current angle, which in some situations is necessary. The wrapped phase values can be shifted by 2π radian intervals, a process known as unwrapping, to obtain a continuous absolute phase relation, as seen in the lower left plot of Fig. 4.1.

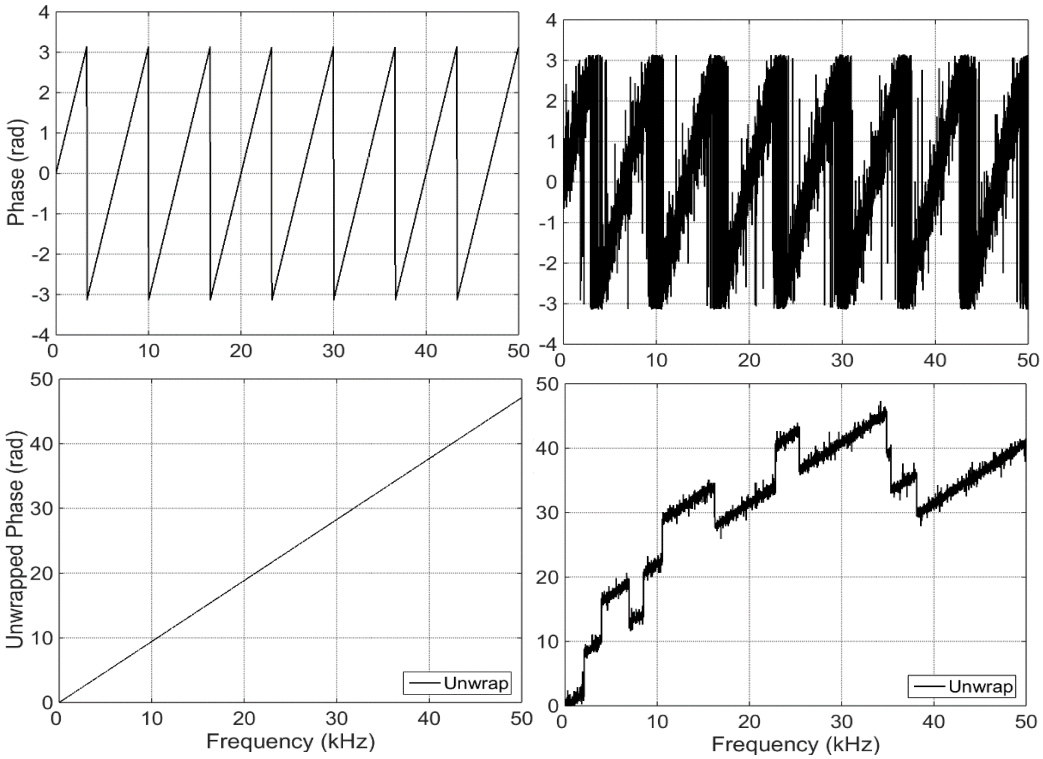

Figure 4.1: Examples of numerical wrapped phase values (top) and the resulting unwrapped phase using MATLAB's function[50] "unwrap" (bottom). The noiseless case (left) is unwrapped perfectly, while the noisy case (right) contains obvious unwrapping errors.

Phase unwrapping is not always so straightforward, most especially when dealing with noisy data. Unwrapping is a common problem in such fields as signal processing, image processing, and optics.[46-48] Many acoustic variables are complex valued in frequency space—obtainable by using a Fourier transform with time domain data. Phase values at high frequencies are often aliased, making unwrapping useful for applications in areas such as beamforming, holography, and sound source localization.[16,18]

Phase unwrapping uses a *transfer function* which, as the name indicates, gives the transformation of the complex-valued pressure recorded at one microphone location relative to that of a second microphone. The complex-valued pressure quantity $\tilde{p}$ can instead be split into a magnitude P and a phase ϕ,[7]

$$\tilde{p}(\omega) = P(\omega)e^{j\phi(\omega)}, \tag{43}$$

where ϕ gives the relative shift in waveforms of the same frequency between –π and π radians as measured by the two microphones. For a plane wave propagating in line with both microphones, the phase changes linearly with increasing frequency. When the frequency is such that the microphones are separated by half of a wavelength, known as the *spatial Nyquist frequency*, the phase can thereafter wrap and become aliased.

Unwrapped phase values can be useful in a variety of situations. In particular, the Phase and Amplitude Gradient Estimator (PAGE) method[18] uses microphone pressure differences and the gradient of the transfer function's phase to obtain active acoustic intensity estimates, $\hat{\boldsymbol{I}}_a$:

$$\hat{\boldsymbol{I}}_a(\omega) = \frac{1}{\omega\rho_0} P^2 \nabla\phi. \tag{44}$$

In order to properly obtain the gradient of the phase, represented by $\nabla\phi$ in Eq. (*21*), phase values must be unwrapped properly. Using the traditional method, the microphone spacing limits the usable bandwidth of results. By using phase unwrapping, the PAGE method can find accurate acoustic intensity values well beyond the spatial Nyquist frequency.[9] Results of this process are in Section 4.4.

4.2 Background

Phase unwrapping can be a difficult challenge in signal processing. There is not necessarily a clearly correct answer in every situation. Even when the trend can be seen visually, unwrapping algorithms often struggle. Even the most appropriate unwrapping can result in erratic jumps, such as when the phase exhibits multiple shifts of approximately π radians in a narrow frequency range. Phase values that are linear in nature, such as plane waves, are simpler to unwrap than rapidly-varying phase values. Li and Levinson[49] show that for linear phase, a high signal-to-noise ratio in

the low frequencies—where the phase is not aliased—leads to the greatest chance of success. At 0 Hz the phase value is necessarily zero. Each frequency bin with its phase value is a data point (f_k, ϕ_k). The goal for unwrapping is to join these points in such a manner as to produce a continuous phase trend. The points are unwrapped by shifting points by any integer multiple of 2π radians:

$$\bar{\phi}_k = \phi_k + 2\pi n, \qquad n = \{0, \pm 1, \pm 2, \dots\}. \tag{45}$$

In Eq. (*45*), ϕ_k is the wrapped phase (between –π and π radians) and $\bar{\phi}_k$ is the unwrapped phase, which is not restricted to a certain range. There are a number of different methods for performing unwrapping, each with its own benefits and limitations.

4.2.1 Simple unwrapping method

Common unwrapping methods, such as MATLAB's *unwrap* function, are conceptually very simple.[50] The unwrapping is performed point-by-point in order of increasing frequency, and relies only upon the single previous data point. The difference between data points is what triggers unwrapping. A cutoff value γ_{cut} is chosen—typically π radians since the wrapped phase is contained in a 2π radian interval. Whenever the difference exceeds the cutoff value, all the following data points are shifted by 2π radians:

$$\bar{\phi}_{k+1} = \phi_{k+1} + 2\pi n_{k+1}, n_{k+1} = \begin{Bmatrix} n_k + 1 & \text{if } \phi_{k+1} - \phi_k < -\gamma_{\text{cut}} \\ n_k - 1 & \text{if } \phi_{k+1} - \phi_k > -\gamma_{\text{cut}} \\ n_k & \text{otherwise} \end{Bmatrix}, n_1 = 0. \tag{46}$$

This ensures that the largest possible phase jump between adjacent points is π radians. This works very well in many circumstances, such as for linearly varying phase values and data with high signal-to-noise ratios; however, many problems can arise. Erroneous phase jumps are often a result of uncorrelated noise between the microphone pair. The algorithm shifts values incorrectly,

even when the phase trend is clearly visible to the human eye. An example of this is visible in the right plots of Fig. 4.1.

4.2.2 Least-squares method

Unfortunately, phase values do not always vary linearly, and signal-to-noise ratios are not always high. Cusack et al.[51] showed that for two-dimensional phase unwrapping, a modified nearest-neighbor algorithm can mitigate problems caused by noise. Huntley[52] also showed that smoothing improves unwrapping. For one-dimensional phase unwrapping, it is therefore reasonable to use a smoothing technique such as the least-squares method.

A least-squares method can prevent many of the unwrapping errors to which the simple unwrapping method is susceptible. Single points with erratic phase values do not trigger an erroneous unwrapping. An additional parameter is necessary in this case: the number of data points N to use for the least-squares fit. To unwrap the point (f_k, ϕ_k), the least-squares method uses the N previously unwrapped frequency data points $\{(f_i, \bar{\phi}_i)\}_{i=k-N}^{k-1}$ to obtain the slope m_k and offset b_k of the fitted line by way of the least-squares equation:

$$\boldsymbol{A}_k^T \boldsymbol{A}_k \boldsymbol{x}_k = \boldsymbol{A}_k^T \boldsymbol{\Phi}_k, \text{where } \boldsymbol{A}_k = \begin{bmatrix} f_{k-N} & 1 \\ f_{k-N+1} & 1 \\ f_{k-N+2} & 1 \\ \vdots & \vdots \\ f_{k-1} & 1 \end{bmatrix}, \boldsymbol{\Phi}_k = \begin{bmatrix} \bar{\phi}_{k-N} \\ \bar{\phi}_{k-N+1} \\ \bar{\phi}_{k-N+2} \\ \vdots \\ \bar{\phi}_{k-1} \end{bmatrix}, \boldsymbol{x}_k = \begin{bmatrix} m_k \\ b_k \end{bmatrix}. \qquad (47)$$

The predicted unwrapped phase value $\tilde{\phi}_k$ for frequency f_k is then $\tilde{\phi}_k = m_k f_k + b_k$. The unwrapped phase value $\bar{\phi}_k$ is found by shifting ϕ_k by 2π intervals to be as close to $\tilde{\phi}_k$ as possible, i.e. n is chosen such that $\left|\tilde{\phi}_k - \bar{\phi}_k\right| = |(m_k f_k + b_k) - (\phi_k + 2\pi n)| < \pi$. This is likewise performed for each point in order of increasing frequency, where $\phi = 0$ at $f = 0$.

The least-squares method can prevent erroneous jumps in certain situations. In frequency ranges of excessive noise, where many phase values are erratic, this method can still give a poorly unwrapped phase. Though the phase itself is expected to be inaccurate in these ranges, unwrapping errors can also shift the phase values for all higher frequencies, hence the need for a better phase unwrapping algorithm.

4.3 Coherence-based approach

Using a coherence-based approach, many unwrapping errors can be avoided, because inaccurate unwrapping usually occurs in frequencies of poor coherence. The algorithm described here shares many similarities with the least-squares approach. The main difference is, naturally, the use of the coherence in order to accomplish unwrapping. Coherence $\gamma_{ij}^2(f_k)$ is a frequency-domain measure of the similarity of the signals received by microphones i and j, with values between zero and one defined as:

$$\gamma_k^2 = \gamma_{ij}^2(f_k) = \frac{\left|G_{ij}(f_k)\right|^2}{G_{ii}(f_k)G_{jj}(f_k)}. \qquad (48)$$

The auto-spectrum of microphone i is represented as G_{ii}, while G_{ij} gives the crosspectrum of microphones i and j. Coherence is often shown on a logarithmic scale and is more useful than linear coherence when applied in this unwrapping algorithm due to the fitting explained below.

4.3.1 Coherence classification

In order to use coherence to prevent erroneous unwrapping, which often occurs in ranges of poor coherence, frequency data points must be given a coherence classification or measure. A basic classification is a division into two groups, one of usable coherence and the other of poor

coherence. There are many possible ways to make this distinction, for example by picking a coherence threshold value. This is useful in some situations, though the method used here takes a different approach. It is done in the following manner:

- The average logarithmic coherence is computed as a threshold value $\langle \gamma_{log}^2 \rangle = \frac{1}{s}\sum_{k=1}^{s} \log_{10} \gamma_k^2$, and all points above this threshold are classified as having usable coherence. Other threshold values can be useful depending on the application.
- A curve is fit to the points below the threshold, using a double exponential model $c_1 e^{c_2 f_k} + c_3 e^{c_4 f_k}$ where c_i is some constant. Other fitting models may be used, though the double exponential is versatile enough to fit many different coherence trends.
- Points above the fitted line are classified as having usable coherence, and those below the line as having poor coherence.

This classification ensures that not too many points are marked as poorly coherent. It also ensures that there will not be long frequency ranges with only points of poor coherence. The dips in coherence are found relatively well using this method. For a visual example of fitting to data, see Fig. 4.2.

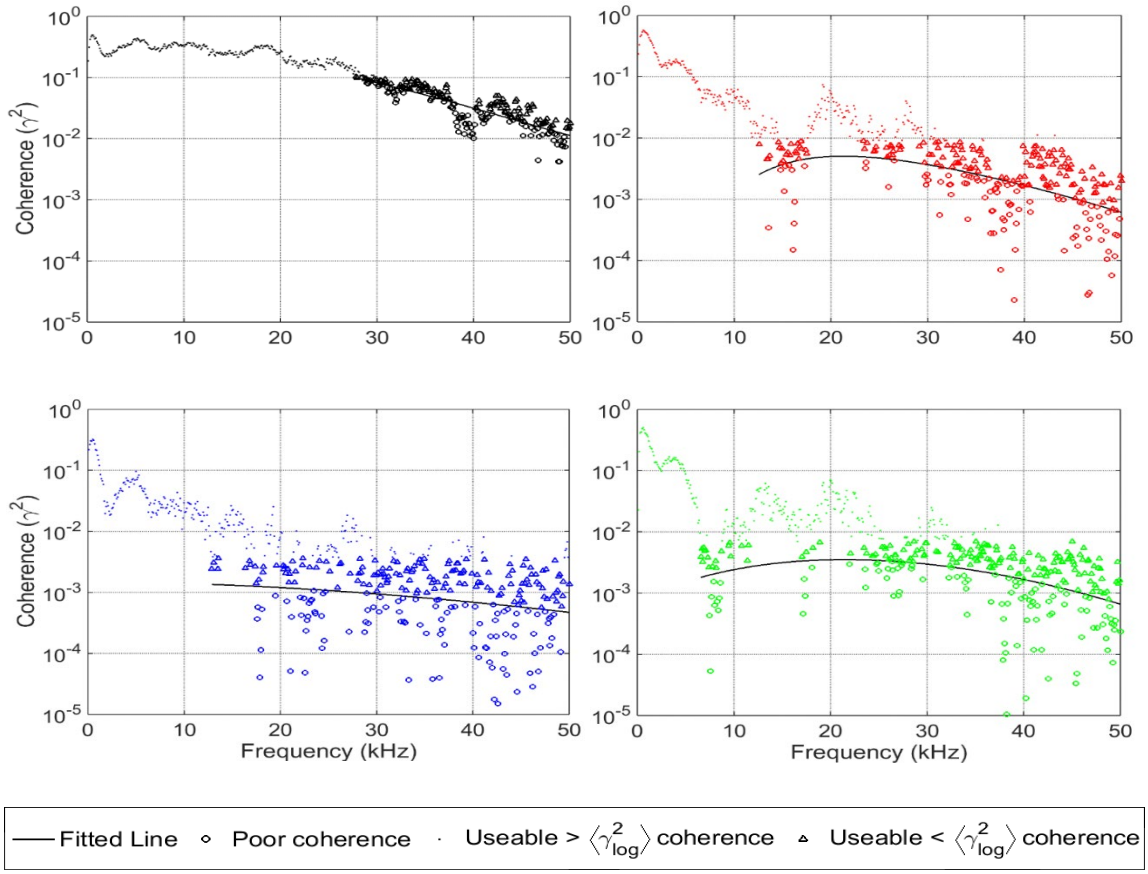

Figure 4.2: Classification of usable coherence and poor coherence for four different microphone pairs. The data for these coherence values come from the jet noise data described in section 4.3.2. The unwrapped phases for these data are seen in Fig. 4.4, with corresponding coloring.

4.3.2 Unwrapping method

After the data points have been classified by their coherence values, the unwrapping is performed using the least-squares approach. The points with usable coherence are first unwrapped independently of those of poor coherence, using the N usable points lower in frequency. Phase values are shifted in 2π intervals so as to be placed as close as possible to the least-squares prediction. The points with poor coherence are not used for unwrapping these points. This ensures that the ranges of poor coherence do not affect the overall phase trend. An example is pictured in the left plot of Fig. 4.3.

In order to unwrap the points of poor coherence, the N closest points, including both points of lower and higher frequencies, with useable coherence are used in the least-squares approach. An example is pictured in the right plot of Fig. 4.3.

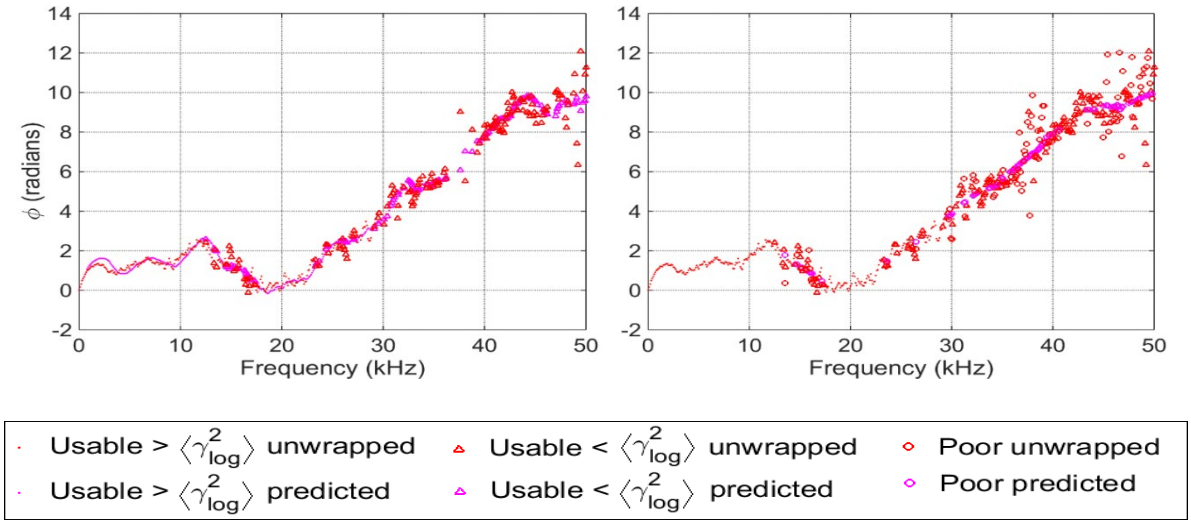

Figure 4.3: The points of usable coherence are unwrapped first using least-squares (left), with N=30 for this case. Then the points of poor coherence are unwrapped to fit the trend (right). As could be expected, the points with poor coherence do not fit as well as the points with usable coherence, just as those above the threshold fit better than those below. These data correspond to the red coherence values seen in Fig. 4.2, and the red line in Fig. 4.4.

The main disadvantage of this approach can be seen when phase values are approximately π radians away from the predicted values. The closest match may be above or below, and this can lead to a jagged-looking unwrapped phase, such as the 38 kHz range in Fig. 4.4. However, an erroneous phase value at $f = f_k$ does not cause erroneous unwrapping that shifts the phase for $f > f_k$ as it does using the simple unwrapping method. The phase can be unwrapped *across* the ranges of poor frequency, not necessarily *in* the ranges of poor frequency. This is what is necessary to find the proper phase gradient. The results using this unwrapping method are seen in the right plot of Fig. 4.4.

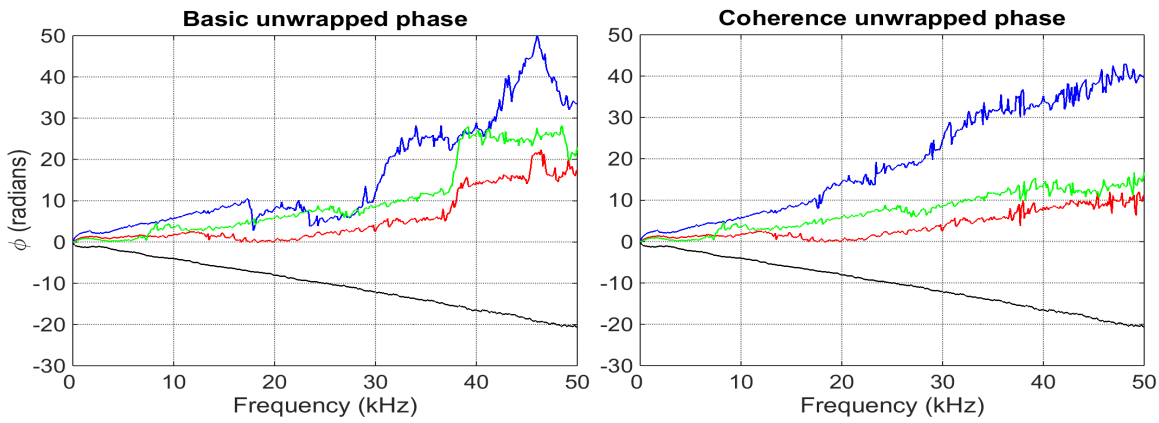

Figure 4.4: The results of basic unwrapping (left) compared to coherence-based unwrapping (right) for four different microphone pairs using jet noise data. The coherence for each set of data is seen in Fig. 4.2 with corresponding colors. The obviously erroneous phase jumps seen using basic unwrapping have been removed by using coherence unwrapping.

4.3.3 Alternative weighting method

A variation can be made to this method by using weighted least-squares in place of regular least-squares. Each point (f_k, ϕ_k) is given a weighting w_k. A simple weighting takes a scaled logarithmic coherence value as the weight. Additionally, points nearer in frequency may be given a larger weighting.

Many different weightings are possible. The weighted least-squares equation is given in Eq. (*49*), using the same definitions as in Eq. (*47*):

$$\boldsymbol{A}_k^T \boldsymbol{W}_k \boldsymbol{A}_k \boldsymbol{x}_k = \boldsymbol{A}_k^T \boldsymbol{W}_k \boldsymbol{\Phi}_k, \text{where } \boldsymbol{W}_k = \begin{bmatrix} w_{k-N} & 0 & 0 & \cdots & 0 \\ 0 & w_{k-N+1} & 0 & \cdots & 0 \\ 0 & 0 & w_{k-N+2} & \ddots & \vdots \\ \vdots & \vdots & \ddots & \ddots & 0 \\ 0 & 0 & \cdots & 0 & w_{k-1} \end{bmatrix}. \quad (49)$$

The same unwrapping procedure described in the previous section is followed in this variation. The points with poor coherence are not used to unwrap the points of usable coherence. Results are very similar in most cases, but not necessarily identical, especially within frequency ranges of poor coherence.

4.4 Experimental results

In addition to numerical data, two different data sets have been investigated in great detail with this phase unwrapping algorithm, namely anechoic chamber measurements of a dipole-like radiation field and jet noise. Active acoustic intensity results for each using the coherence-based phase unwrapping algorithm are compared to that using the MATLAB *unwrap* function,[50] using the Phase and Amplitude Gradient Estimator (PAGE) Method.[18] As explained previously, this method uses the gradient of the phase and therefore needs accurately unwrapped phase values to produce accurate active acoustic intensity vectors above the spatial Nyquist frequency. The acoustic intensity direction can be greatly impacted by incorrectly unwrapped phase values.

4.4.1 Anechoic experiment

4.4.1.1 Experimental setup

Measurements were made in the anechoic chamber at BYU by D. K. Torrie[7] in order to test the efficacy of the PAGE method. A two-dimensional probe consisting of three microphones in an equilateral triangle arrangement around a center microphone was used for the receiver. The microphone radius is 2 inches. The source consisted of the middle two elements (or one of the middle elements for the monopole case) of a loudspeaker array consisting of four 6.3 cm loudspeakers spaced 17.78 cm apart.[7] For most frequencies, the coherence is very high, exceeding 0.99. However, due to the lobe patterns of a dipole at low frequencies and more complex interference patterns at higher frequencies, the coherence drops markedly at specific frequencies and locations for which one microphone is located in an interference null. Coherence and phase values for microphone pairs with the probe at a single location are shown in Fig. 4.5.

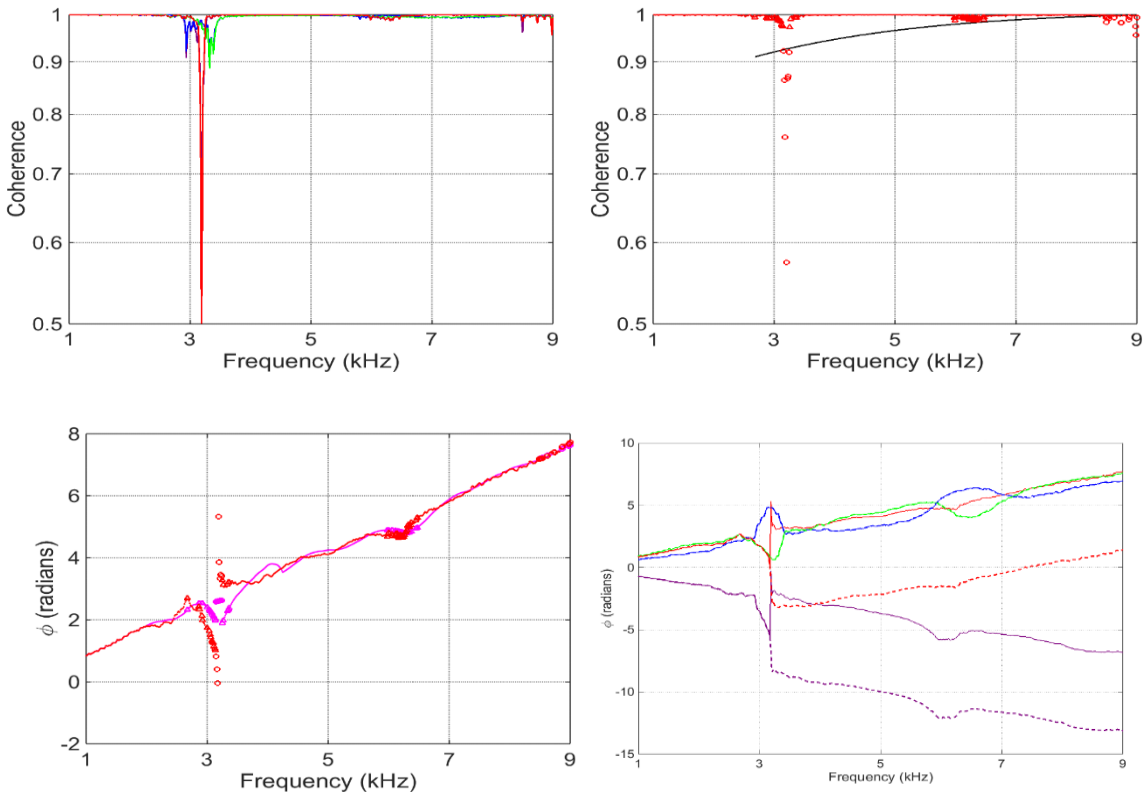

Figure 4.5: For comparison, the results of the unwrapping algorithm for the dipole case are shown. The red lines in each are the same microphone pair. The magenta line (bottom left) gives predicted phase values. The dashed lines (bottom right) show the simple unwrapping results, and the solid lines the coherence-based results. See previous figures for detailed explanations.

4.4.1.2 Results

The coherence-based approach can deal with unwrapping errors in frequency ranges that exhibit poor coherence. Fig. 4.6 shows a spatial map of acoustic intensity vectors for the given frequency. The unwrapping is done across frequency for each position individually. When unwrapping errors have occurred at lower frequencies the vectors appear incorrect.

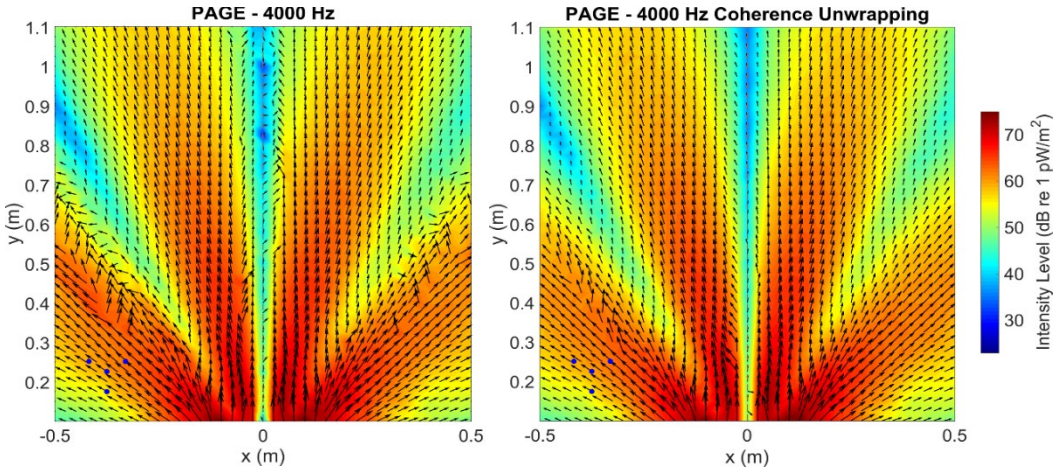

Figure 4.6: A comparison of using simple unwrapping (left) and coherence-based unwrapping (right) to calculate active acoustic intensity using the PAGE method. Many of the erroneous vectors have been markedly improved. The blue dots represent the probe microphones for the selected location.

Something important to note is that the intensity vectors within frequency nulls are not necessarily improved. This, however, is not the goal; instead, the vectors should be valid for frequencies *above* which a frequency null has swept across the probe location. We are concerned with unwrapping *across* frequencies that exhibit poor coherence (when the vector is in a null), rather than unwrapping *in* the frequency ranges of poor coherence. For the spatial map, the erroneous vectors in the areas with high intensity are the result of unwrapping errors at lower frequencies, when this position was in a null. By using coherence unwrapping, many of these errors are avoided.

4.4.2 Jet noise experiment

4.4.2.1 Experimental setup

Acoustical measurements were made at a jet facility at the Hypersonic High-enthalpy Wind Tunnel at Kashiwa Campus of the University of Tokyo. An unheated jet was ideally expanded

through a 20-mm diameter converging-diverging nozzle for a design Mach number of 1.8. Although the facility is not anechoic, nearby reflecting surfaces were wrapped in fiberglass to limit reflections.[53] The same microphone probe configuration described in the dipole experiment was used to obtain measurements. The data used to describe the unwrapping method come from this experiment.

4.4.2.2 Results

Whereas the dipole experiment measurements exhibit excellent coherence, the jet noise experiment measurements exhibits poor coherence between probe microphone pairs, with typical values of less than 0.01. In spite of this extremely low coherence, the phase values still vary rather linearly with frequency. There are relative peaks and dips in coherence across the frequency range of interest. The coherence-fitting algorithm described above works well with this, catching the dips and appropriately classifying frequency ranges of poor coherence. The large phase jumps in these ranges result in a very poorly unwrapped phase when using the simple approach. The coherence-based approach, on the other hand, is not thrown off by these false jumps, and recovers remarkably well.

Figure 4.7 contains spatial maps for the acoustic intensity in the jet noise experiment. The upper figures show the results using regular (left) and coherence-based unwrapping (right). To compare the two, the plots have been superimposed (bottom) and the vectors have been colored. The results using the coherence-based approach vary more smoothly in space, as we would expect to happen physically.

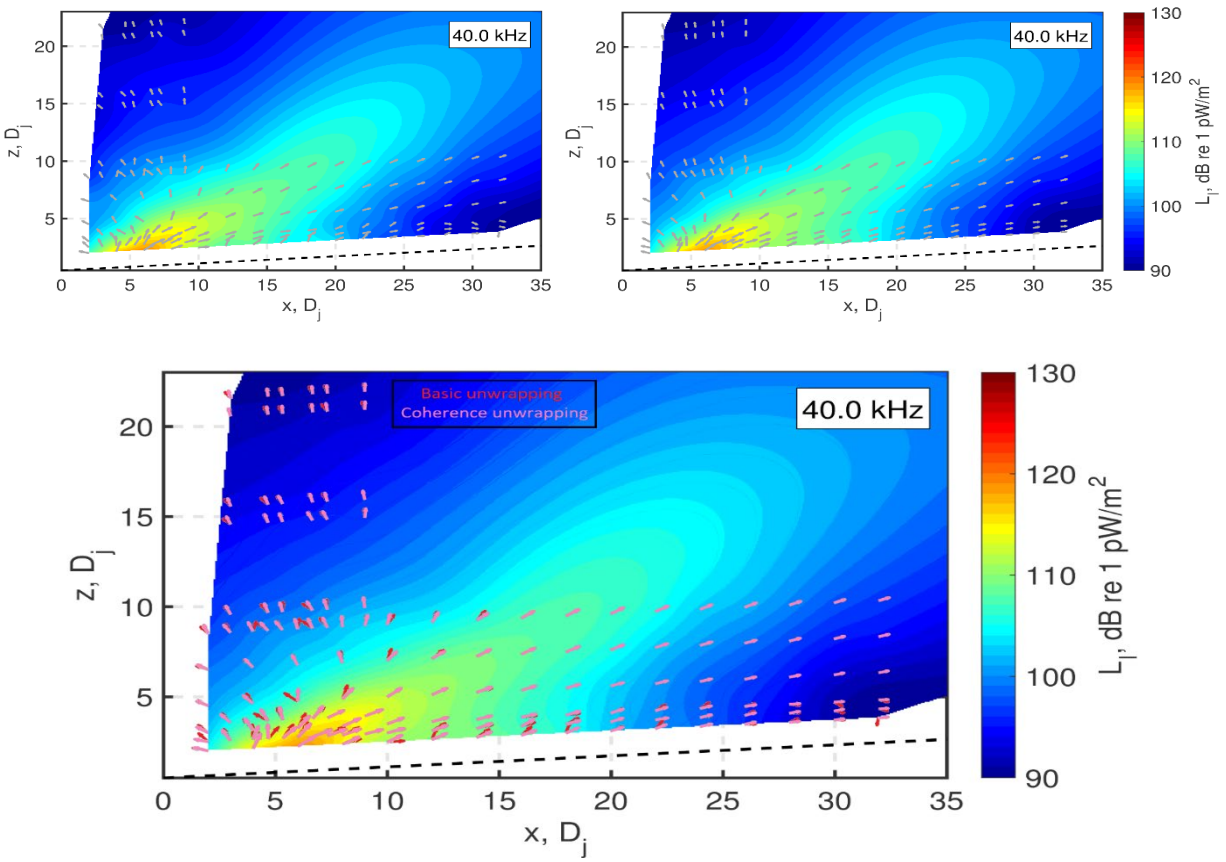

Figure 4.7: Active acoustic intensity vector plots resulting from using simple unwrapping (top left) and coherence-based unwrapping (top right). To aid with visual comparison, these plots have been superimposed (bottom) with differently-colored vectors.

4.5 Future Work

This phase unwrapping algorithm has been applied to situations other than active acoustic intensity, such as for beamforming, and has shown marked improvements.[54] Investigations into higher-order PAGE calculations for finding active acoustic intensity are currently ongoing.[55] Preliminary results of this method combined with coherence unwrapping using the anechoic chamber data show further improvements, and can be seen in Fig. 4.8.

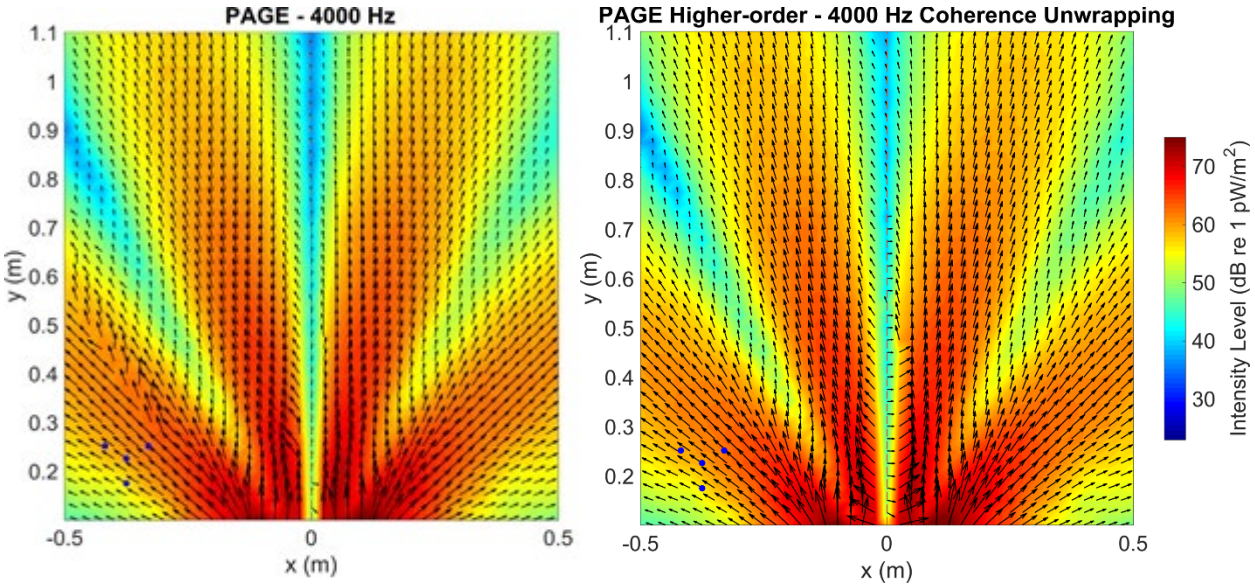

Figure 4.8: Active acoustic intensity vector plots using coherence unwrapping with the PAGE calculation (left) and coherence unwrapping with a higher-order PAGE calculation (right).

4.6 Conclusion

A coherence-based phase unwrapping algorithm can better determine absolute phase values than can simple unwrapping methods. Phase unwrapping is a problem that may not always have a viable solution. Some frequency ranges contain so many jumps that one cannot be sure what the phase is supposed to be. In other situations, a phase trend can be picked out visually, but algorithms can produce results with many false jumps. There is not a one-case-fits-all solution.

In spite of these difficulties, it is possible to improve results by using a coherence-based approach. Phase unwrapping errors are often the result of trying to unwrap in ranges of relatively poor coherence. By giving ranges of poor coherence no weight (or less weight) in unwrapping, a more viable phase trend can be obtained. This in turn leads to less error in active acoustic intensity vectors using the PAGE method, which can increase the bandwidth to well beyond the spatial Nyquist frequency.

Chapter 5

A coherence-based phase and amplitude gradient estimator method for calculating active acoustic intensity

The Phase and Amplitude Gradient Estimator (PAGE) method[9] has been developed as an alternative to the traditional p-p method for calculating energy-based acoustic measures such as active acoustic intensity. While this method shows many marked improvements over the traditional method, such as a wider valid frequency bandwidth for broadband sources, contaminating noise can lead to inaccurate results. Contaminating noise degrades performance for both the traditional and PAGE methods and causes probe microphone pairs to exhibit low coherence. When coherence is low, better estimates of the pressure magnitude and gradient can be obtained by using a coherence-based approach, which yields a more accurate intensity estimate. This coherence-based approach to the PAGE method, known as the CPAGE method, employs two main coherence-based adjustments. The pressure magnitude adjustment mitigates the negative impact of uncorrelated contaminating noise and improves intensity magnitude calculation. The phase gradient adjustment uses coherence as a weighting to calculate the phase gradient for the probe, and improves primarily the calculation of intensity direction. Though requiring a greater computation time than the PAGE method, the CPAGE method is shown to improve intensity calculations, both in magnitude and direction, in the presence of noise.

5.1 Introduction

Coherence is an important measure in many signal processing applications, including beamforming,[56] underwater acoustics,[57] and intensity calculations.[58] It is a frequency-space measure that gives the similarity of signals received by a microphone pair, and ranges between values of zero and one. Low coherence is often indicative of extraneous noise and can also be caused by multiple sources or nonlinear effects.[20] As such, it can give insight into the nature of a sound field.

Coherence is defined by using the auto and cross-spectra for two microphones μ and ν as

$$\gamma_{\mu\nu}^2(\omega) = \frac{\left|G_{\mu\nu}(\omega)\right|^2}{G_{\mu\mu}(\omega)G_{\nu\nu}(\omega)}, \tag{50}$$

where ω is the angular frequency, $G_{\mu\mu}$ and $G_{\nu\nu}$ are auto-spectra, and $G_{\mu\nu}$ is the cross-spectrum. Although $G_{\mu\nu}$ can be imaginary, the auto-spectra are purely real, and so the coherence will always be real-valued and between zero and one.[13] For a probe consisting of n microphones, there will be $n_p = \frac{n(n-1)}{2}$ microphone pairs, and hence n_p coherence spectra. These coherence spectra are useful because, as the coherence is a measure of the similarity of signals as measured by the microphones, it can be used to account for the effects of contaminating noise, and improve intensity calculations.

Active acoustic intensity, which is a frequency and spatially-dependent vector measuring the propagation of sound energy, is useful for a number of applications, including source characterization and localization.[15] To calculate the intensity, both the pressure and particle velocity are necessary. Some methods exist to measure particle velocity, though many methods instead use a multi-microphone probe to measure pressure at different spatial locations and then obtain a value for the particle velocity using the calculated pressure gradient. Different methods

have different ways to obtain the pressure gradient, which can result in different calculated intensity vectors.[14]

A commonly-used method for acoustic intensity, known as the p-p or traditional method, calculates the pressure gradient by using real and imaginary parts of the complex pressure. Using the five-microphone orthogonal probe pictured in Fig. 5.1, where the coordinate system is defined in the caption, the two-dimensional intensity is given by

$$\boldsymbol{I}(\omega) = \frac{\mathrm{Im}\{G_{12}(\omega)\} - \mathrm{Im}\{G_{13}(\omega)\}}{4a\rho_0\omega}\hat{x} + \frac{\mathrm{Im}\{G_{15}(\omega)\} - \mathrm{Im}\{G_{14}(\omega)\}}{4a\rho_0\omega}\hat{y}, \qquad (51)$$

where ρ_0 is the air density and a is the microphone spacing. The traditional method is fairly robust to uncorrelated contaminating noise, as it uses cross-spectral values to calculate the intensity, and cross-spectral values are not impacted by uncorrelated noise. For correlated contaminating noise—such as noise emitted by additional sources—results are more complicated. However, this method can only be used for frequencies below the spatial Nyquist frequency, defined as when the microphone spacing is equal to one-half of an acoustic wavelength, i.e. the sound speed divided by $2a$. Even below this frequency, the intensity magnitude estimate rolls off,[9] and so the traditional method is only used for frequencies well below the spatial Nyquist frequency[8]—level bias errors due to processing are about 1 dB at half the spatial Nyquist frequency.[10]

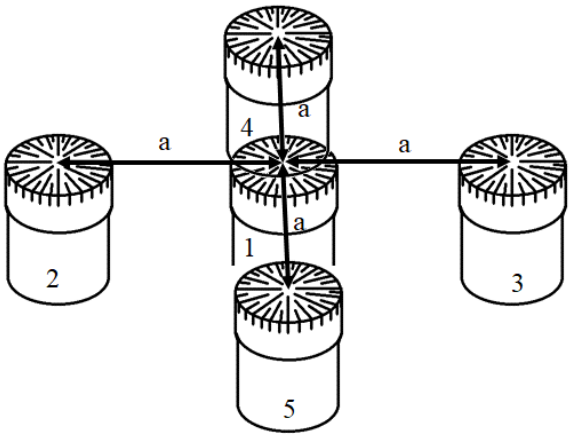

Figure 5.1: A five-microphone orthogonal probe used for 2-dimensional intensity experiments. For the coordinate system defined, microphone 1 is in the center, while $\hat{x}$ points in the direction from microphone 1 to microphone 3, and $\hat{y}$ points in the direction from microphone 1 to microphone 4. The microphones in numerical order are then positioned at locations $(0,0), (-a, 0), (a, 0), (0, a), (0, -a)$.

Another method known as the Phase and Amplitude Gradient Estimator (PAGE) method[9] uses the magnitude and phase of the complex pressure, instead of real and imaginary parts. By using phase unwrapping,[12] this method can yield reliable intensity estimates well above the spatial Nyquist frequency for radiating sources.[27] The general equation for the PAGE method intensity estimate is

$$\boldsymbol{I}(\omega) = \frac{1}{\rho_0 \omega} P^2(\omega) \nabla \phi(\omega), \tag{52}$$

where P is the pressure magnitude, and $\nabla\phi$ is the phase gradient. Using the five-microphone orthogonal probe in Fig. 5.1, the PAGE intensity is calculated as

$$\boldsymbol{I}(\omega) = \frac{-G_{11}(\omega) \arg\{G_{23}(\omega)\}}{4a\rho_0\omega} \hat{x} + \frac{-G_{11}(\omega) \arg\{G_{54}(\omega)\}}{4a\rho_0\omega} \hat{y}, \tag{53}$$

where G_{11} is the auto-spectrum of the middle microphone. Note that the argument of the transfer function is equivalent to the argument of the cross-spectrum, since the transfer function is simply a complex cross-spectrum divided by the product of real-valued auto-spectra. The auto-spectra

are affected by noise, and because of this, though the PAGE method can be used for higher frequencies, contaminating noise can reduce the usefulness of the PAGE method.[10]

The calculation bias errors for both pressure-gradient based intensity methods have been studied, [7] including the effects of different probe configurations and rotation, as well as with contaminating noise.[10] Bias errors for the PAGE method are essentially caused by a combination of two separate mechanisms: errors due to pressure magnitude and errors due to phase gradient calculation. Because errors are the result of two mechanisms, two main adjustments can be made. Both adjustments make use of the coherence measured by the microphone probe. These adjustments can be implemented into the PAGE method calculation; the resulting approach is called the CPAGE method, for the Coherence-based Phase and Amplitude Gradient Estimator method. The pressure magnitude adjustment is discussed in Section 5.2, and the phase gradient adjustment is discussed in Section 5.3. Experimental validation for these corrections is given in Section 5.4.

5.2 Pressure magnitude adjustment

Using the PAGE method, one type of error in intensity calculations caused by contaminating noise is encountered when obtaining the pressure magnitude estimate. Because auto-spectral values are used, as seen in Eq. (*52*), the pressure of any contaminating noise is included in the pressure measurements and therefore in the intensity calculation. The pressure magnitude is squared to obtain the auto-spectrum, and so even small errors have a large impact on intensity calculations. In Chapter 2, a magnitude adjustment was found that can reduce the pressure magnitude bias errors of the PAGE method.[10] This correction relies upon the estimate of the pressure magnitude.

Probe geometry determines how the pressure value is obtained. There are two qualitatively different types of probes: those with a microphone located at the geometric center of the probe, and those without. When there is a microphone at the probe center, the magnitude of the pressure measured by this microphone is taken to be pressure magnitude, and no calculation is needed:

$$P^2(\omega) = |\tilde{p}_c(\omega)|^2, \tag{54}$$

where the subscript *c* indicates that this is the probe's center microphone. For probes without a center microphone, the pressure magnitude is calculated by averaging the pressure magnitude values obtained at all of the microphones:

$$P^2(\omega) = \left(\frac{1}{n}\sum_{i=1}^{n}|\tilde{p}_i(\omega)|\right)^2. \tag{55}$$

The PAGE method uses the pressure magnitude from Eqs. (*54*) and (*55*) directly, while the CPAGE method makes an adjustment to the pressure magnitude.

The bias errors of both the PAGE and traditional methods in the presence of contaminating noise are investigated in Chapter 2.[10] Because the traditional method incorporates cross spectra, it is unaffected by uncorrelated noise in some cases, such as when the contaminating noise is plane-wave like.[10] For the PAGE method, however, uncorrelated noise simply adds to the overall pressure magnitude, increasing the magnitude of the auto-spectrum and therefore the intensity magnitude. However, by using the coherence values of the probe microphones, the pressure magnitude of the uncorrelated noise relative to that of the signal can be calculated. The coherence can therefore be used to account for the additional pressure magnitude caused by the contaminating noise. The resulting pressure estimate will therefore more accurately estimate the pressure magnitude of the sound source of interest, rather than the combined pressure of the source and contaminating noise (this approach can be used to reduce errors in signals that contain wind noise, for example).

As a basic example, consider a case where all microphones in a probe measure the combined pressure from uncorrelated plane-wave-like noise and a plane wave signal that are of equal amplitude, i.e., the signal-to-noise ratio, SNR, is zero. The PAGE-calculated pressure is double what would be calculated without the contaminating noise, resulting in a +3 dB bias caused by the contaminating noise (see Fig. 2.3). The coherence gives the amount of contamination measured between each microphone pair, so if the coherence values are the same for each microphone pair, the exact amount of contamination caused by uncorrelated noise—and hence the SNR—can be found. Removing the pressure caused by the contaminating noise would make the calculation bias error go to zero.

Unfortunately, in practice coherence values are not identical for all probe microphone pairs, and so obtaining the "effective" SNR for the probe is nontrivial. When microphone pairs have different coherence values, an estimated SNR—or an effective coherence for the probe—must be calculated. This is not as simple as averaging all coherence values, however. As an example, consider the five-microphone orthogonal probe in Fig. 5.1, for a case where all microphones record the desired the signal, while a single microphone also measures additional pressure from uncorrelated noise (e.g. electrical noise). For this probe, there are ten separate microphone pairs, and with only one microphone picking up a contaminated signal, the coherence of four of these microphone pairs is reduced. Averaging the coherence across all microphone pairs gives a skewed result of the effective probe coherence or overall SNR.

There are many possible solutions to the problem of estimating the SNR; the CPAGE method uses one that is easy to implement, and gives a conservative pressure magnitude adjustment. The maximum coherence value across all microphone pairs at a particular frequency is used as the effective probe coherence. Using the maximum coherence value ensures that only

noise measured by all microphones is removed and therefore will not cause an over-correction. Using the pressure magnitude P—which is obtained from the composite signal of the source and noise together, as given in Eqs. (*54*) and (*55*)—the adjusted pressure magnitude utilized by the CPAGE method is calculated as

$$P^2_{\mathrm{CPAGE}}(\omega) = \left(\max_{\mu,\nu} \left\{ \sqrt{\gamma^2_{\mu\nu}(\omega)} \right\} P(\omega) \right)^2 = \max_{\mu,\nu} \{ \gamma^2_{\mu\nu}(\omega) \} P^2(\omega). \qquad (56)$$

Note that any pressure adjustment leads to a reduction of the central pressure value, since the coherence can never exceed a value of one. This adjustment is reasonable because contaminating noise always serves to increase, rather than decrease, the total pressure magnitude. The multiplicative factor $\sqrt{\gamma^2_{\mu\nu}}$ is explained in Section 2.3.1, and causes the calculation bias errors of the CPAGE method for a plane wave source and uncorrelated noise to go to zero, while causing a reduction in bias errors for other source and noise combinations.

The adjustment in Eq. (*56*) is most effective when all microphones record uncorrelated contaminating noise. All microphone pairs must exhibit a decrease in coherence at the same frequency in order for any correction to be made. When microphone pairs demonstrate vastly different coherence values—whether due to correlated contaminating noise or different levels of uncorrelated contaminating noise—an adjustment to the phase gradient is more useful.

5.3 Phase gradient adjustment

The first adjustment utilized by the CPAGE method improves the intensity magnitude calculation; the phase gradient adjustment can have some impact on intensity magnitude, though primarily is of use in improving the intensity direction. Using the PAGE method, the intensity calculation is given in Eq. (*52*), and calculating the intensity direction relies upon estimating the

phase gradient, $\nabla\phi$. This frequency-dependent phase gradient is calculated by using the phase of the transfer function between probe microphone pairs, then performing a least-squares fit to obtain a phase gradient for the probe:

$$\nabla\phi = (\mathrm{X}^{\mathrm{T}}\mathrm{X})^{-1}\mathrm{X}^{\mathrm{T}}\Delta\phi, \tag{57}$$

where X and $\Delta\phi$ are defined below.

The matrix or vector X is of size $n_p \times d$ where n_p is the number of probe microphone pairs ($n_p = \frac{n(n-1)}{2}$ for a probe consisting of n microphones) and d is probe intensity-measurement dimensionality. The matrix X is composed of the physical distance between probe microphone positions:

$$\mathrm{X} = \begin{bmatrix} x_2 - x_1 & \cdots & x_n - x_1 & x_3 - x_2 & \cdots & x_n - x_{n-1} \\ y_2 - y_1 & \cdots & y_n - y_1 & y_3 - y_2 & \cdots & y_n - y_{n-1} \\ z_2 - z_1 & \cdots & z_n - z_1 & z_3 - z_2 & \cdots & z_n - z_{n-1} \end{bmatrix}^{\mathrm{T}}. \tag{58}$$

where $x, y,$ and z are orthogonal coordinates in three-dimensional space, and the subscripts give the probe microphone numbers. For one- or two-dimensional intensity probes, only the first or second columns, respectively, of X are used. Because the physical positions of the probe are not frequency dependent, the pseudoinverse $(\mathrm{X}^{\mathrm{T}}\mathrm{X})^{-1}\mathrm{X}^{\mathrm{T}}$ utilized by the PAGE method is the same for all frequencies, and must only be computed once.

The vector $\Delta\phi$—not to be confused with $\nabla\phi$, the phase gradient—is of length n_p, and gives the measured phase differences between microphone pairs. Phase differences are given by the argument of the transfer function (or cross-spectrum here), and are frequency-dependent:

$$\Delta\phi = \begin{bmatrix} \arg\{G_{12}\} & \cdots & \arg\{G_{1n}\} & \arg\{G_{23}\} & \cdots & \arg\{G_{n-1,n}\} \end{bmatrix}^{T}. \tag{59}$$

Because measured phase differences lie in a 2π radian interval, this requires the use of phase unwrapping to get accurate phase differences above the spatial Nyquist frequency.[12] The

vector $\Delta\phi$, therefore, must contain unwrapped transfer-function phase differences to be useful above the spatial Nyquist frequency.

The phase gradient adjustment implemented by the CPAGE method is conceptually simple: instead of using a least-squares method, a weighted least-squares method is used. The weighted least-squares method is similar to the least-squares method, though—as the name implies—it allows for data points (phase differences) to be given different weights or importance in the fitting algorithm. The weights used for the CPAGE method are the square roots of the coherence values between microphone pairs, $\sqrt{\gamma_{\mu\nu}^2}$, the same values used in the pressure magnitude adjustment. Note that the weights used are frequency-dependent. These weights are combined into a diagonal matrix of size $n_p \times n_p$,

$$\mathrm{W} = \mathrm{diag}\left[\sqrt{\gamma_{12}^2} \quad \cdots \quad \sqrt{\gamma_{1n}^2} \quad \sqrt{\gamma_{23}^2} \quad \cdots \quad \sqrt{\gamma_{n,n-1}^2}\right], \tag{60}$$

where W is frequency-dependent. The frequency-dependent phase gradient obtained by the CPAGE method using a weighted least-squares algorithm is then

$$\nabla\phi = (\mathrm{X}^{\mathrm{T}}\mathrm{W}\mathrm{X})^{-1}\mathrm{X}^{\mathrm{T}}\mathrm{W}\Delta\phi. \tag{61}$$

Equation (*61*) uses the weighted pseudoinverse $(\mathrm{X}^{\mathrm{T}}\mathrm{W}\mathrm{X})^{-1}\mathrm{X}^{\mathrm{T}}\mathrm{W}$. Unlike the unweighted pseudoinverse, the weighted pseudoinverse varies with frequency, since the weighting matrix itself is frequency dependent. The main disadvantage to this is that a pseudoinverse must be computed for each frequency, which increases overall computation time. However, the phase gradient adjustment allows the CPAGE method to improve intensity calculation (most especially intensity direction) when contaminating noise is present.

5.4 Experimental verification

The two coherence-based adjustments to the PAGE method explained are uniquely suited for different situations. The magnitude adjustment—Eq. (*56*)—is most applicable when all probe microphone measurements include uncorrelated noise, while the phase gradient adjustment—Eq. (*61*)—is most applicable when only some of the microphones are contaminated by noise, or when the contaminating noise is self-correlated. The CPAGE method uses both the pressure magnitude and phase gradient adjustments simultaneously, though, depending on the situation, one adjustment can have a much larger impact than the other. Two different experiments are used to show the effects of each adjustment individually. Experimental results show how the CPAGE method calculation differs from the PAGE method calculation when microphone signals contain contaminating noise.

Measurements were taken in BYU's large anechoic chamber, described in related publications.[11,27] The five-microphone orthogonal probe for two-dimensional intensity calculation—pictured in Fig. 5.1—was used, where the probe radius $a = 0.25$ m (see Fig. 5.2). This relatively large probe radius was used so that individual microphones could be more easily subjected to contaminating noise. The source used for all experiments was a loudspeaker emitting broadband noise. The calculation bias errors for the CPAGE and PAGE method are compared. Rather than using an analytical intensity for comparison, the results of the PAGE method in the absence of noise are used as the benchmark value. This choice allows bias errors to show the differences in how both methods handle contaminating noise. A bias error of zero means that the contaminating noise has no effect on intensity calculation. The magnitude and direction bias errors are explicitly defined, respectively, as

$$L_{\epsilon,\boldsymbol{I}} = 10\log_{10}\left(\frac{|\boldsymbol{I}_{\text{noise}}|}{|\boldsymbol{I}|}\right) \text{ dB}, \tag{62}$$

$$\theta_{\epsilon,\boldsymbol{I}} = \theta_{\text{noise}} - \theta, \tag{63}$$

where $|\boldsymbol{I}|$ and θ are the magnitude and direction, respectively, of the intensity as calculated by the PAGE method in the absence of contaminating noise, and $|\boldsymbol{I}_{\text{noise}}|$ and θ_{noise} are the calculated intensity magnitude and direction of either method when contaminating noise is present. Bias errors for the traditional method are not shown as the spatial Nyquist frequency for this probe is 686 Hz, and so for most frequencies of interest (beyond about 200 Hz) the traditional method intensity calculations are unreliable.[8]

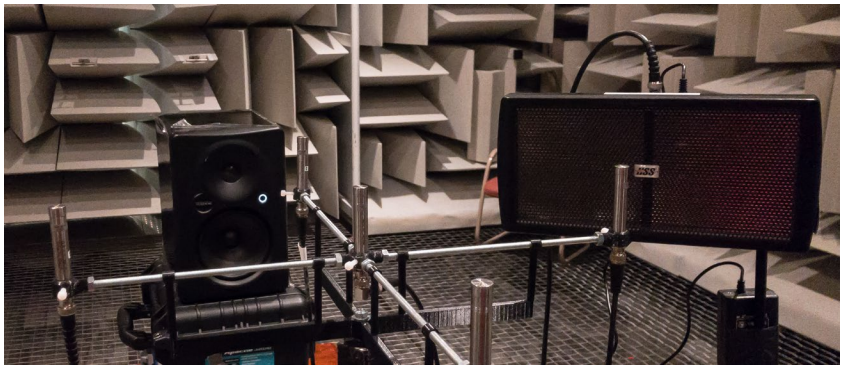

Figure 5.2: Experimental setup. The five-microphone orthogonal probe has a radius of $a = 0.25\ m$. The loudspeaker was used as the source for both experiments, while the parametric speaker array was used as the noise source for the phase gradient adjustment experiment.

5.4.1 Pressure magnitude adjustment experiment

To show the effectiveness of the coherence-based pressure magnitude adjustment, all microphone signals were contaminated. Measurements were first taken of the source alone—the results of the PAGE method for these measurements give the benchmark values. The signals acquired were then contaminated with computer-generated broadband white noise, with an independent contamination signal for each microphone. Because the contaminating signals were of approximately equal amplitude for each microphone, the resulting coherence values for all

microphone pairs were also of similar amplitude. The contaminated signals had much larger pressure magnitudes than the uncontaminated signals (SNR ≈ -6 dB). This meant that the PAGE method calculated a much larger intensity magnitude for the contaminated case, resulting in a large level bias error due to noise.

The CPAGE method can account for the uncorrelated contaminating noise, resulting in much smaller level bias errors than the PAGE method. Because intensity direction calculation uses arguments of cross-spectra, which are largely unaffected by uncorrelated contaminating noise, the calculated intensity direction for both methods should match the noiseless case, resulting in only small angular bias errors.

The results for this experiment are seen in Fig. 5.3. Sound pressure levels obtained from auto-spectral values for two of the probe microphones (numbered 1 and 2 in Fig. 5.1) are shown in Fig. 5.3(a). The solid lines give the sound pressure levels of the source alone, while the dashed lines are the results obtained from the contaminated signals. The coherence of the contaminated signals for the four microphone pairs which include the center microphone (number 1) are shown in Fig. 5.3(b).

The level bias errors for the PAGE and CPAGE method due to the contaminating noise are shown in Fig. 5.3(c). Because the contaminating noise is much louder than the source, the PAGE method shows consistently large bias errors at all frequencies: calculated levels are a result of the noise, rather than of the source. As expected, the CPAGE method can correctly account—at least in part—for the contaminating uncorrelated noise. At all frequencies, this results in a smaller magnitude bias for the CPAGE method. The PAGE method calculates a larger magnitude because of the contaminating noise, while variation in the CPAGE method magnitude follows the same

trend across frequency but with lower bias errors. As expected, the angular bias errors for both methods are nearly zero, as shown in Fig. 5.3(d).

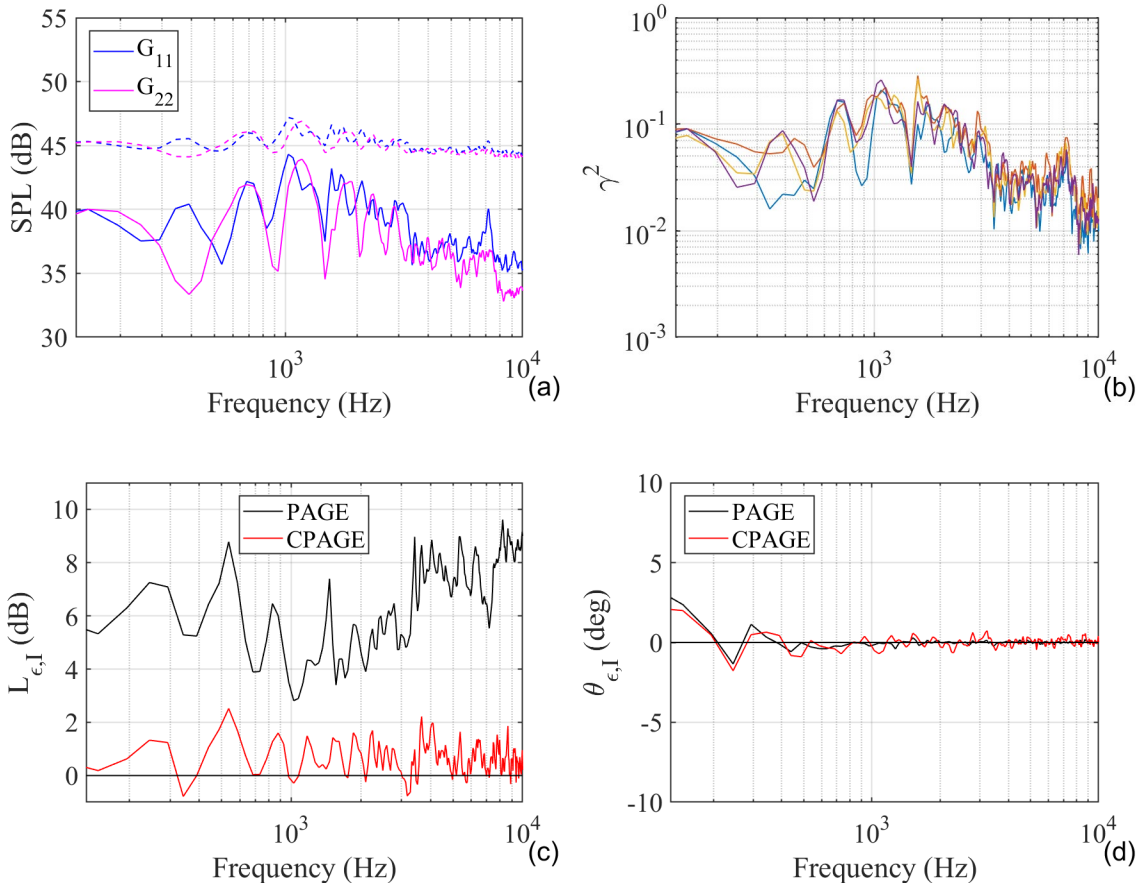

Figure 5.3: Bias errors for the PAGE and CPAGE methods—in comparison to the noiseless PAGE intensity results—caused by adding uncorrelated broadband white noise to the signals recorded by all probe microphones independently. Sound pressure levels obtained from microphone auto-spectral values are shown in (a), where the solid lines are for the source alone, and the dashed lines are for the contaminated signal. The coherence of the contaminated signals for various microphone pairs is shown in (b). The CPAGE method is seen to have reduced magnitude bias errors (c), while the angular bias is mostly unchanged from that of the PAGE method (d).

5.4.2 Phase gradient adjustment experiment

To test the effectiveness of the coherence-based phase gradient adjustment, the same experimental setup was used, but with a different noise source. An American Technology Corporation HSS 450 parametric speaker array, which is designed to have a spatially-narrow

intensity lobe, was pointed at microphone 2 (as numbered in Fig. 5.1). A minor amount of contaminating noise could be picked up by the other microphones, but for most frequencies the contamination was minimal. The level of the contaminating noise at microphone 2 was much larger than the signal amplitude (SNR $10 - 20$ dB), effectively rendering this microphone's signal useless for measuring the source, while having a very small impact on the signals measured by the other microphones.

Because the coherence values for the microphone pairs that do not include microphone 2 are largely unaffected by the contaminating noise, the center pressure correction is minimal for most frequencies. The cross-spectral values obtained using the signal of microphone 2 are erroneous, however, which gives an incorrect phase gradient. The coherence for all pairs including microphone 2 are poor, however. Therefore, a weighted pressure gradient can be used to more accurately calculate the intensity direction. Experimental results are seen in Fig. 5.4.

Figure 5.4(a) shows the sound pressure levels obtained from the auto-spectral values for microphones 1 and 2, where again the solid line is the uncontaminated signal and the dashed line includes the contaminating noise. The noise has a very small impact on the signal of microphone 1, while the signal of microphone 2 is vastly different, and essentially gives the sound pressure level of the noise rather than the source. The coherence of the contaminated signals for the four probe microphone pairs which include the center microphone (number 1) are shown in Fig. 5.3(b). Two of the coherence spectra are always near unity, and one exhibits a few dips at certain frequencies. The other coherence spectrum is much lower than all the others and corresponds to the coherence between microphones 1 and 2. Figure 5.3(c) shows the intensity level bias errors for both methods are similar, though there are some differences.

The intensity direction bias errors are shown in Fig. 5.3(d). The PAGE method shows large errors at nearly all frequencies. For some frequencies, the CPAGE method corrects the intensity direction nearly perfectly; interestingly, at other frequencies the correction is still an improvement over the PAGE method, but is not entirely effective. This resulting intensity direction bias errors appear jagged across frequency, much as the coherence values do. Indeed, the jagged nature of the coherence (of all microphone pairs, though only one pair containing microphone 2 is pictured) across frequency causes the somewhat jagged nature of the calculated intensity direction. The bias errors for the CPAGE method are certainly reduced, though the inconsistency across frequency suggests that a different phase gradient weighting or regularization may be more useful.

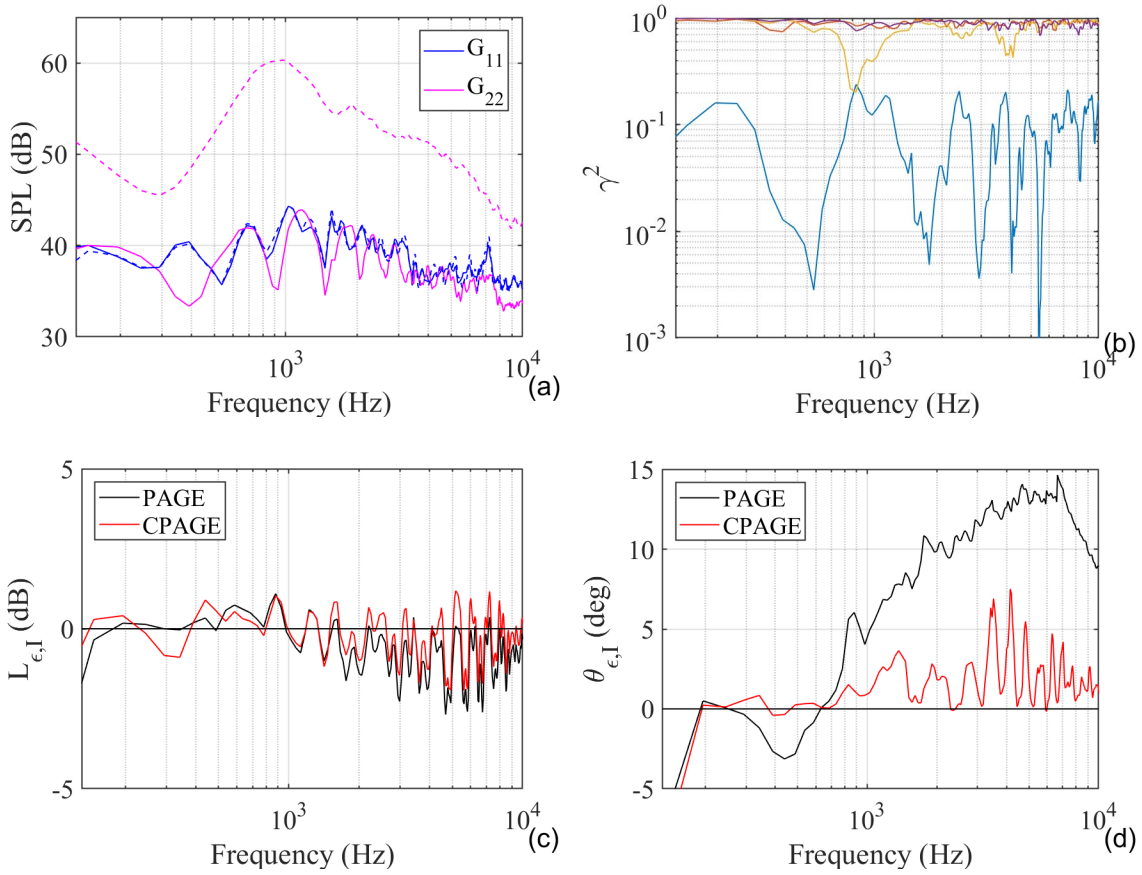

Figure 5.4: Similar to Fig. 5.3, where instead of uncorrelated contaminating noise the parametric speaker array was used to contaminate the signal of microphone 2. In (a) the level of contamination of the signal of microphone 2 is apparent, while the signal of microphone 1 is largely unaffected. In (b) the coherence between microphones 1 and 2 is very low, while other pairs including microphone 1 are much larger.

5.5 Conclusions

By using coherence in its calculations, the CPAGE method reduces the intensity calculation bias errors of the PAGE method. Two main adjustments are made. A coherence-based magnitude adjustment can account for uncorrelated noise measured by all microphones, and improves intensity magnitude calculation. A coherence-weighted pressure gradient calculation can account for different levels of noise measured by microphones, and improves intensity direction calculation. These corrections together make the CPAGE method better able to calculate intensity vectors in the presence of contaminating noise.

Though only active acoustic intensity results are investigated herein, the calculation of other energy-based acoustic measures—such as reactive intensity, potential energy density, kinetic energy density, and specific acoustic impedance, as well as directional pressure[59]—could also be improved with the CPAGE method. Coherence can effectively measure the signal contamination, and as such can account for contaminating noise recorded while measuring source properties.

The CPAGE method is limited in many of the same ways as the PAGE method. It relies upon correct phase unwrapping and broadband signals to be accurate above the spatial Nyquist frequency, and is effected by scattering. As shown in Section 5.4.2, without regularization the CPAGE method can show more accuracy at some frequencies than others, resulting in a jagged intensity direction across frequency. Though the CPAGE method is not ideal for every situation, it broadens the applications of the PAGE method because it is more robust to contaminating noise.

The effectiveness of the CPAGE method is best seen in sound fields that contain a large amount of contaminating noise. One application which is currently being investigated deals with contaminating wind noise at low frequencies. This sound field can exhibit very low coherence,

and requires the use of large microphone probes. The CPAGE method is thought to be doubly useful in this situation, as it can deal with low coherence and can be used for high frequencies even with large microphone spacing. This application, as well as other future work, may help to further validate the effectiveness of the CPAGE method in calculating active acoustic intensity.

5.6 Chapter 5 Appendix

The CPAGE method uses two main adjustments to calculate intensity. However, there is another possible adjustment which is useful in very special cases. The adjustment proposed here should, in practice, rarely be necessary, though is worth considering for completeness. This correction is useful when the pressure measured by a probe's center microphone at a particular frequency is considered to be of dubious validity. This can result from poor experimental setup, where—for whatever reason—the center microphone records mostly noise instead of actual signal at a particular frequency. If this is known in practice then the experimental setup should clearly be changed, but if further data acquisition is unfeasible, this additional adjustment can prove useful.

The CPAGE method only uses this correction at frequencies where the coherence of the center microphone with all other microphones is less than the coherence of all outer microphone pairs,

$$\max_{\mu}\{\gamma_{c\mu}^2(\omega)\} < \min_{\mu,\nu\neq c}\{\gamma_{\mu\nu}^2(\omega)\}, \tag{64}$$

where the subscript c signifies the center microphone, and μ and ν label the probe microphones. When the condition in Eq. (*64*) is true, then instead of using the pressure measured at the center microphone, the weighted average pressure of the other microphones should be used. In other words, at these frequencies, the CPAGE method treats the probe as if there is no center

microphone, since the measured center pressure is considered to be more erroneous than the measured pressure of all other probe microphones. Intensity probes are generally more accurate when a probe has a center microphone,[45] so this correction is very rarely necessary. Because the CPAGE method calculates a pseudoinverse at every frequency to obtain the pressure gradient, the condition in Eq. (*64*) can be checked without having a large impact on computation time.

Chapter 6

Conclusion

Coherence can be used to improve the calculation of active acoustic intensity. Coherence can be used at many places in intensity calculation, including phase unwrapping, dealing with narrowband signals, adjusting pressure magnitude to account for contaminating noise, and improved phase gradient calculation. Pressure gradient methods like the traditional and PAGE methods require the use of a multi-microphone probe to calculate intensity, and so coherence—which is a pairwise microphone measure—can be easily calculated and included in processing to yield a more stable method, known as the CPAGE method.

Coherence can be used to improve transfer function phase unwrapping. Below the spatial Nyquist frequency, phase values do not need to be unwrapped, but above this frequency the PAGE method needs to have correctly unwrapped phase values to estimate intensity. By using the coherence in phase unwrapping, phase values can be more properly unwrapped. This leads to better phase gradient and hence intensity value calculations.

With better unwrapped phase values, more accurate phase gradients can be obtained. The CPAGE method further improves phase gradient calculations by using a coherence-weighted least-squares algorithm, where the coherence of each microphone pairs gives the relative weight for the phase difference measured. In cases of near-zero coherence, this may cause larger adjustments than wanted, though regularization could be used to account for this possibility.

The bias errors for the PAGE method illustrate rather clearly how contaminating noise can negatively impact intensity calculation. From these bias errors, a pressure magnitude correction

term is found. This correction term works best for uncorrelated contaminating noise, though is also useful for other situations. The pressure magnitude adjustment utilized by the CPAGE method is very conservative, and further investigations may lead to a more useful way to apply this adjustment.

The CPAGE method is a useful tool, which in many cases can better calculate the intensity of a source in the presence of contaminating noise. This method is not a perfect solution for every situation, however, but rather an improvement in many situations. There are problems and limitations with this method just as there are with any other method. Below the spatial Nyquist frequency, unwrapping is not a problem, but above the spatial Nyquist frequency erroneous phase unwrapping can occur for both the PAGE and CPAGE methods: transfer function phases may not be locally linear or even continuous—room modes and scattering can cause physical phase jumps. The CPAGE method can adjust for problems the PAGE method has when dealing with noise, but does not deal with other possible problems. The CPAGE method is better at handling uncorrelated noise for a plane wave source, but is also useful in other source and noise situations, and can make adjustments without needing any knowledge of the source or noise type.

Though active acoustic intensity is the focus of this thesis, the CPAGE method can be used to obtain other energy-based acoustic measures, which include reactive intensity, potential energy density, kinetic energy density, and specific acoustic impedance. Just as the PAGE method is better suited to some of these calculations than the traditional method, the CPAGE method can implement further adjustments to improve calculations.

6.1 Contributions

The PAGE method is still relatively new, and has proven to be remarkably effective in certain situations. Contributions from this research serve to augment the usability of the PAGE method, and include (1) better phase unwrapping techniques, (2) a better understanding of calculation bias errors, (3) applications of the PAGE method to narrowband source investigation, and (4) the CPAGE method—that utilizes improved coherence-based calculation techniques to give more reliable pressure magnitude and phase gradient values—which can better deal with contaminating noise in a sound field.

The real benefit of the PAGE method is its ability to be used up to and even above the spatial Nyquist frequency. Above the spatial Nyquist frequency, phase unwrapping must be performed correctly to give accurate results: improved phase unwrapping is therefore key to application of the PAGE method at higher frequencies. By using coherence, phase unwrapping can be performed more reliably—though the unwrapped phase values can still be erroneous, such as when physical phase jumps occur in highly reactive fields.[18,59]

Previous investigations of the bias errors for the traditional and PAGE methods ignored the effects of both probe rotation and contaminating noise.[8] Including both of these effects leads to a better understanding of the situations in which each method is most effective. The traditional method is useful for low frequencies, and is fairly robust to uncorrelated contaminating noise. The PAGE method is an improvement in many ways, including extending the useable bandwidth, though contaminating noise can cause errors in calculating intensity magnitude and direction. Using the CPAGE method, these bias errors can be reduced. The CPAGE method can be useful in areas of research including beamforming, underwater acoustics, and especially aeroacoustics.

Because it relies upon phase unwrapping at higher frequencies, the PAGE method is most useful when measuring a broadband noise source. For measuring narrowband sources above the spatial Nyquist frequency, additive low-level broadband noise can improve PAGE method calculations. Limitations of this method yield specific guidelines for when additive noise is useful.

Finally, the CPAGE method incorporates improved processing techniques. This resultant method is more robust to contaminating noise, and incorporates both a pressure magnitude and phase gradient correction. Since all sound fields contain some level of contaminating noise, the CPAGE method takes the benefits of the PAGE method calculations and improves them to better handle a wider variety of situations.

6.2 Future work

Many uses of coherence have been found to be useful, but phase unwrapping, a pressure magnitude adjustment, and a phase gradient adjustment are simply a few places in intensity calculation where coherence can be utilized. As mentioned, calculation of other energy-based acoustic measures can likely benefit from utilizing coherence and the CPAGE method. Future investigations are necessary to validate this claim.

Initial applications of the PAGE method to study the infrasound frequency range are currently being conducted. Since contaminating noise can occur in this frequency range (caused by wind noise, for example), the more robust CPAGE calculations may give more accurate results. Different types of noise could further portray possible weaknesses of this method.

As before mentioned, different types of regularization—especially in the weighted least-squares pressure gradient calculation—may increase the effectiveness of the CPAGE method

calculations across frequency. Different magnitude corrections are also possible. Further investigation may yield better adjustments than those which are currently employed.

Contaminating noise is always going to be a challenge. Though not always bad—and if used in the right way potentially even useful—noise has an undeniable impact on acoustic measurements. A better understanding of the effects of noise can lead to improved calculation techniques. Methods which are better able to handle contaminating noise are more useful in a greater number of situations, and key to dealing with noise is using coherence.

Bibliography

[1] M. E. Weber, “Wideband, frequency-domain beamforming for coherent signal processing,” J. Acoust. Soc. Am. **74**, S76 (1983).

[2] J. V. Candy, “Model-Based Signal Processing,” J. Acoust. Soc. Am. **119**, 2553 (2006).

[3] R. M. Fitzgerald, A. N. Guthrie, J. D. Shaffer, and D. A. Nutile, “Low-frequency acoustic coherence in the deep ocean,” J. Acoust. Soc. Am. **55**, S58 (1974).

[4] R. Hickling, and A. W. Brown. "Determining the direction to a sound source in air using vector sound-intensity probes." J. Acoust. Soc. Am. **129**, 219–224 (2011).

[5] F. J. Fahy, “Measurement of acoustic intensity using the cross-spectral density of two microphone signals,” J. Acoust. Soc. Am. **62**, 1057–1059 (1977).

[6] F. J. Fahy, "A technique for measuring sound intensity with a sound level meter," Noise Control Eng. **9**, 155–162 (1977).

[7] D. K. Torrie, E. B. Whiting, K. L. Gee, T. B. Neilsen and S. D. Sommerfeldt, "Initial Laboratory Experiments to Validate a Phase and Amplitude Gradient Estimator Method for the Calculation of Acoustic Intensity from Broadband Sources," Proc. Mtgs. Acoust. **23**, (2017).

[8] E. B. Whiting, J. S. Lawrence, K. L. Gee, T. B. Neilsen, and S. D. Sommerfeldt, “Bias error analysis for phase and amplitude gradient estimation of acoustic intensity and specific acoustic impedance,” J. Acoust. Soc. Am. **142**, 2208-2218 (2017).

[9] D. C. Thomas, B. Y. Christensen and K. L. Gee, "Phase and amplitude gradient method for the estimation of acoustic vector quantities," J. Acoust. Soc. Am. **137**, 3366-3376 (2015).

[10] M. R. Cook, K. L. Gee, T. B. Neilsen, and S. D. Sommerfeldt, “The effects of contaminating noise on the calculation of acoustic intensity,” accepted to J. Acoust. Soc. Am. (2018).

[11] M. R. Cook, K. F. Succo, K. L. Gee, S. D. Sommerfeldt, and T. B. Neilsen, “Bandwidth extension of narrowband-signal intensity calculation using additive, low-level broadband noise,” submitted to J. Acoust. Soc. Am. (2019).

[12] M. R. Cook, K. L. Gee, S. D. Sommerfeldt, and T. B. Neilsen, "Coherence-based phase unwrapping for broadband acoustic signals," Proc. Mtgs. Acoust. **30**, 055005 (2017).

[13] F. J. Fahy, *Sound Intensity* (Spon, London, 1995), pp. 1–295.

[14] M. J. Crocker, "Measurement of Sound Intensity," in Handbook of Acoustical Measurements and Noise Control, New York, McGraw-Hill, 1991, pp. 14.1-14.17.

[15] J. Y. Chung, “Cross-spectral method of measuring acoustic intensity without error caused by instrument phase mismatch,” J. Acoust. Soc. Am. **64**, 1613–1616 (1978).

[16] J. A. Mann and J. Tichy, "Acoustic intensity analysis: Distinguishing energy propagation and wave-front propagation," J. Acoust. Soc. Am. **90**, (1991).

[17] E. B. Whiting, J. S. Lawrence, K. L. Gee, T. B. Neilsen, and S. D. Sommerfeldt, “Bias error analysis for phase and amplitude gradient estimation of acoustic intensity and specific acoustic impedance,” J. Acoust. Soc. Am. **142**, 2208–2218 (2017).

[18] E. B. Whiting, “Energy Quantity Estimation in Radiated Acoustic Fields,” M. S. Thesis, Brigham Young University, Provo, Utah (2016).

[19] J. S. Lawrence, E. B. Whiting, K. L. Gee, R. D. Rasband, T. B. Neilsen, and S. D. Sommerfeldt, “Three-microphone probe bias error for acoustic intensity and specific acoustic impedance,” J. Acoust. Soc. Am. **143**, EL81 (2018).

[20] J. S. Bendat and A. G. Piersol, *Random Data: Analysis and Measurement Procedures* (Hoboken, New Jersey, 2010).

[21] L. S. Goodfriend, “Correction chart for background noise,” Noise Control **4**(3), 56 (1958).

[22] C. H. Oppenheimer, “A statistical background noise correction sensitive to the steadiness of background noise,” J. Acoust. Soc. Am. **140**, 2888 (2016).

[23] E. Y. Lo and M. C. Junger, “Signal-to-noise enhancement by underwater intensity measurements,” J. Acoust. Soc. Am. **82**, 1450 (1987).

[24] J. S. Lawrence, K. L. Gee, T. B. Neilsen, and S. D. Sommerfeldt, “Higher-order estimation of active and reactive acoustic intensity,” Proc. Mtgs. Acoust. **30**, 055004 (2017).

[25] S. E. Bard, “A study of background noise variability in acoustical measurement laboratories,” J. Acoust. Soc. Am. **132**, 2086 (2012).

[26] C. H. Oppenheimer, “An alternate background noise correction sensitive to the steadiness of background noise,” ECMA TR/107 (2015).

[27] K. F. Succo, S. D. Sommerfeldt, K. L. Gee, T. B. Neilsen, “Acoustic intensity of narrowband sources using the phase and amplitude gradient estimator method,” Proc. Mtgs. Acoust. **30**, 030015 (2018).

[28] ANSI/ASA S1.9:1996, Instruments for the Measurement of Sound Intensity (Acoust. Soc. Am., Melville, NY, 1996).

[29] G. Pavić, "Measurement of sound intensity," J. Sound Vib. **51**, 533-545 (1977).

[30] F. Jacobsen, "Intensity Techniques," in *Handbook of Signal Processing in Acosutics* (Springer, New York, NY), pp. 1109-1127 (2008).

[31] F. Jacobsen, "Sound Intensity," in *Springer Handbook of Acoustics* (Springer, New York, NY), pp. 1053-1075 (2007).

[32] F. Jacobsen, "Random errors in sound intensity estimation," J. Sound Vib. **128**, 247-257 (1989).

[33] A. F. Seybert, "Statistical errors in acoustic intensity measurements," J. Sound Vib. **75**, 519-526 (1981).

[34] T. Loyau and J.-C. Pascal, "Statistical errors in the estimation of the magnitude and direction of the complex acoustic intensity vector," J. Acoust. Soc. Am. **97**, 2942-2962 (1995).

[35] C. P. Wiederhold, K. L. Gee, J. D. Blotter, and S. D. Sommerfeldt, "Comparison of methods for processing acoustic intensity from orthogonal multimicrophone probes," J. Acoust. Soc. Am. **131**, 2841-2852 (2012).

[36] J.-C. Pascal and J.-F. Li, "A systematic method to obtain 3D finite-difference formulations for acoustic intensity and other energy quantities," J. Sound Vib. **310**, 1093-1111 (2008).

[37] C. P. Wiederhold, K. L. Gee, J. D. Blotter, S. D. Sommerfeldt, and J. H. Giraud, "Comparison of multimicrophone probe design and processing methods in measuring acoustic intensity," J. Acoust. Soc. Am. **135**, 2797-2807 (2014).

[38] F. Jacobsen,"A simple and effective correction for phase mis-match in intensity probes," Appl. Acoust. **33**, 165-180 (1991).

[39] T. Yanagisawa and N. Koike, "Cancellation of both phase mismatch and position errors with rotating microphones in sound intensity measurements," J. Sound Vib. **113**, 117-126 (1987).

[40] T. Iino, H. Tatekawa, H. Mizukawa, and H. Suzuki, "Numerical evaluation of three-dimensional sound intensity measurement accuracies and a proposal for an error correction method," Acoust. Sci. Technol. **34**, 34-41 (2013).

[41] B. Y. Christensen, "Investigation of a New Method of Estimating Acoustic Intensity and Its Application to Rocket Noise." M. S. thesis, Brigham Young University, Provo, UT (2014).

[42] J. A. Mann, J. Tichy, and A. J. Romano, "Instantaneous and time-averaged energy transfer in acoustic fields," J. Acoust. Soc. Am. **82**, 17-30 (1987).

[43] J. A. Mann and J. Tichy, "Near-field Identification of Vibration Sources, Resonant Cavities, and Diffraction Using Acoustic Intensity Measurements," J. Acoust. Soc. Am. **90**, 720-729 (1991).

[44] K. L. Gee, M. Akamine, K. Okamoto, T. B. Neilsen, M. R. Cook, S. Teramoto, and T. Okunuki, "Characterization of Supersonic Laboratory-Scale Jet Noise with Vector Acoustic Intensity," 23rd AOAACEAS Aeroacoustics Conference, AIAA Aviation Forum, (AIAA 2017-3519).

[45] M. T. Rose, R. D. Rasband, K. L. Gee, and S. D. Sommerfeldt, "Comparison of multi-microphone probes and estimation methods for pressure-based acoustic intensity," Proc. Mtgs. Acoust. **26**, 030004 (2016).

[46] D. C. Ghiglia and L. A. Romero, "Robust two-dimensional weighted and unweighted phase unwrapping that uses fast transforms and iterative methods," J. Acoust. Soc. Am. **11**, 107-117 (1994).

[47] K. Itoh, "Analysis of the phase unwrapping algorithm," Applied Optics **21**, 2470 (1982).

[48] J. Tribolet, "A new phase unwrapping algorithm," IEEE Trans. Acoust., Speech, and Sig. Proc. **25**, 170-177 (1977).

[49] D. Li and S. E. Levinson, "A linear phase unwrapping method for binaural sound source localization on a robot," in *International Conference on Robotics & Automation, Proceedings of the IEEE*, (Washington, DC, May 2002).

[50] The MathWorks, Inc., function *unwrap.m,* (1984-2005).

[51] R. Cusak, J. M. Huntley and H. T. Goldrein, "Improved noise-immune phase-unwrapping algorithm," Appl. Optics **34**, 781-789 (1995).

[52] J. M. Huntley, "Noise-immune phase unwrapping algorithm," Appl. Optics **28**, 3268-3270 (1989).

[53] A. T. Wall, K. L. Gee, T. B. Neilsen and D. W. Krueger, "Cylindrical acoustical holography applied to full-scale jet noise," J. Acoust. Soc. Am. **136**, 1120-1128 (2014).

[54] C. B. Goates, B. M. Harker, K. L. Gee and T. B. Neilsen, "Extending the usable bandwidth of an acoustic beamforming array using phase unwrapping and array interpolation," J. Acoust. Soc. Am. **141**, 3912 (2017).

[55] J. S. Lawrence, K. L. Gee, T. B. Neilsen and S. D. Sommerfeldt, "Higher-order estimation of active and reactive acoustic intensity," Proc. Mtgs. Acoust. **30**, 055004 (2017).

[56] M. E. Weber, "Wideband, frequency-domain beamforming for coherent signal processing," J. Acoust. Soc. Am. **74**, S76 (1983).

[57] A. I. Malekhanov and A. G. Sazontov, "Large-array acoustic signal processing in random deep-water channels: Effects of coherence," J. Acoust. Soc. Am. **97**, 3294 (1995).

[58] J. A. Clark, “Measurement of coherence with a vector acoustic intensity probe,” J. Acoust. Soc. Am. **81**, S43 (1987).

[59] J. S. Lawrence, K. L. Gee, T. B. Neilsen, and S. D. Sommerfeldt, “Highly directional pressure sensing using the phase gradient,” J. Acoust. Soc. Am. **144**, EL346 (2018).